รหัสโครงการ SUT7-706-51-36-31

รายงานการวิจัย

การศึกษาเกี่ยวกับประสิทธิผลของการตกผลึกอะมิโนเอซิดบริสุทธิ์

(A Study into the effectiveness of crystallization for separation of amino acids)

ได้รับทุนอุดหนุนการวิจัยจาก

มหาวิทยาลัยเทคโนโลยีสุรนารี

ผลงานวิจัยเป็นความรับผิดชอบของหัวหน้าโครงการวิจัยแต่เพียงผู้เดียว

รหัสโครงการ SUT7-706-51-36-31

รายงานการวิจัย

การศึกษาเกี่ยวกับประสิทธิผลของการตกผลึกอะมิโนเอซิดบริสุทธิ์

(A Study into the effectiveness of crystallization for separation of amino acids)

คณะผู้วิจัย

หัวหน้าโครงการ

ศาสตราจารย์ ดร.เอเดรียน ฟลัด

สาขาวิชาวิศวกรรมเคมี

สำนักวิชาวิศวกรรมศาสตร์

มหาวิทยาลัยเทคโนโลยีสุรนารี

ผู้ร่วมวิจัย

นายวิรพงษ์ วันทา นายวัชรกานต์ ศรีมหาพรหม

ได้รับทุนอุดหนุนการวิจัยจากมหาวิทยาลัยเทคโนโลยีสุรนารี ปีงบประมาณ พ.ศ. 2551-2553

ผลงานวิจัยเป็นความรับผิดชอบของหัวหน้าโครงการวิจัยแต่เพียงผู้เดียว

กุมภาพันธ์ 2555

Acknowledgements

The research which has been presented in this report is based on the research of students who have had their study or their research entirely or partially funded by this grant, Mr. Watcharagarn Srimahaprom and Dr. Lek Wantha. Parts of this work have been taken or altered from sections of their Theses.

บทคัดย่อ

งานวิจัยนี้ได้ทำการวัดอัตราการตกผลึกของสาร DL-methionine hydrochloride และวัดความบริสุทธ์ของสารดังกล่าว กับเวลาในการตกผลึก งานวิจัยส่วนนี้ได้รับการตีพิมพ์ในวารสาร Journal of Prince of Songkhla University และ วารสารต่างประเทศ : Journal of Crystal Growth. นอกจากนี้ได้ทำการวัดอัตราการเปลี่ยนสถานะของผลึก 2 ชนิด ของกรดอะมิโนเอซิด ซึ่งงานวิจัยส่วนนี้ได้ตีพิมพ์ในวารสารต่างประเทศอีก 4 ฉบับ

Abstract

The current study has successfully measured the kinetics of the key mechanisms responsible for the preferential crystallization of DL-methionine hydrochloride, and measured the product purity as a function of time for a preferential crystallization of this species. The work has resulted in a published international journal paper (in J. Crystal Growth) as well as a paper accepted for publication in the journal of Prince of Songkhla University. We have also been successful in measurement of the thermodynamic and kinetic mechanisms for the solution mediated phase transformation between two crystalline polymorphs of an amino acid. We have used the racemic amino acid DL-methionine. The results have been very successful in validated the mechanisms, and the work has resulted in several international journal articles.

Contents

Figures

Tables

Chapter I
Introduction

1.1 Background and Significance

Crystallization is a separation and purification process where there is a phase transition of one or more species from an amorphous solid, liquid or gaseous state to a crystalline state. In crystallization from solution a species crystallizes from a liquid mixture, which will occur only if the solute concentration exceeds its solubility. This type of solution is said to be supersaturated. Supersaturation can be obtained by many methods such as cooling, evaporation, vacuum, pressure, and reaction, or a combination of these processes. Evaporative crystallization is one of the most common processes used in industrial crystallizers. It is a process in which the mixture requires heating to achieve a supersaturated state. Crystallization is used in the production of a wide range of materials from bulk commodity chemicals to specialty chemicals and pharmaceuticals.

Amino acids are among the most biologically significant molecules. They are the basic components of all proteins and are therefore essential in human and animal nutrition. The alpha amino acids (those significant in biochemistry) are those in which both the acid group and the amine group are attached to the same carbon, the alpha carbon. A side chain (R) is also attached to this carbon, and the side chain determines the amino acid. The simplest amino acid has the side chain H, and is called glycine. Amino acids (except glycine) are chiral molecules which means that they potentially exist as two different molecules, usually referred to as the D- and L- forms of the molecule. These forms are referred to as enantiomers. These molecules are different (non-interchangeable) molecules but have, in general, the same physical and chemical properties since they are mirror images of each other. The two forms of alanine (the alpha amino acid with a side chain of CH_3) are shown in Figure 1.1 as an example.

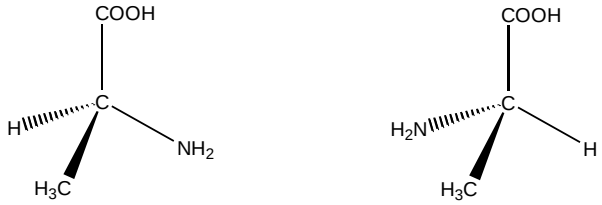

Figure 1.1 L- and D-alanine. The L- form is the one shown on the left.

Under a wide range of conditions the amine group is protonated (NH_3^+) and the carboxylic acid group is deprotonated (COO^-), making the amino acid a zwitterion. There are 21 proteinogenic (used in the production of proteins) amino acids; all of these are alpha amino acids, and they vary only in the side chain (R) involved in the amino acid. Details of these can be found in any organic chemistry or biochemistry text.

If an amino acid is produced by a biological process the necessary form (the L-form) will be produced, however if it is prepared by a traditional chemical synthesis then the product will be an equimolar (racemic) mixture of the desired form and the counter-enantiomer. In some cases the racemic mixture will be suitable for use or sale but in many cases the two enantiomeric forms need to be separated from each other before sale. This may be done by a range of techniques, including chromatography, however crystallization is the most economic method in nearly all cases. There are two methods that may be used that rely on crystallization. The first method is to add a second chiral molecule in a pure enantiomeric form that crystallize with the target molecule as a diastereomer salt. The two forms (for instance D-additive·L-enantiomer and D-additive·D-enantiomer) will have different solubilities, and thus the lower solubility product can be crystallized with very high purity. This method can give a very good separation of the target molecule but is potentially expensive due to the need to use a chiral molecule as an additive, although in many cases the additive can be recovered after separation for the salt containing the target molecule. A second method is to use preferential crystallization which is a kinetic-based separation. This method does not require any additives and hence is potentially cheaper. The trouble with the method is that it can be difficult to apply in practice, and little is known about the optimum operation in such crystallizations. If the process is not applied very well either the product purity or the product yield will be low. One objective of this study is to better understand, and better enable optimization of the operation of preferential crystallization.

A second concern in the crystallization of amino acids (along with a wide range of other products) is that of polymorphism. Polymorphism is a phenomenon where more than one crystal structure is possible for a particular solute, and is a significant problem when the energies of the polymorphs are sufficiently similar that any of several polymorphs may crystallize; the thermodynamically stable polymorph may not be the form initially crystallizing. In fact, when the energies of the polymorphic forms are similar Ostwald's Rule of Stages suggests that the stable polymorph *will not* be the first form to crystallize; note however that this law is not always true. There are two particular cases where the

crystallization of polymorphic forms may lead to problems in processing. The first case is where the stable form is the preferred product, yet the initial crystalline product is a metastable form: in the case it is necessary to wait until the polymorph transformation from the metastable for to the stable form is complete before the product is harvested. The second case is where the metastable polymorph crystallizes first and is also the desired product: in this case the crystallization should be forced to be as quick as possible and the product needs to be harvested before a significant fraction has converted into the stable polymorph. Another objective of the current study is to study the solution mediated transformation of polymorphs of amino acids to better enable design of crystallizers producing the desired polymorphic form of the amino acid.

1.2 Objectives

1.2.1 Objectives of Preferential Crystallization Study

The objectives of this study are the following:

(1) To study the preferential crystallization of an amino acid to better understand preferential crystallization from racemic mixtures of amino acids and enable better design of crystallizers for such applications. In this work we attempt to separate the enantiomers of methionine (D- and L-methionine) from each other. Since methionine is a racemic compound (it crystallizes into a co-crystal of D-methionine and L-methionine from a racemic solution) it is necessary to convert the methionine enantiomers into the methionine hydrochloride (met·HCl) enantiomers since met·HCl is a conglomerate crystal form; this means that it will crystallize into a mechanical mixture of the two pure crystal phases, L-methionine hydrochloride and D-methionine hydrochloride. For this species it is possible to separate the enantiomers into pure compounds using preferential crystallization. This work entails several lower level objectives:

(A) Determination of the atmospheric pressure phase diagram of the system water(1)- L-methionine hydrochloride(2)- D-methionine hydrochloride(3) between 4 and 40ºC, which is the likely temperature range useful for the preferential crystallization. This is essentially just the solubility of the two enantiomers in aqueous solutions which contain both enantiomers.

(B) The next measurement necessary for the design of the preferential crystallization system is the crystal growth rate for the two enantiomeric forms in aqueous solutions containing both enantiomers, and particularly for racemic aqueous solutions since the crystallizations will occur close to the racemic solution composition. An objective of the

current study is to make these measurements. It is also necessary to know the secondary nucleation threshold in order to operate the crystallizer correctly, and also to enable accurate measurement of growth rates; these measurements have also been undertaken in the current study. It is not necessary to measure nucleation rates since preferential crystallizations are seeded batch crystallizations. Nucleation is avoided since the counter-enantiomer may nucleate which would reduce the purity of the product.

(C) The third objective of the work is to determine the feasibility of the preferential crystallization of the species methionine hydrochloride. This is done by conducting small scale methionine hydrochloride preferential crystallization experiments and measuring the change in the composition of the crystalline phase over batch time.

1.2.1 Objectives of Solution Mediated Polymorph Transformation (SMT) Study

The SMT study has the aim to model the SMT of a pair of amino acid polymorphs; in this instance the pair of α- and γ-DL-met were chosen, with γ-DL-met being the stable polymorph (and therefore α-DL-met being the metastable polymorph) in this pair. The modeling is to be based on first principles, i.e. measurement of the kinetic rates and equilibria for the fundamental processes, and then putting these processes together into population balance models for both polymorphs.

(A) The first objective of the SMT study was to measure the basic equilibria and kinetic rate equations that are necessary to describe all of the fundamental processes involved in the SMT. The equilibrium processes involved are primarily the solubilities of the two polymorphic forms, α- and γ-DL-met. The metastable zone width (the concentration driving force required before nucleation can occur) is also an important consideration for the SMT. Kinetic rates necessary are the rates of crystal growth, dissolution, and nucleation for the polymorphic forms of DL-met. Since only γ-DL-met is likely to nucleate under the conditions in the SMT study, then only its nucleation rate is required. Since only the α-form can dissolve under the conditions in the SMT study (since it is the metastable form) then only the dissolution rates of this polymorph are required.

(B) The second objective in the SMT study is a study of the rate of SMT between the two ploymorphs of DL-met. This is performed to determine rates of transfer between the metastable polymorph and the stable polymorph to compliment and test the theoretical modeling, which will be performed later.

1.3 Scope of the Work

1.3.1 Overall scope and assumptions of the preferential crystallization study

The preferential crystallization study has the following scope;

(A) Measurement of the phase diagram with respect to solid-liquid equilibrium for the system D-met·HCl : L-met·HCl : water, at 1 atmosphere and between 5 and 40ºC, which are likely operating conditions for the crystallizations.

(B) Secondary nucleation thresholds of the enantiomers of methionine in both pure enantiomer aqueous solutions and racemic aqueous solutions in order to test the viability of preferential crystallization, and as an aid to crystal growth experiments.

(C) Measurements of average growth rates and growth rate distributions for the enantiomers of met·HCl in pure enantiomer aqueous solutions, and also in aqueous solutions containing a racemic solution of the enantiomers. The former growth rates are likely to be the maximum possible growth rates for the enantiomer, whereas the latter are likely to be similar to those seen in preferential crystallizations where the solution remains close to racemic.

(D) Tests for the ability of preferential crystallization to separate and purify the enantiomers of met·HCl. The tests will be done at low temperatures which should be the most convenient for preferential crystallization.

1.3.2 Overall scope and assumptions of the SMT study

(A) The thermodynamic characteristics of the polymorphs in the study (α- and γ-DL-met) will be characterized using a range of techniques including powder X-Ray diffraction (PXRD) and differential scanning calorimetry (DSC) in order to find the melting points of the enantiomers, the heat of fusion of the enantiomers, and other basic thermodynamic properties. Thermodynamic conclusions for the type of polymorphic system involved will be reached using the results of this study.

(B) The solubility (solid-liquid equilibrium) for the two polymorphs studied C) will be measured at atmospheric pressure and at a range of temperatures suitable for crystallization studies, in this case 5 - 70ºC. This will allow for crystallization studies and SMT studies to be performed, and also allow for confirmation of the type of polymorphic system in evidence for DL-met.

(C) The secondary nucleation threshold will be measured over a similar range of temperatures to the solubility measurements to enable batch crystallization studies to be conducted in a suitable region of the phase diagram, and to assist in modeling of the SMT

behavior. The nucleation rates of the stable polymorph, (γ-DL-met) which is the only polymorph likely to nucleate under the conditions of the SMT study, will be studied between 18 and 35ºC. The narrower range of temperature used here is due to the difficulties of accurate nucleation kinetics at very low temperatures (where rates are extremely small) and at high temperatures (where rates are too large).

(D) Growth and dissolution rates of the two polymorphs will be measured between 10 and 40 ºC, which will allow for models of the growth and dissolution mechanisms to be created. These models are necessary for the model of the SMT behavior in the system.

(E) Measurements of the SMT of the metastable polymorph (α-DL-met) to the stable polymorph (γ-DL-met) will be performed at 25ºC to obtain data to compare the full population balance models to. These experiments will be performed both within and outside of the instantaneous secondary nucleation threshold; this will allow the study of the mechanism of SMT both when the stable form nucleates immediately, and when there is a significant time delay between the seeding of the metastable form and the creation of the stable form nuclei.

1.4 Outcomes of the research

The outcomes of this research are following:

- The operation of preferential crystallization units, which are designed to efficiently separate enantiomers, will be better understood. These units are very significant for industrial production of many chemicals, and in particular for production of many pharmaceuticals. The viability of preferential crystallization from aqueous solution will be tested for a specific example, methionine hydrochloride.

- Better understanding of the phenomena of solution mediated transformation (SMT) in industrial crystallization units. This allows for better, more polymorphically pure product, and better operation of industrial crystallization units in processes where more than one crystalline polymorph is possible.

- The study aids in the design of industrial crystallizers.

- The study has strengthened the knowledge of separation involving crystallization in the process industries in Thailand through development of researchers in the area.

Chapter II

Ternary Phase Diagram of D-Methionine Hydrochloride - L-Methionine Hydrochloride - Water

2.1 Introduction

The synthesis and separation of enantiomers of organic compounds into their pure chiral species has received increasing interest recently, particularly due to their significance in pharmaceuticals (Collins, Sheldrake, and Crosby, 1992; Davankov, 1997). More than 50% of active pharmaceutical ingredients produced are known to be chiral, and hence enantioseparation and recovery of the solid enantiomer from solution are very significant (Lorenz and Seidel-Morgenstern, 2002; Tulashie, Lorenz, Malwade, and Seidel-Morgenstern, 2010). For instance, the market for single enantiomer chiral drugs was approximately 100 billion US$ in 2000 (Maier, Franco, and Lindner, 2001). Thus separation of racemic mixtures into pure enantiomers is essential.

The application of crystallization processes for the separation and purification of enantiomers requires measurements of solid-liquid equilibria (SLE) data (phase diagrams) describing the melting behavior of two enantiomers (the binary melting point phase diagram) and/or the solubility behavior of the system L-enantiomer/D-enantiomer/solvent (the ternary solubility diagram) (Lorenz, Perlberg, Sapoundjiev, Elsner, and Seidel-Morgenstern, 2006). Knowledge of the SLE data can allow for optimization of the separation processes and also for increases in the productivity. This chapter will focus on solubility data. A solubility method based on the classical isothermal method and using the refractive index technique was used in the study.

2.2 Theory

2.2.1 Enantiomers and Racemates

A mixture containing an equal amount of both enantiomers is called *a racemic mixture* except for when a crystal racemate (a repeating unit containing both enantiomers) is formed. A racemic solution has the same boiling point, refractive index, and density in the liquid state as the pure individual enantiomers (Červinka, 1995). There are three different crystal forms into which a racemic solution can crystallize. In the first, the crystalline racemic mixture is a *conglomerate*; it is an equimolar mechanical mixture of single crystals of the two pure enantiomer. Conglomerate forming compounds are very

few, only 5–10 % (Jacques, Collet, and Wilen, 1981). The most common type of crystalline racemic mixture is *racemic compound* or *true racemate*, where the two enantiomers are present in equal amounts in a well-defined arrangement within the crystal lattice (Jacques, Collet and Wilen, 1981; Moss, 1996). Around 90–95 % of racematic mixtures form a racemic compound in the solid phase and thus are more difficult to separate by preferential crystallization (Lorenz, Perlberg, Sapoundjiev, Elsner, and Seidel-Morgenstern, 2006). The third possibility corresponds to the formation of a *racemic solid solution*: the term *pseudoracemate* is used to designate this case, which is rather rare.

2.3.3 Ternary Phase Diagrams for Enantiomeric Systems

Essential basic knowledge for the design and optimization of crystallization processes are the fundamental solid/liquid equilibrium (SLE) data of the corresponding phase diagrams. The essential phase diagrams which have to be known are the binary phase diagram that describes the melting behavior of the two enantiomers, and for crystallization from solution, the ternary phase diagram describing the solubility behavior of the two enantiomers in the presence of a suitable solvent. Binary phase diagram are usually determined by thermal analysis techniques.

Figure 2.1 shows typical solubility phase diagrams for conglomerates, racemic compounds, and solid solution forming systems in an equilateral triangle. These diagrams consist of the three vertexes of the triangle which represent the pure components: the solvent on top, the (+)- and (–)-enantiomers on left and right respectively. The concentration units can be mole or weight fractions of the component represented on the axis. Each point inside the diagram indicates a ternary mixture consisting of all three components. Figure 2.1(a) presents the ternary solubility diagram of conglomerates that consists of (a) a 1-phase region of an unsaturated (clear solution) on the solvent top corner, (b) below the equilibrium conditions which will be contained two 2-phase regions of a saturated solution and crystals of one or two enantiomers, and (c) a 3-phase region under the equilibrium conditions which consists of the saturated solution will be a racemic mixture of the two enantiomers and the crystals will be a mechanical mixture of the two enantiomers.

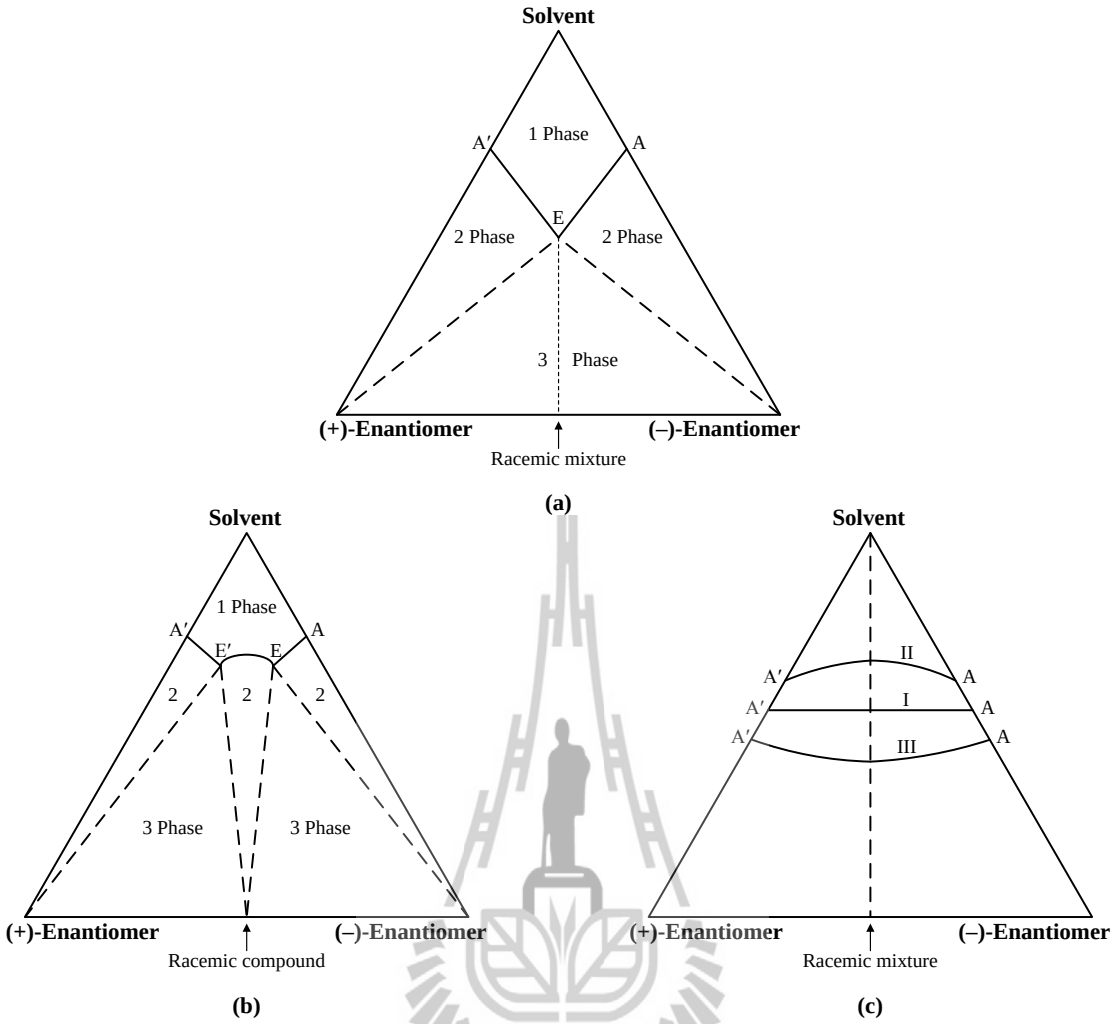

Figure 2.1 Illustration of typical solubility ternary phase diagrams of enantiomeric systems under isothermal conditions: (a) conglomerate, (b) racemic compound, and (c) pseudoracemate.

Figure 2.1(b) presents the majority of enantiomeric systems (up to 90% of the systems found in nature). It presents a solubility ternary phase diagram of a racemic compound, which is more complicated than the conglomerate system due to the existence of two eutectic points (E) in the binary (+)/(–) enantiomeric system. The diagram shows differences to the conglomerate system with respect to (a) the shape of 1-phase region of the undersaturated solution, (b) the shape of the 2-phase regions (crystals of one or two enantiomers and saturated solution), (c) another 2-phase region appears due to the solid phase of the racemic crystals in the saturated solution, and (d) there are two separate 3-phase regions in which the solid phase will be mechanical mixtures of one enantiomer and

the racemic compound, and the saturated solution will be a racemic mixture of the two enantiomers (Lorenz, Perlberg, Sapoundjiev, Elsner, and Seidel-Morgenstern, 2006). The ternary phase diagram of a pseudoracemate is illustrated in Figure 2.1(c). The solubilities of the pure enantiomers are represented by points *A* and *A′*. In the case of type I, the solubility of the pseudoracemate is equal to the enantiomers and the solubility curve is the horizontal line *AÁ*. In the types II and III, the pseudoracemate is more and less soluble than the enantiomers, respectively (Jacques, Collet, and Wilen, 1981).

2.4 Experimental Procedure

2.4.1 Materials

DL-methionine (DL-Met) and L-methionine (L-Met) were purchased from Acros Organics with purity greater than 99% and 98% respectively. Hydrochloric acid 37% (HCl) analytical reagent grade was purchased from Carlo Erba. These two methionine amino acids were reacted to form methionine hydrochloride in the batch crystallizer shown in Figure 2.2, using hydrochloric acid 37% as a reagent. 5.97 g of DL- or 5.97 g of L-Met was dissolved in 10 cm^3 of hydrochloric acid 37% in a 0.5 L glass vessel with a sealed glass lid (to reduce solvent loss) at higher than room temperature until dissolution was complete, and then the solution was kept in a water bath at a constant temperature of 10°C. The solution was agitated by a centrally located four-blade propeller for around 24 hours. The precipitated DL-methionine hydrochloride (DL-Met·HCl) or L-methionine hydrochloride (L-Met·HCl) was collected by filtration with a 110 mm diameter number 42 ashless filter paper (Whatman, US). Solution was filtered through a buchner funnel and aspirator (Eyela model A-3S, Tokyo Rikakikai Company Limited, Japan), and washed with 5 ml of hydrochloric acid 37% at 10°C (Shiraiwa, Miyazaki, Watanabe, and Kurokawa, 1997). Both solid products were dried over silica gel in a desiccator. Deionized water (18.2 MΩ·cm) was used as a solvent in the preparation of all aqueous solutions throughout the experiments.

2.4.2 Determination of the Concentration Calibration Curve of DL-Methionine Hydrochloride

The calibration curve for the concentration of DL-Met·HCl in water was measured at 25°C using an automatic digital refractometer (Model RFM340, Bellingham and Stanley

Limited, UK) with temperature control to within ±0.3°C. The precision of the refractive index determination was ±0.00001 refractive index unit. All solutions were prepared in laboratory glass bottles with screw caps (Schott Duran, Germany) and varying the mass of DL-Met·HCl. The solution samples were removed after 24, 29, 34, and 39 hours and they were filtered through a 0.45 μm cellulose acetate membrane filter in a 47 mm filter holder (Millipore Swinnex Filter Holder, USA) connected to a 20 mL disposable syringe (Nipro Medical Corporation, Thailand). Solutions were analyzed for DL-Met·HCl content by solution concentration measurement and pH values using a RFM340 automatic digital refractometer and pH meter (Model CyberScan pH510, Eutech Instrument Private Company Limited, Singapore), respectively.

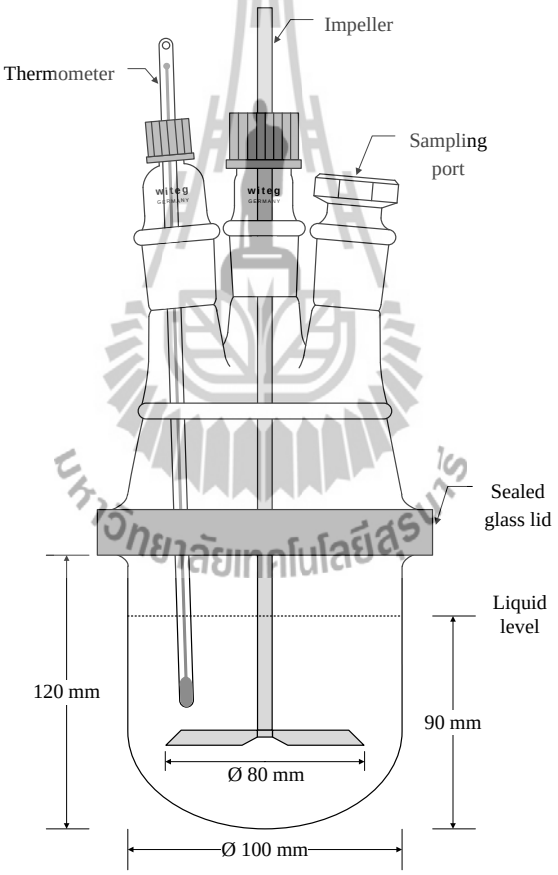

Figure 2.2 The 0.5 litre glass batch crystallizer for preparing the methionine hydrochloride.

2.4.3 Determination of the Solubility of Methionine Hydrochloride in Water System for Pure Enantiomer and Racemic Mixture Compositions

The solubility data of the racemic conglomerate (DL-Met·HCl) and pure methionine hydrochloride (L-/D-Met·HCl) in water were measured at 5, 10, 25, and 40°C by means of the equilibrium solubility method using an RFM340 automatic digital refractometer for analyzing Met·HCl content. 20 ml of deionized water was added into a 100 ml laboratory glass bottle with a screw cap (Schott Duran, Germany) which was placed in a 3 liter beaker on a magnetic stirrer plate. Constant temperature water at either 40, 25, 10, or 5^{o}C (depending on the experimental temperature desired) was circulated through the 3 L beaker to maintain a constant solution temperature. The solubility experiments for DL-Met·HCl were started at 40°C. The solid DL-Met·HCl was added to water in a glass bottle with a screw cap in excess of the saturation condition at 40°C. The solution was stirred with a magnetic stirrer bar at all times for 48 hours, which is enough time to reach equilibrium. Secondly, around 2 ml of solution sample at 40°C was taken to separate the liquid from the solid using a 0.45 μm cellulose acetate membrane filter with a 250 ml filter holder with receiver (Nalgene Labware, USA) connected to an aspirator, through which solution could be filtered within a few seconds at room temperature. Then liquid samples, diluted at a ratio by mass of 1:4 (liquid solution : deionized water) were kept in a water bath at 25°C for an hour. Finally, the concentration of the solution was measured using refractive index at 25°C using a RFM340 automatic digital refractometer. To ensure DL-Met·HCl and L-Met·HCl solution concentrations were at equilibrium, measurements were repeated every hour for about 4 hours to check the concentration was constant. After measurement at 40°C the solution temperature was decreased to 25, 10, and 5°C respectively, and the saturation concentration measured at the new temperatures. The solubility of L-Met·HCl was first determined at 5°C, then 10, 25, and 40°C respectively, using the same methods as used for the DL-Met·HCl solubility experiments.

2.4.4 Determination of the Solubility of Mixtures of Methionine Hydrochloride Enantiomers in Water

A 75% L-Met·HCl and 25% D-Met·HCl enantiomeric mixture was used to study the solubility data for intermediate compositions of the Met·HCl enantiomers in water. This was done by mixing DL-Met·HCl and L-Met·HCl in a 1:1 ratio. This system was also

measured at 5, 10, 25, and 40°C using the same measurement techniques and an experimental procedure similar to those given in sections 2.4.3. The method starts at low temperature, as for L-Met·HCl. The solid amino acids of DL- and L-Met·HCl were added into a 10 g of deionized water in a 100 ml of laboratory glass bottle and screw cap at 1.00 g amounts at each time until it was in excess of the saturation condition at 5°C, and then the concentration measured. This method was repeated at the other saturation temperatures. The solution concentration at each temperature was measured at 25°C using refractive index measured using a RFM340 automatic digital refractometer. This was repeated every hour for about 4 hours to ensure the solubility had been reached.

2.5 Results and Discussion

2.5.1 DL-Methionine Hydrochloride Solubility Calibration Curve

The calibration curve used to obtain DL-Met·HCl concentration at 25°C is shown in Figure 2.3.

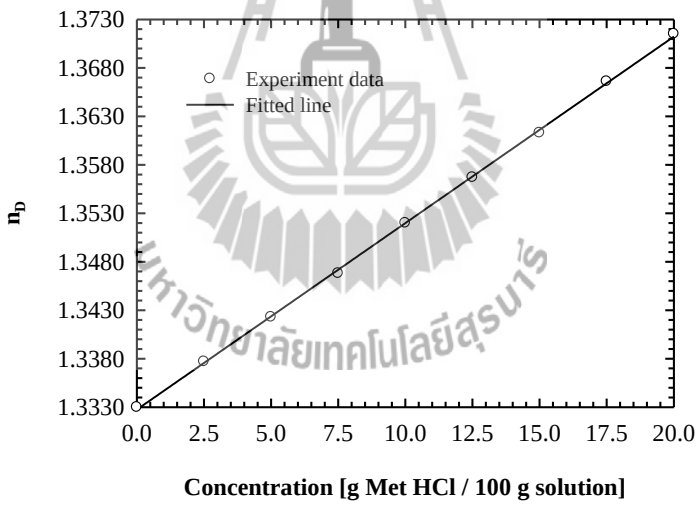

Figure 2.3 Refractive index for the calibration curve of DL-methionine hydrochloride (DL-Met·HCl) in water at 25°C.

2.5.2 Solubility of the Methionine Hydrochloride Species in water

The experimental data for solubilities of the three enantiomeric mixtures in water (Racemic conglomerate, pure enantiomer, and mixture compositions) obtained in this work are summarized in Table 2.1. Solubilities of racemic and pure enantiomeric methionine hydrochloride as a function of temperature are shown in Figure 2.4 and Figure 2.5,

respectively. The solubility of a pure enantiomer of methionine hydrochloride in water is compared with the solubility of the racemic conglomerate mixture in Figure 2.6.

Table 2.1 Average value of solubility results, and standard deviation (2σ) for the racemic conglomerate mixture, pure enantiomer, and 75 : 25 mixture of methionine hydrochloride enantiomers in water at four temperatures.

Temperature (°C)	DL-Met·HCl		L-Met·HCl		75%L- , 25%D-Met·HCl	
	Run	g/100 g H_2O ± 2σ	*Run*	g/100 g H_2O ± 2σ	*Run*	g/100 g H_2O ± 2σ
5	3	262 ± 33	3	168 ± 17	3	129 ± 13
10	3	284 ± 35	3	170 ± 12	3	162 ± 17
25	3	315 ± 10	3	191 ± 12	3	235 ± 5
40	3	387 ± 53	3	224 ± 21	3	284 ± 22

Figure 2.4 and Figure 2.5 shows the relationship between the solubility of DL-Met·HCl in water and L-Met·HCl in water as a function of temperature respectively, where both solubility data show an increasing tendency with increasing temperature. Solid lines (DL-Met·HCl and L-Met·HCl) are best fitted trendlines of both Met·HCl compound solubility data which fitted using a quadratic polynomial equation, with the relationship of the solubility data being

$$C^{*}_{\text{DL-Met·HCl}} = 260.0426 + 1.0216T + 0.0533T^{2} \text{ and}$$

$$C^{*}_{\text{L-Met·HCl}} = 165.2585 + 0.2265T + 0.0311T^{2}$$

where C* represents the solubility concentration in g Met·HCl / 100 g water, and T represents the experimental temperature in degree Celsius. Dashed-dot lines are the solubility relationship that can be observed from data with 95% confidence intervals, which shows a confidence region of DL-Met·HCl and L-Met·HCl solubility data along the solid lines. Long dashed line curves are 95% prediction limits, which shown probability scope of DL-Met·HCl and L-Met·HCl solubility data over the range of experimental temperatures investigated in this study.

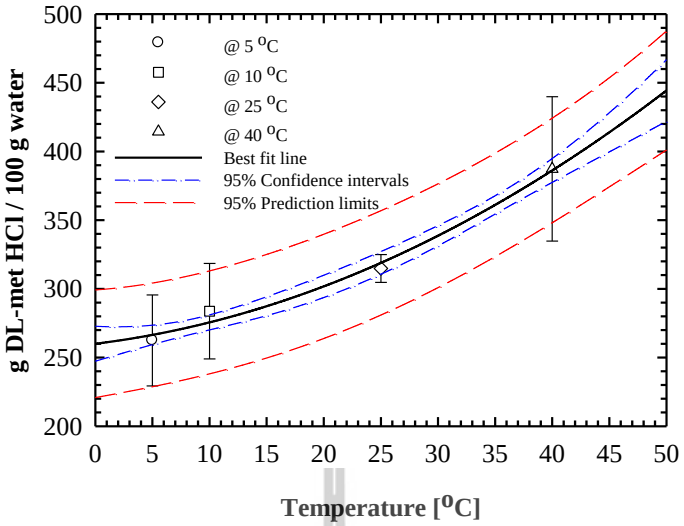

Figure 2.4 Solubility data for the conglomerate DL-methionine hydrochloride (DL-Met·HCl) in water.

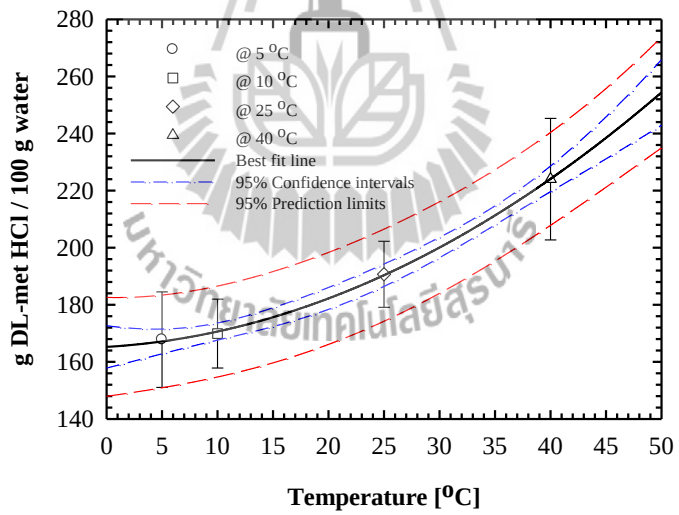

Figure 2.5 Solubility data for L-methionine hydrochloride (L-Met·HCl) in water.

Figure 2.6 shows a comparison between the solubility of the conglomerate form of methionine hydrochloride in water solvent and the racemic form of methionine in water in a temperature range of 0°C to 50°C. This shows that the solubility of DL-Met is lower than the two enantiomers forms (L- and D-Met), but the solubility of DL-Met·HCl form is higher than that of L- and D-Met·HCl which making the conglomerate more stable than the

racemic compound, as theoretically expected (Flood, 2008). Both the solubility of the conglomerate and racemic crystals increased with increasing temperature, and the solubility of the conglomerate of the hydrochloride form of methionine is very much higher than the solubility of the racemate form of methionine.

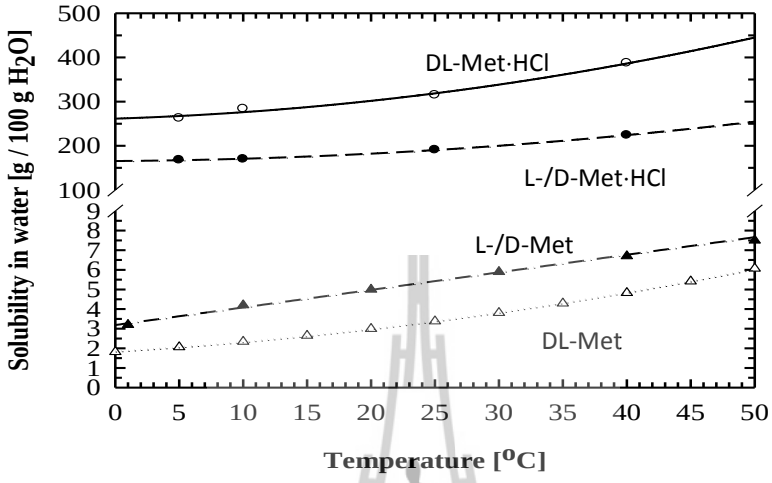

Figure 2.6 Solubility of the (○) conglomerate DL-Met·HCl (from this work) and (●) L-/D-Met·HCl (from this work) in water compared to solubility literature data of (△) DL-Met (replotted from Dalton and Schmidt, 1935) and (▲) L-/D-Met (replotted from Polenske and Lorenz, 2009) in water.

2.5.3 Ternary Solubility Phase Diagram of the Methionine Hydrochloride Enantiomers in Water

The appropriate solubility data for the ternary phase diagram of methionine hydrochloride enantiomers in water are presented in Figure 2.7. 3 runs of experiment in the ternary phase diagram L-Met·HCl + D-Met·HCl + water have been measured giving solubilities at temperature ranges between 5°C and 40°C covering the whole range of enantiomeric compositions.

Figure 2.7 presents the ternary solubility phase equilibria of enantiomeric methionine hydrochloride in water in mole fraction units. The solubility is strongly dependent on temperature with an increase in temperature resulting in a rapid rise in solubility.

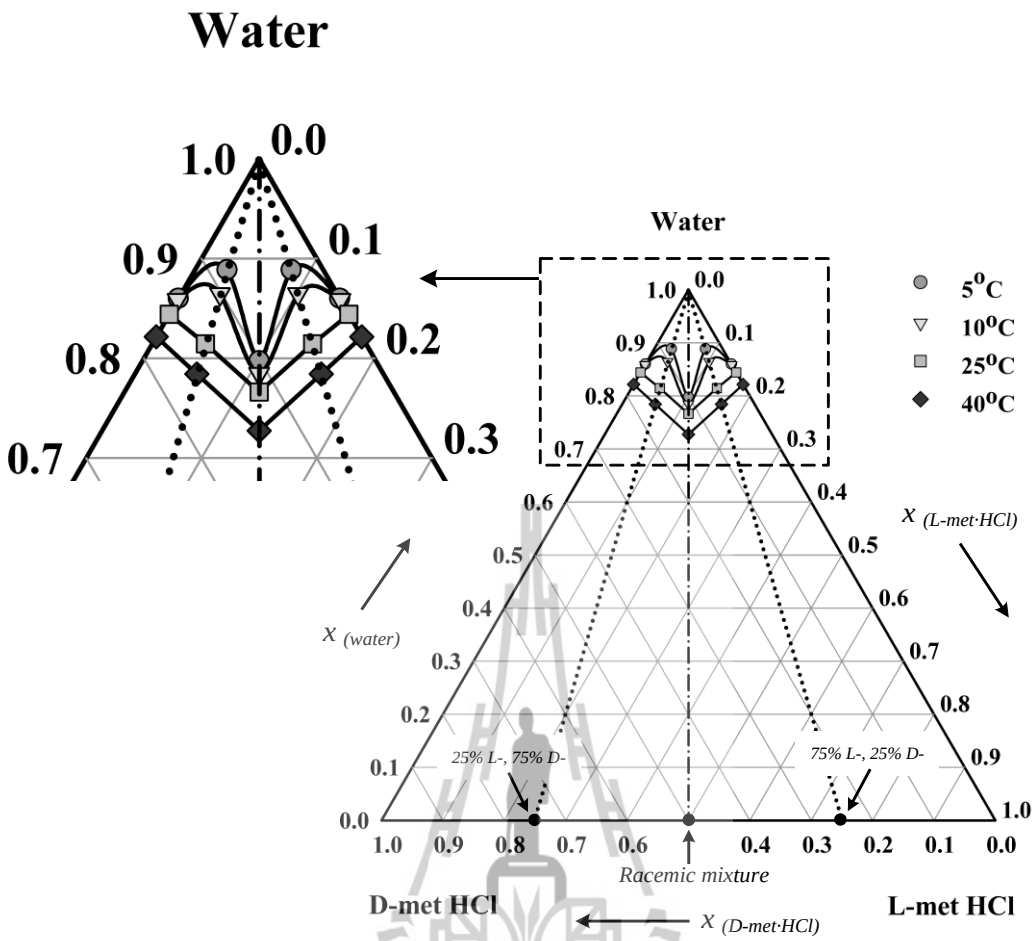

Figure 2.7 Ternary phase diagram for L-methionine hydrochloride (L-Met·HCl) + D-methionine hydrochloride (D-Met·HCl) + water. The phase diagram is shown for isotherms at 5°C, 10°C, 25°C, and 40°C (from top to bottom). The isotherm lines are just guides to the eye.

2.6 Conclusions

This work measured the solubility of the enantiomeric methionine hydrochloride in three forms (racemic mixture, pure enantiomer, and 75% L- + 25% D-Met·HCl mixture) in water over the temperature range of 5°C to 40°C using an isothermal solubility method based on a classical solubility measurement. The ternary solubility phase diagram of L-Met·HCl + D-Met·HCl + water is in accordance with the typical ternary phase diagram for a conglomerate forming species.

2.7 References

Červinka, O. (1995). Enantioselective reactions in organic chemistry. Hertfordshire, England: Ellis Horwood.

Collins, A. N., Sheldrake, G. N., and Crosby, J. (1992). Chirality in industry: The commercial manufacture and applications of optically active compounds. Chichester: John Wiley & Sons.

Dalton, J. B. and Schmidt, C. L. A. (1935). The solubilities of certain amino acids and related compounds in water, the densities of their solutions at twenty-five degrees, and the calculated heats of solution and partial molal volume. II. Journal of Biological Chemistry 109: 241-248.

Davankov, V. A. (1997). Analytical chiral separation methods. Pure and Applied Chemistry 69(7): 1469-1474.

Flood, A. E. (2008). Recent patents on the optical resolution of amino acid enantiomers by crystallization from solution. Recent Patents on Materials Sciences 1: 98-115.

Fujiwara, M., Nagy, Z. K., Chew, J. W., and Braatz, R. D. (2005). First-principles and direct design approaches for the control of pharmaceutical crystallization. Journal of Process Control 15: 493-504.

Jacques, J., Collet, A., and Wilen, S. H. (1981). Enantiomers, racemates, and resolutions. New York: John Wiley & Sons.

Kurosawa, I., Teja, A. S., and Rousseau, R. W. (2005). Solubility measurements in the L-isoleucine + L-valine + water systems at 298 K. Industrial and Engineering Chemistry Research 44: 3284-3288.

Lorenz, H., Perlberg, A., Sapoundjiev, D., Elsner, M. P., and Seidel-Morgenstern, A. (2006). Crystallization of enantiomers. Chemical Engineering and Processing 45: 863-873.

Lorenz, H. and Seidel-Morgenstern, A. (2002). Binary and ternary phase diagrams of two enantiomers in solvent systems. Thermochimica Acta 382: 129-142.

Maier, N. M., Franco, P., and Lindner, W. (2001). Separation of enantiomers: Needs, challenges, perspectives. Journal of Chromatography A 906(1-2): 3-33.

Moss, G. P. (1996). Basic terminology of stereochemistry (IUPAC Recommendations 1996). Pure and Applied Chemistry 68(12): 2193-2222.

Polenske, D. and Lorenz, H. (2009). Solubility and metastable zone width of the methionine enantiomers and their mixtures in water. Journal of Chemical and Engineering Data 54: 2277-2280.

Shiraiwa, T., Miyazaki, H., Watanabe, T., and Kurokawa, H. (1997). Optical resolution by preferential crystallization of DL-methionine hydrochloride. Chirality 9: 48-51.

Tulashie, S. K., Lorenz, H., Malwade, C. R., and Seidel-Morgenstern, A. (2010). Ternary solubility phase diagrams of mandelic acid and N-methylephedrine in chiral solvents with different carbon chain lengths. Crystal Growth & Design 10: 4023-4029.

Chapter III

Crystal growth rates and growth rate distribution for L-methionine hydrochloride single crystals in supersaturated solutions of methionine hydrochloride

3.1 Abstract

In this chapter, basic properties of the crystallization of the L-enantiomer of DL-Methionine Hydrochloride (DL-Met·HCl) were studied in order to assist in understanding and modeling of the preferential crystallization of DL-Met·HCl. In this work, the primary nucleation threshold (PNT), secondary nucleation threshold (SNT), and the crystal growth rate distribution of L-Methionine Hydrochloride (L-Met·HCl) crystals in methionine hydrochloride (Met·HCl) solutions were studied. The experimental data in this chapter will help to efficiently operate preferential crystallization of L-Met·HCl, and allow the optimization of the resolution time and operating condition of the preferential crystallization. The primary and secondary nucleation threshold of DL-Methionine Hydrochloride (DL-Met·HCl) in aqueous solution were measured based on induction time measurements for relative supersaturations (σ) of 0.01, 0.02, 0.03, 0.04, and 0.05, which were performed isothermally at 10°C in an agitated glass batch crystallizer with a constant temperature jacket. The method used gives a satisfactory experimental result for the PNT and SNT of D- or L-Met·HCl in aqueous solution. The results show that the induction time dependence on the relative supersaturation is an increase in induction time as the relative supersaturation decreases for both nucleation thresholds. The crystal growth rate and growth rate distribution (GRD) of L-Met·HCl single crystal in DL- and L-Met·HCl solutions at 10°C were determined by means of a small-cell crystallizer connected to a stereomicroscope with a digital camera, using relative supersaturations (σ) of 0.005, 0.01, and 0.02. The experimental data shows that the crystal growth rate depends strongly on the relative supersaturation of the Met·HCl solution, especially from pure L-Met·HCl supersaturated solution, and there is a wide crystal growth rate distribution from both types of supersaturated solution. The results will be used to determine the experimental conditions of the preferential crystallization of DL-Met·HCl.

3.2 Introduction

Nucleation is one of the most important factors to control in industrial crystallization processes, since it controls crystal product quality aspects, such as the kind

of solid state, crystal size distributions, and purity of the product crystals. In most cases, knowledge of nucleation will be used to control the crystal growth processes. Nucleation is the formation of new crystals suspended in the solution. Crystal growth is the growth of these crystals to larger sizes through deposition of solute from the solution. Both nucleation and crystal growth require a supersaturated environment in order to occur. Crystal nucleation has been classified as primary nucleation when it takes place without the help of seed crystals and as secondary nucleation when seed crystals are present in a supersaturated solution (Shimizu, Tsukamoto, Horita, and Tadaki, 1984). Although in industrial crystallization, the secondary nucleation mechanism is considered to be the more important for controlling the size distribution of product crystals, it has not been well understood, and in most cases nucleation is necessarily avoided or minimized in crystallization processes since it is difficult to control and gives a bad product size distribution. If possible, the operation is usually undertaken in the metastable zone or the nucleation threshold, and crystallization is initiated through the addition of seed crystals, thus avoiding large amounts of nucleation (Garside and Davey, 1980; Larson, 1981). Over the last several decades, nucleation in solution has been the subject of extensive study. The results obtained are numerous and provide insight into a particular aspect the process, but usually without showing its interrelation with other such aspects or its significance for nucleation in general.

The crystal growth process is a process in which molecules or ions (or atoms) are incorporated into the crystal lattice. Although growth of crystals in a supersaturated solution is a complex process and involves a large number of steps, it usual can be described by two successive mechanisms, that are mass transfer (by diffusion or convection) of solute molecules from the bulk solution to the crystal surface, and integration of solute molecules into the surface (a reaction step) (Randolph and Larson, 1988). A technique to better understand nucleation of molecules involves the measurement of nucleation time by the induction time technique. The induction time, t_{ind}, refers to the time that elapses after the creation of supersaturation in solution until a new phase is detected, and is an experimentally accessible quantity (Kuldipkumar, Kwon, and Zhang, 2007). The induction time thus measured allows for a connection to be made between nucleation theory and experimental investigation.

This work aims to systematically study the primary and secondary nucleation threshold of DL-Met·HCl in aqueous solution at various relative supersaturation by means

of induction time by the turbidity technique, and also determine the growth rate distribution of L-Met·HCl crystals in DL- and L-Met·HCl solution with different relative supersaturation using a small-cell crystallizer. The work will elucidate the relationship between induction time and the relative supersaturation of DL-Met·HCl solution and also the relationship between the relative supersaturation and the crystal growth rate. The solubility data of DL- and L-Met·HCl from the previous chapter will be used here to calculate the amount of Met·HCl species required in the aqueous solutions for a particular supersaturation value. This should improve understanding of the kinetics of nucleation and crystal growth of L-Met·HCl crystals in Met·HCl solutions. Moreover, important crystallization parameters will be estimated in order to predict the suitable operating condition for preferential crystallization of DL-Met·HCl and including the purity of desired crystal form.

3.3 Theory

Solution crystallization is considered to be a two-step process: nucleation, or the birth of crystals, and crystal growth, which involves subsequent growth of existing crystals. One of requirements for bulk crystallization is that the solution should exceed its solubility at a given temperature, i.e., the solution should be supersaturated (Chattopadhyay, Erdemir, Evans, Ilavsky, Amenitsch, Segre, and Myerson, 2005).

3.3.1 Fundamentals of Nucleation

Nucleation is a key step in the crystallization process, since it can control crystal product quality aspects such as the kind of solid state, size, crystal size distribution (CSD) and purity of product particles. There is a statistical process of a new phase (nuclei) in a supersaturated existing phase (Funakoshi and Matsuoka, 2008; Jiang and ter Horst, 2011). Nucleation from solution can be divided into two distinct types, which are primary nucleation and secondary nucleation. Primary nucleation is the formation of nuclei that are able to grow without presence of any crystalline matter, whereas secondary nucleation requires the presence of crystals.

Primary nucleation is used to describe nucleation when the nucleation mechanism does not depend on the presence of suspended solute crystals in the solution. This is further divided into homogeneous mechanisms (where there are no external nucleation sites available, as could be caused by the walls of the vessel, dust particles, crystals or solids of other solute etc.) and heterogeneous mechanisms (where there is the presence of foreign

suspended dust particles or apparatus surfaces). Secondary nucleation is more significant than primary nucleation, and can be called the main source of the nuclei occurring in the majority of industrial crystallization units, since the vessel is run continuously having solute crystals inside. Secondary nucleation can occur by contact nucleation, shear nucleation, fracture nucleation, attrition nuclei, and needle breeding. Randolph and Larson (1988) also propose an initial breeding nucleation mechanism, which is the important nucleation source of nuclei in a seeded system.

3.3.2 Induction Time Measurement

The induction time is usually defined as time needed for the first nucleation events to be detected in a solution kept at a constant supercooling (Kubota, 2008). It should be related to the metastable zone width (MSZW, ΔT_m), because the induction time and the MSZW are closely related with crystal nucleation kinetics. The MSZW has been defined as the supercooling at which the first crystals appear when the solution is cooled at a constant rate. The induction time is defined as the time elapsed from attainment of a constant supersaturation to the appearance of first crystals. The induction time is affected by several parameters such as the initial supersaturation, temperature, pH, agitation speed, and the presence of additives/impurities (Kuldipkumar, Kwon, and Zhang, 2007).

3.3.3 Methods to Study Crystal Growth

Crystal growth rate (typically termed G and expressed in terms of micrometers per time) is a function of supersaturation, with higher supersaturations resulting in higher growth rates (Barrett, Smith, Worlitschek, Bracken, O'Sullivan, and O'Grady, 2005). In general, the crystal growth mechanism is determined by measuring the growth rates and then fitting the measured rates to the expressions describing the different crystal growth mechanisms (Kuldipkumar, Kwon, and Zhang, 2007). Crystal growth rate data can be obtained by a number of experimental methods. Two main groups can be differentiated. The first group comprises methods that measure the growth of a single crystal to obtain the needed data, e.g. recirculation apparatus or flow apparatus (Myerson and Ginde, 2002), or microscopic cells (Rodriguez-Hornedo and Murphy, 1999). Single crystal growth techniques, which can focus on growth rates of individual faces, are predominantly used for fundamental studies relating to growth mechanisms. The second group of methods involves the growth of a suspension of crystals, e.g. in agitated vessels (Mullin, 2001), or fluidized beds (Phillips and Epstein, 2004). Measurements made on populations of crystals

are useful for determining overall mass transfer rates and for observing size-dependent growth or growth rate dispersion.

3.4 Experimental Procedure

3.4.1 Materials

DL- and L-Met·HCl compounds were prepared by the method shown in Section 2.4.1. The solutions of DL- and L-Met·HCl in water were prepared in the relative supersaturation (σ) range between 0.005 and 0.05 (for experiments at 10°C) at a high temperature, around 45-50°C for about 30 to 40 minutes to ensure that no nuclei remained. The L-Met·HCl crystals were prepared as seed crystals used in the secondary nucleation threshold experiments and also as single crystals in crystal growth rate experiments. The size of L-Met·HCl crystals used in the experiments was 100-600 μm.

3.4.2 Determination the Induction Times (t_{ind}) of Primary and Secondary Nucleation Threshold for DL-Methionine Hydrochloride in Water Solvent System

The apparatus for measuring induction time consists of a 400 ml glass batch crystallizer with a jacket with a four-blade impeller and an overhead stirrer. The glass batch crystallizer with jacket was connected to circulating water at constant temperature from a cooling bath, and the solution temperature in the glass batch crystallizer was confirmed using a thermometer, and the temperature was controlled to within ±0.5°C. The solution was agitated at 350 rpm at all times by a four-blade impeller connected to an overhead stirrer. The primary and secondary nucleation threshold experiments were modified from the method of Srisa-nga et al. and using the relationship between nucleation and induction time at a constant supercooling to determine both nucleation thresholds (Srisa-nga, Flood, and White, 2006; Kubota, 2010). 20 g of supersaturation concentration of DL-Met·HCl in water was prepared at 0.01, 0.02, 0.03, 0.04, and 0.05 of relative supersaturation (σ) based on solubility data, which was dissolved at 45-50°C for about 30 to 40 minutes in a 100 ml laboratory glass bottles and screw caps (Schott Duran, Germany) to ensure a homogenized solution, and that no nuclei existed in the solution. The clear solution was cooled down instantaneously to 10±0.5°C by pouring the solution (at 45-50°C) from a glass bottle to the glass batch crystallizer which was kept at constantly temperature (10°C).

The solution was held at 10°C until the induction time (t_{ind}) was reached. For SNT experiments, approximately 0.2 g of L-Met·HCl as seed crystals was added into the

solution before the start of the experiment, since secondary nucleation is induced by the added seeds. Nucleation was observed by eye at particular time intervals, with nucleation being indicated by clouding due to the very fine nuclei particles. The timing was stopped when the solution began to change from a clear solution to become a turbid solution which was clearly visible. Primary nucleation threshold experiments were the same as the secondary nucleation threshold experiments, but the primary nucleation threshold experiment does not have seed crystals added before the start of the induction time measurement. The same steps were repeated for 0.01, 0.02, 0.03, 0.04, and 0.05 relative supersaturation (σ) of DL-Met·HCl solution, for both primary and secondary nucleation threshold measurements.

3.4.3 Determination the Mean Crystal Growth Rates and Growth Rate Distribution of L-Methionine Hydrochloride Single Crystal in DL- and L-Methionine Hydrochloride Supersaturated Solution by Small-Cell Crystallizer

The mean crystal growth rate and growth rate distribution measurement of L-Met·HCl single crystals in DL-Met·HCl and L-Met·HCl supersaturated solutions were studied via a small-cell crystallizer with a stereomicroscope. The small-cell crystallizer was constructed of stainless steel and was of circular cross-section with an internal diameter of 60 mm. The supersaturated solution was held in the upper section (the growth section) which had a capacity of about 70 ml, and contains a glass cover slip upon which the single crystals grow. The lower section, which is separated from the growth section with an acrylic plate, is used for circulation of constant temperature water at 10°C from a water bath maintained to within ±0.5°C, to hold the liquid solution in growth section at 10°C, which was checked the solution temperature in growth section by thermometer. Circular cover glasses (acrylic plates) were used to separate the supersaturated solution and water, and also used to close the solution chamber at the upper section and circulating water chamber at the lower section from the atmosphere, sealing being achieved with O-rings (Garside, and Larson, 1978; Lowe, Ogden, McKinnon, and Parkinson, 2002).

50 ml of DL- and L-Met·HCl solutions were prepared at 0.005, 0.01, and 0.02 of relative supersaturation (σ) (with reference to the saturation concentration at 10°C) at a high temperature (45-50°C), which is above the solubility temperature, to ensure that the solution is homogeneous and no ghost nuclei remained in the solution. Nine L-Met·HCl single crystals were attached on the 20×20 mm glass cover slip. The size of L-Met·HCl

seed crystals used in the experiment were 200-500 μm. The L-Met·HCl single crystal glass cover slip was taken into the solution chamber (upper section) in the small-cell crystallizer in which Met·HCl supersaturated solutions were maintained at 10±0.5°C by constant temperature water circulation. The crystal size is monitored directly throughout the experiment using a stereomicroscope (model SZX9, Olympus Optical Co., Ltd., Japan) equipped with a microscope digital camera (model DP11 type C-mount CCD camera plus hand switch, Olympus Optical Co., Ltd., Japan) connected to a computer to operate the software for image processing and analysis (Olympus Camedia Master version 1.11). The crystal size was measured by the changes in the dimensions of single crystals by measuring the scale calibrated by a standard wire at magnification 6.3x, 16x, 25x, and 64x. In this experiment, the two visible dimensions of the single crystals can be observed, the width and the length, but measurement of the crystal size to determine the growth rate is done only on crystal side that significantly changes and is most easily measured, that is the width of the single crystals.

3.5 Results and Discussion

3.5.1 Effect of Supersaturated Solution of DL-Methionine Hydrochloride to the Induction Time for Primary and Secondary Nucleation Threshold Measurement

The effect of various supersaturations on the induction time of the measured PNT and SNT of DL-Met·HCl solution are shown in Figure 3.1 and Figure 3.2, respectively. These figures show the time dependence of the relative supersaturation of the PNT and SNT, with the induction time increasing as the relative supersaturation of the PNT and SNT decreases. The induction time of the SNT is less than the induction time of the PNT because of the influence of L-Met·HCl seed crystals on the SNT experiment, which induced the birth of new crystals in the supersaturated solution.

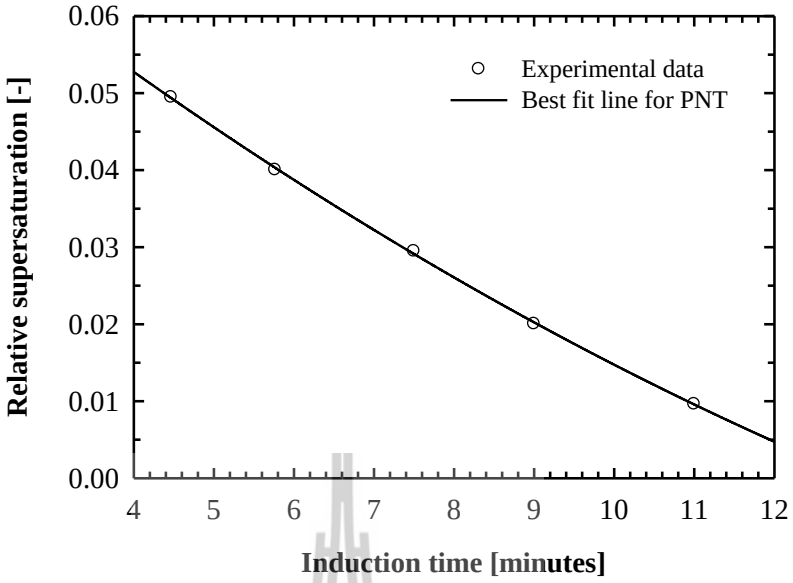

Figure 3.1 Effect of supersaturation on the induction time for the primary nucleation threshold (PNT) of DL-Met·HCl solution.

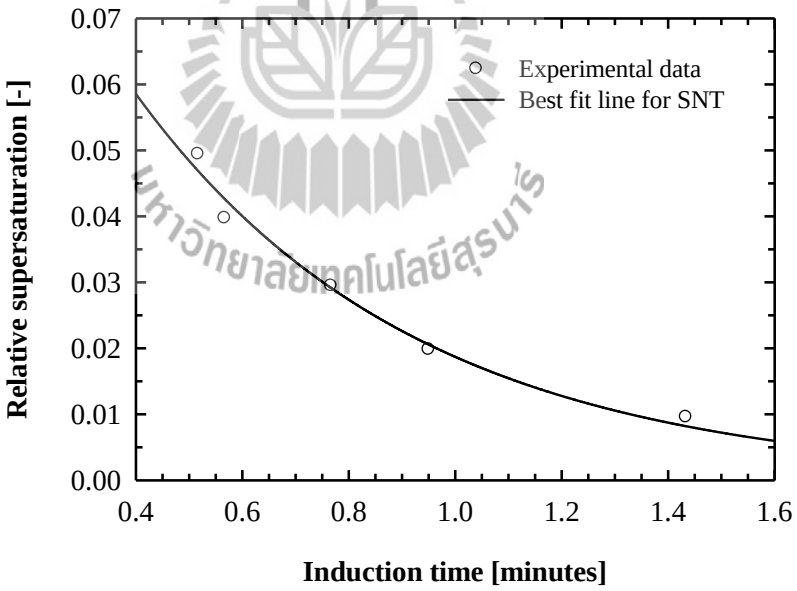

Figure 3.2 Effect of supersaturation on the induction time for the secondary nucleation threshold (SNT) of DL-Met·HCl solution.

3.5.2 Growth Rate Distribution of L-Met·HCl Single Crystal in DL- and L-Met·HCl Solution at Various Relative Supersaturation

The crystal growth rates of L-Met·HCl single crystals in Met·HCl solution were studied with a small-cell crystallizer, and the size of crystals were observed using a stereomicroscope equipped with a digital camera. Nine parent crystals of L-Met·HCl were attached with latex glue onto a glass cover slip within the supersaturated solution of Met·HCl at 10°C; the temperature was maintained by circulating constant temperature water from a cooling bath. The size of the crystals was observed and recorded by a stereomicroscope with a digital camera, with each parent crystal being recorded every 10 minutes until 50 minutes cycle times were completed.

For L-Met·HCl parent crystals in DL-Met·HCl supersaturated solution ($\sigma = 0.005$) at 10°C, the parent crystals grew in the length direction significantly more than in the width direction, and also small particle which were attached on the single crystal at the initial time (which could not be seen with the naked eye). They were grown mostly sideways on the parent crystals, which made the large parent crystal unable to grow as expected. The growth of small crystals on the surface of the parent crystal was quite disorganized, like a group of small needle-like crystals grown from the surface of parent crystal. Due to the imperfection of the crystal surface the growth is therefore not the growth of single crystals. For L-Met·HCl parent crystal in L-Met·HCl supersaturated solution ($\sigma = 0.005$) at 10°C the parent crystals were grown in both directions (the width and the length) which is the same with growth in DL-Met·HCl supersaturated solution, and also the small crystals were grown on the sideways of parent crystal also well. This may be because of small crystals attached to the single crystal at the initial time, as in the growth in DL-Met·HCl supersbaturated solution.

However, the growth of small crystals on the parent crystals in L-Met·HCl supersaturated solutions was more orderly and resulted in more perfect shape more than the growth in DL-Met·HCl supersaturated solutions. The L-Met·HCl small crystal in L-Met·HCl supersaturated solution grow significantly in both visible directions (the width and the length), but the L-Met·HCl small crystal in DL-Met·HCl supersaturated solution grow significantly in the length direction only. This may be due to the DL-Met·HCl supersaturated solution has the D-Met·HCl acting as a growth inhibitor of L-Met·HCl. This modifies the growth behavior of the L-Met·HCl crystals in the DL-Met·HCl supersaturated solutions.

After recording all crystal growth data completely with the stereomicroscope; 9 L-Met·HCl parent crystals grown in DL-Met·HCl supersaturated solutions ($\sigma = 0.005$, $\sigma =$

0.01, σ = 0.02) at 10°C; 9 L-Met·HCl parent crystals grown in L-Met·HCl supersaturated solution (σ = 0.005, σ = 0.01, σ = 0.02) at 10°C, the crystal size was measured by comparison with a scale calibrated by a standard wire at various magnifications, e.g. 6.3x, 16x, 25x, and 40x. The standard wire was calibrated by measuring the diameter of the wire on a photomicrograph of the desired magnification, and then printing the photomicrograph at a size equal to that of the crystal image. After measurement of the size of standard wire using a ruler and comparison to the actual size of the standard wire (which was known via measurement with a micrometer), the actual dimensions of the crystal could be calculated.

The growth is not only of single crystals as expected, so that the small crystal particles growing on top of each parent crystal were also selected to determine the growth data, as shown in Figure 3.3. This shows a L-Met·HCl parent crystal in L-Met·HCl supersaturated solution (σ = 0.005) at 10°C using a magnification of 25x, with a sample time of 50 minutes. The 4 crystal particles shown were selected to represent growth data of this condition by measurement of the growth only in the direction of the width of the crystals. The reason that only the growth of the width was chosen is that the length direction is out of the photomicrograph frame for some conditions. Thus, it was not possible to measure the growth of the length of the crystals continuously over time. The small crystals attached to each parent crystal were measured at various sampling times. From the data obtained we can plot the relationship between the sampling time (minutes) and the width of the crystals (μm) as shown in Figure 3.4. From Figure 3.4, the graph shows the straight line of 4 crystals at various time; where all data represents the growth data of L-Met·HCl in L-Met·HCl solution at 10°C. After this, the slope of each graph line can be determined which will give the crystal growth rate (μm/min) of the crystals. There are 9 positions of the L-Met·HCl single crystal in each experimental condition. There are 6 experimental conditions as mentioned above.

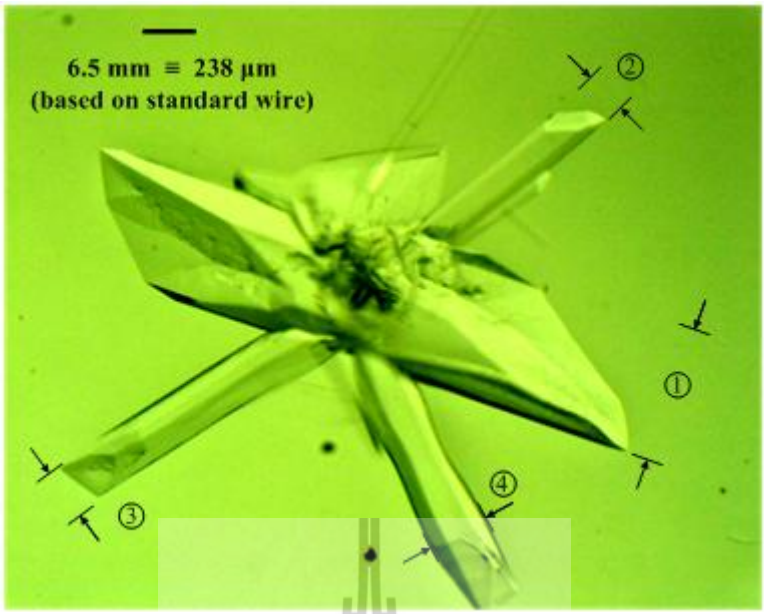

Figure 3.3 An example of measuring the size of L-Met·HCl crystals in L-Met·HCl solution (σ = 0.005) at 10°C,sample time 50 minutes, and magnification 25x.

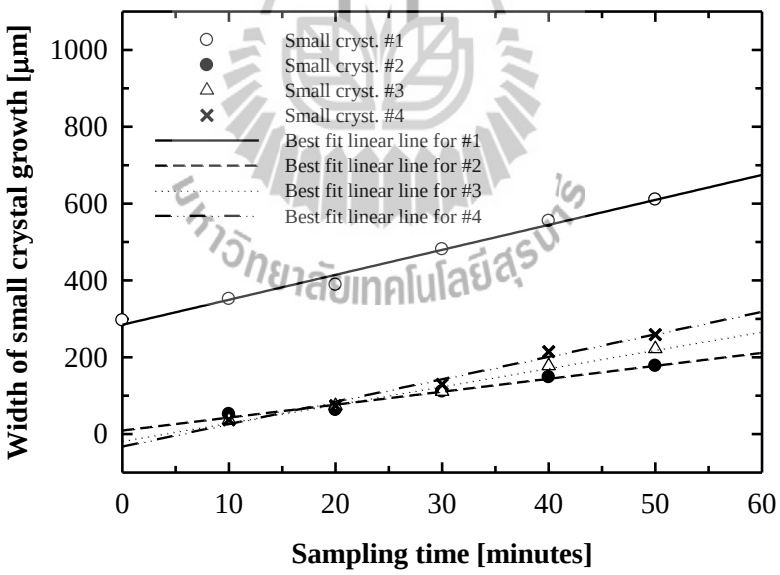

Figure 3.4 The results of crystal growth; relationship between sampling time (minutes) versus the width of crystal (µm) at the following conditions : L-Met·HCl parent crystal in L-Met·HCl supersaturated solution (σ = 0.005), 10°C, magnification 25x.

There are 321 total data for the crystal growth rate, and these data represent 54 parent crystals at 6 experimental conditions. These data can be plotted to show the relationship between growth rate (μm/min) versus number of crystals (#), which represents the probability distribution of L-Met·HCl single crystal growth rates in both DL- and L-Met·HCl supersaturated solutions. This can also be plotted using the empirical representation of a growth rate data distribution, using a log-normal distribution. The log-normal growth rate distribution is simply a normal distribution in terms of log*G*. Thus the log-normal distribution expressed as a density function is distributed about values of log*G* and is given as (Randolph and Larson, 1988):

$$f(\log G) = [(2\pi)^{1/2} \log \sigma']^{-1} \times exp\left[-\left(\frac{\log G/\overline{G'}}{\sqrt{2} \log \sigma'} \right)^2 \right] \quad (3.1)$$

where *G* is the independent growth rate variable, $\overline{G'}$ is the geometric mean growth rate, and σ' is the geometric standard deviation.

The results in L-Met·HCl supersaturated solution (Figure 3.6) show a much wider range than the growth rate distribution in DL-Met·HCl supersaturated solution (Figure 3.5). This is because, L-Met·HCl single crystal can be grown in the L-Met·HCl supersaturated solution better than the growth in the DL-Met·HCl supersaturated solution, which there have the effect of D-Met·HCl acting as a growth inhibitor of L-Met·HCl. Hence, the growth rate distribution of L-Met·HCl single crystal in L-Met·HCl supersaturated solution are more than growth rate distribution of L-Met·HCl single crystal in DL-Met·HCl supersaturated solution. The mean growth rate ($\overline{G}$) is a function of the relative supersaturation (σ) value, nevertheless. The mean growth rate of L-Met·HCl single crystal in both Met·HCl supersaturated solution at σ = 0.01 were reduced from the expected values as shown in Figure 3.7. The L-Met·HCl solution concentration has constant value throughout the experiments also.

3.5.3 Mean Growth Rate of L-Met·HCl Single Crystal in DL- and L-Met·HCl Supersaturated Solution

The predicted growth rate distributions were calculated using the crystal growth rate of each crystal. The growth rate distributions of each experimental condition can be determined as shown in Figure 3.5 and Figure 3.6, assuming log-normal distributions. This

allows for analysis of the mean growth rate for each condition, shown in Table 3.1, and also the geometric standard deviation.

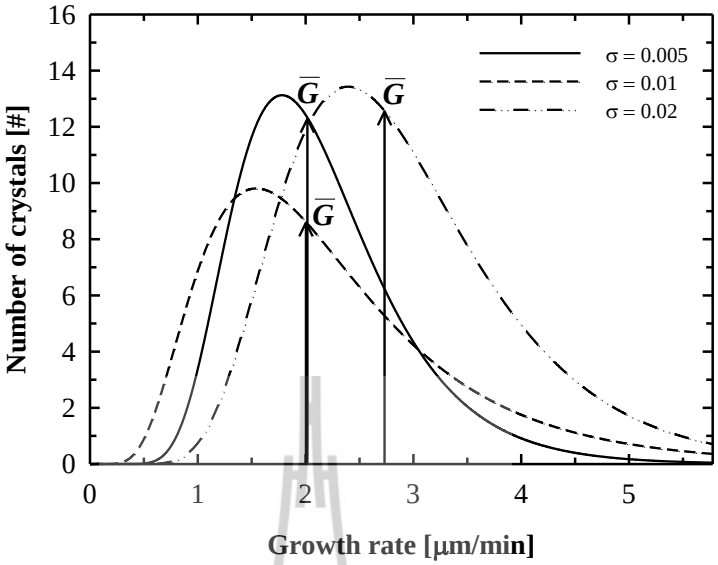

Figure 3.5 Mean growth rates of L-Met·HCl parent crystals in DL-Met·HCl supersaturated solution from a small-cell crystallizer run at 10°C with different relative supersaturations.

Table 3.1 Mean growth rates of L-Met·HCl single crystal in DL- and L-Met·HCl supersaturated solution from the small-cell crystallizer run at 10°C with different relative supersaturations.

DL-Met·HCl supersaturated solution		L-Met·HCl supersaturated solution	
Relative Supersaturation (σ)	Mean growth rate ($\overline{G}$; μm/min)	Relative Supersaturation (σ)	Mean growth rate ($\overline{G}$; μm/min)
0.005	2.0141	0.005	5.1269
0.01	2.0077	0.01	3.5817
0.02	2.7319	0.02	18.4250

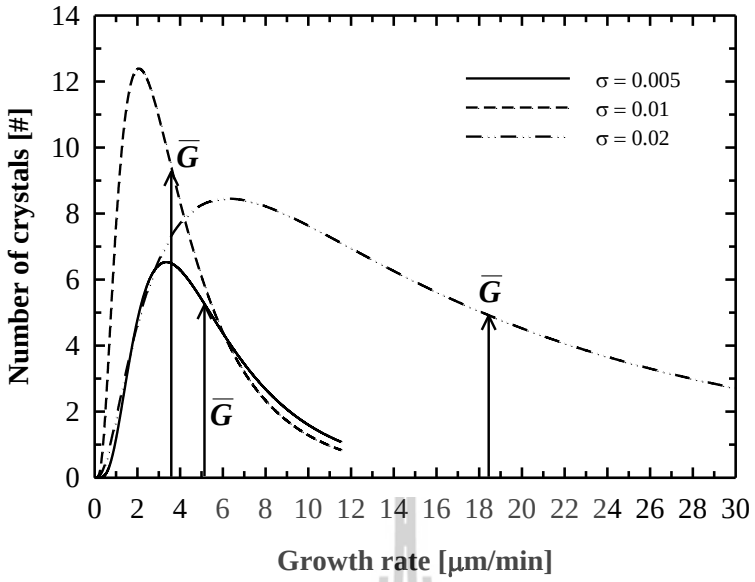

Figure 3.6 Mean growth rates of L-Met·HCl parent crystals in L-Met·HCl supersaturated solution at 10°C with different relative supersaturations.

Figures 3.5 and 3.6 show the growth rate distributions of L-Met·HCl single crystals in DL- and L-Met·HCl supersaturated solution. From Figure 3.5, it can be seen that the growth rate distribution of L-Met·HCl single crystal in DL-Met·HCl solution of three relative supersaturation were quite similar values, and also the mean growth rate did not differ much. Figure 3.6 shows the growth rate distribution in L-Met·HCl supersaturated solutions, and it is seen that at $\sigma = 0.02$ the growth rate distribution was quite wide compared to solutions at $\sigma = 0.005$ and $\sigma = 0.01$. However, by comparison between growth rate distribution in DL-Met·HCl supersaturated solution and growth rate distribution in L-Met·HCl supersaturated solution, it was found that the growth rate distribution of L-Met·HCl parent crystal in L-Met·HCl supersaturated solution was wider than the growth rate distribution of L-Met·HCl parent crystal in DL-Met·HCl supersaturated solution. The mean growth rates of each relative supersaturation are shown in Table 3.1. Data from Table 3.1 can be plotted to show the relationship between relative supersaturation versus mean growth rate (μm/min) as shown in Figure 3.7. It can be seen that, at constant temperature, the mean growth rates increase with increasing relative supersaturation, and also growth rate of L-Met·HCl single crystal in L-Met·HCl supersaturated solution is faster than growth rate in DL-Met·HCl supersaturated solution.

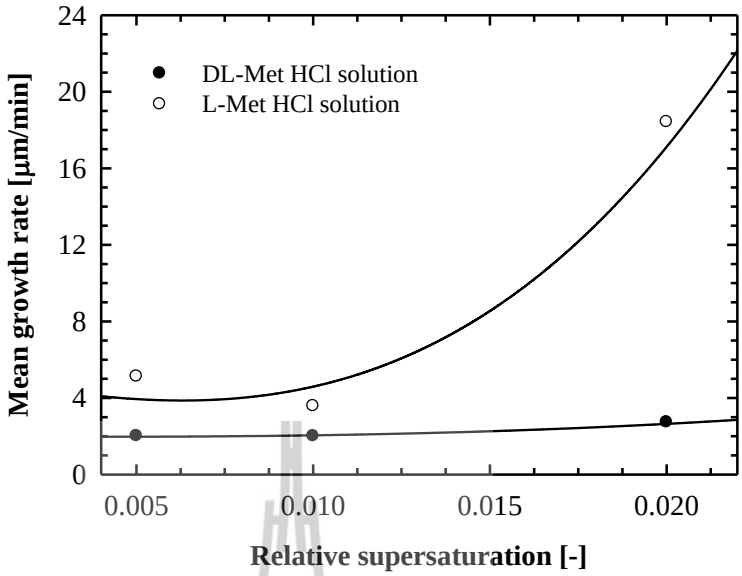

Figure 3.7 Mean growth rates for L-Met·HCl parent crystals as a function of relative supersaturation of DL- and L-Met·HCl supersaturated solution at 10°C.

3.6 Conclusions

The primary and secondary nucleation threshold measurements of DL-Met·HCl solution were determined with a modified method using the relationship between nucleation time and induction time measurement at a constant supercooling (10°C) in a glass batch crystallizer with a closed jacket system. There is simple method for measurement of the nucleation threshold by using observation of the change of the turbidity of the solutions with the naked eye, which allows measurements of the primary and secondary nucleation thresholds of DL-Met·HCl solution. From the experimental results, it can be indicated that, the induction time dependence of the relative supersaturation of the primary and secondary nucleation thresholds. The induction time increases as the relative supersaturation of primary and secondary nucleation threshold decreases, and also the induction time of the secondary nucleation threshold is less than the induction time of the primary nucleation threshold because of the influence of L-Met·HCl seed crystals. The rate of secondary nucleation is increased by the added seeds resulting in the nucleation threshold for secondary nucleation being larger than that for primary nucleation.

The growth rate distribution and the mean growth rate of L-Met·HCl crystals in Met·HCl supersaturated solution were studied to optimize the operation of the preferential

crystallization of DL-Met·HCl. These data were determined in a small-cell crystallizer and the stereomicroscope with the digital camera at constant 10°C in a stagnant solution. From the experimental results, it is found that the parent crystals are not a single crystal due to the imperfection of the crystal surface. They have the small crystal particles attached on the surface of a parent crystal at the initial time. They were grown mostly on sideways on the parent crystal, and were grown very well in both directions (the width and the length) into the supersaturated solution with different relative supersaturation (σ). Nevertheless, the growth of L-Met·HCl parent crystals in L-Met·HCl supersaturated solution are grown orderly and perfect shape rather than the growth of L-Met·HCl parent crystals in DL-Met·HCl supersaturated solution. The latter grow in a disorganized way, like the group of needle small crystals grown from the surface of parent crystal. This is because of the concentration of L-Met·HCl form in both supersaturated solutions is not equal. The L-Met·HCl supersaturated solution has pure L-Met·HCl substance only (100% L-Met·HCl), but the DL-Met·HCl supersaturated solution has L-Met·HCl substance and D-Met·HCl substance in each a half (50% L-Met·HCl + 50% D-Met·HCl). Furthermore, the DL-Met·HCl supersaturated solution has the effect of D-Met·HCl acting as a growth inhibitor of L-Met·HCl, that makes the growth of L-Met·HCl parent crystals in DL-Met·HCl supersaturated solution does not good shape as it should over time and also were grown more slowly than the growth into pure L-Met·HCl supersaturated solution.

The crystal growth rate depends strongly on the relative supersaturation (especially from pure L-Met·HCl supersaturated solutions), with the crystal growth rate at $\sigma = 0.02 > \sigma = 0.01 > \sigma = 0.005$. Also there is a wide crystal growth rate distribution from both types of supersaturated solution. Hence, the mean growth rate ($\overline{G}$) of L-Met·HCl single crystals in L-Met·HCl supersaturated solution is larger than the mean growth rate from DL-Met·HCl supersaturated solution.

The results of primary and secondary nucleation threshold, and also the growth rate and growth rate distribution of L-Met·HCl single crystals in Met·HCl supersaturated solution can lead to the efficient operation of preferential crystallization experiments in the next chapter. We need to know the suitable resolution time on seeding, including L-Met·HCl crystals growth behavior on preferential crystallization for high purity of the crystal (the desired crystal form) and cost effectiveness in manufacturing.

3.7 References

Barrett, P., Smith, B., Worlitschek, J., Bracken, V., O'Sullivan, B., and O'Grady, D. (2005). A review of the use of process analytical technology for the understanding and optimization of production batch crystallization processes. Organic Process Research & Development 9(3): 348-355.

Chattopadhyay, S., Erdemir, D., Evans, J. M. B., Ilavsky, J., Amenitsch, H., Segre, C. U., and Myerson, A. S. (2005). SAXS study of the nucleation of glycine crystals from a supersaturated solution. Crystal Growth & Design 5(2): 523-527.

Funakoshi, K. and Matsuoka, M. (2008). Primary nucleation of threonine crystals from ternary solutions. Crystal Growth & Design 8(5): 1754-1759.

Garside, J. and Davey, R. J. (1980). Invited review secondary contact nucleation: Kinetics, growth and scale-up. Chemical Engineering Communications 4: 393-424.

Garside, J. and Larson, M. A. (1978). Direct observation of secondary nuclei production. Journal of Crystal Growth 43: 694-704.

Jiang, S. and ter Horst, J. H. (2011). Crystal nucleation rates from probability distributions of induction times. Crystal Growth & Design 11: 256-261.

Kubota, N. (2008). A new interpretation of metastable zone widths measured for unseeded solutions. Journal of Crystal Growth 310: 629-634.

Kubota, N. (2010). A unified interpretation of metastable zone widths and induction times measured for seeded solutions. Journal of Crystal Growth 312: 548-554.

Kuldipkumar, A., Kwon, G. S., and Zhang, G. G. Z. (2007). Determining the growth mechanism of tolazamide by induction time measurement. Crystal Growth & Design 7(2): 234-242.

Larson, M. A. (1981). Secondary nucleation: An analysis. Chemical Engineering Communications 12: 161-169.

Lowe, J., Ogdena, M., McKinnon, A., and Parkinson, G. (2002). Crystal growth of sodium oxalate from aqueous solution. Journal of Crystal Growth 237-239: 408-413.

Mullin, J. W. (2001). Crystallization. Oxford: Butterworth-Heinemann.

Myerson, A. S. and Ginde, R. (2002). Crystals, crystal growth, and nucleation. In A. S. Myerson (Ed.), Handbook of industrial crystallization (pp. 33-65). Boston: Butterworth-Heinemann.

Phillips, V. R. and Epstein, N. (2004). Growth of nickel sulfate in a laboratory-scale fluidized-bed crystallizer. AIChE Journal 20(4): 678-687.

Randolph, A. D. and Larson, M. A. (1988). Theory of particulate processes: Analysis and techniques of continuous crystallization. California: Academic Press.

Rodríguez-Hornedo, N. and Murphy, D. (1999). Significance of controlling crystallization mechanisms and kinetics in pharmaceutical systems. Journal of Pharmaceutical Sciences 88(7): 651-660.

Shimizu, K., Tsukamoto, K., Horita, J., and Tadaki, T. (1984). Origin of secondary nucleation as revealed by isotopic labelling. Journal of Crystal Growth 69: 623-626.

Srisa-nga, S., Flood, A. E., and White, E. T. (2006). The secondary nucleation threshold and crystal growth of α-glucose monohydrate in aqueous solution. Crystal Growth & Design 6(3): 795-801.

Chapter IV

The Purification of L-Methionine Hydrochloride via Optical Resolution of DL-Methionine Hydrochloride by Preferential Crystallization

4.1 Abstract

Solubility data, the ternary phase diagram of met·HCl (which is a conglomerate forming system), the primary and secondary nucleation threshold, mean growth rate, and growth rate distributions (GRD) have already been discussed. This chapter deals with the resolution of DL-met·HCl using preferential crystallization to separate the desired enantiomer (L-met·HCl) from the racemic solution (DL-met·HCl). The study is an attempt to improve the efficiency and economics of the optical resolution of methionine. All experiments were operated in a batch crystallizer at low temperature and various relative supersaturations of L-met·HCl. L-met·HCl crystals were used as a homochiral seed to induce the desired enantiomer (L-met·HCl) from DL-met·HCl aqueous solution. The optical activity measurement via polarimetry was used to evaluate the percent purity of the product crystal (w.r.t. L-met·HCl). The results reveal the purity of L-met·HCl crystal decreased rapidly to the equilibrium value over time, due to the influence of the nucleation threshold of the counter enantiomer being small. Using preferential crystallization to separate the enantiomers of met·HCl from an aqueous solution to obtain a high purity product appears to be very difficult; this study cannot separate the desired enantiomer to close to 100% purity. A process in which a tailor-made additive agent is used to inhibit the primary nucleation of the undesired enantiomer (D-met·HCl) may enable the optical resolution from aqueous solution to be more effective.

4.2 Introduction

The chiral nature of drugs is a major concern in the pharmaceutical industry, since the two molecules in a pair of enantiomers have different pharmacological activities. Only one possible form of two enantiomers can be found in chiral drugs and other chiral molecules from natural sources, and also by semi-synthesis. A mixture of both enantiomers is obtained from total synthesis. The pure enantiomers of chiral molecules can be developed commercially by two alternative approaches, that are (i) enantioselective synthesis of the desired enantiomer, or (ii) separation of both isomers from a racemic

mixture. The separation is focused on the target molecule or on one of its chemical precursors obtained from the ordinary synthetic procedures. Both operation methods have advantages and disadvantages. Crystallization is basically a separation technique that is used to separate the desirable substances from impurities or from by-products that come from secondary reactions in their synthesis. Crystallization can also separate the pure enantiomers from a racemate or an enantiomerically enriched sample (Jacques, Collet, and Wilen, 1981; Bayley and Vaidya, 1992; Wood, 1997).

Resolution by crystallization includes direct crystallization (preferential crystallization or spontaneous resolution) (Coquerel, 2007) and diastereomeric crystallization (classical resolution) (Kozma, 2001). Preferential crystallization (or resolution by entrainment) is an attractive technology to separate racemic mixtures of the group of conglomerate forming systems into their pure enantiomers, due to the advantages of obtaining directly a solid product and economic considerations. It is an effective and comparatively cheap technology for the production of pure enantiomers at different scale. However, the direct crystallization of pure enantiomers from racemic solutions is limited to conglomerates (5–10% of all chiral systems). Unfortunately, the major part of the chiral substances belongs to the racemic compound forming systems (Lorenz, Polenske, and Seidel-Morgenstern, 2006). Preferential crystallization is based on the selective crystallization of one species out of a slightly supersaturated solution of a racemic mixture. The supersaturated binary mixture is induced with pure crystals of one of the enantiomers, and only the crystals of the same kind of enantiomer are allowed to grow selectively for a certain period of time before the counter species nucleates (Nohira and Sakai, 2004; Polenske, Lorenz, and Seidel-Morgenstern, 2009). Moreover, crystallization is often used in combination with other enantioselective techniques, such as enantioselective synthesis, enzymatic kinetic resolution or simulated moving bed (SMB) chromatography (Collins, Sheldrake, and Crosby, 1997; Blehaut and Nicoud, 1998; Seebach, Hoffmann, Sting, Kinkel, Schulte, and Küsters, 1998).

This work aims to study the optimum mechanism of preferential crystallization to separate the pure enantiomer of L-met·HCl from a racemic solution of DL-met·HCl to gain the maximum percentage purity of the product crystals from the enriched solution. There is also a study of the viability of the preferential crystallization of L-met·HCl in aqueous solution of DL-met·HCl at various relative supersaturations. The process design is based on the knowledge of solid-liquid equilibrium (SLE), nucleation and growth rate kinetics to

define the optimum operating parameters, such as crystallization temperature, resolution time, and initial supersaturation. Moreover, the study was performed in an attempt to improve the efficiency and economics of the optical resolution of methionine. In the following section the liquid phase and product crystal analysis using polarimetry and refractometry is described.

4.3 Theory

4.3.1 Principle of Preferential Crystallization

Preferential crystallization is one of the most successful processes to resolve many racemates in conglomerate forming systems into the pure enantiomers (Gou, Lorenz, and Seidel-Morgenstern, 2011). Enantiomers are substances with identical physical and chemical properties, but different metabolic effects. The principle of a kinetically controlled preferential crystallization processcan be illustrated in a ternary phase diagram as shown in Figure 4.1. The corners of the diagram represent the pure solvent and two pure enantiomers (D-enantiomer and L-enantiomer). The crystallization starts from a saturated solution at temperature $T_{cryst}+\Delta T$. It is rapidly cooled down to the crystallization temperature T_{cryst} within the metastable zone. The solution becomes supersaturated but nuclei do not appear in the solution (as no spontaneous primary nucleation will occur). Point A represents the initial mixture of two enantiomers and a solvent. The separation process can be well processed using an enantiomeric excess, but it is not strictly necessary. If the crystallizer is seeded with seeds of both enantiomers (D-enantiomer and L-enantiomer) at point A, the two types of crystal will start to grow and also induce the secondary nucleation, as the two enantiomers are being produced simultaneously. The process will eventually end at point E, which represents the equilibrium point for the temperature T_{cryst}. In the equilibrium state, the liquid phase will have a racemic composition (point E) and the solid phase will consist of a mixture of crystals of both enantiomers (Elsner, Menéndez, Muslera, and Seidel-Morgenstern, 2005). However, the aforementioned process is not an example of enantioselective preferential crystallization.

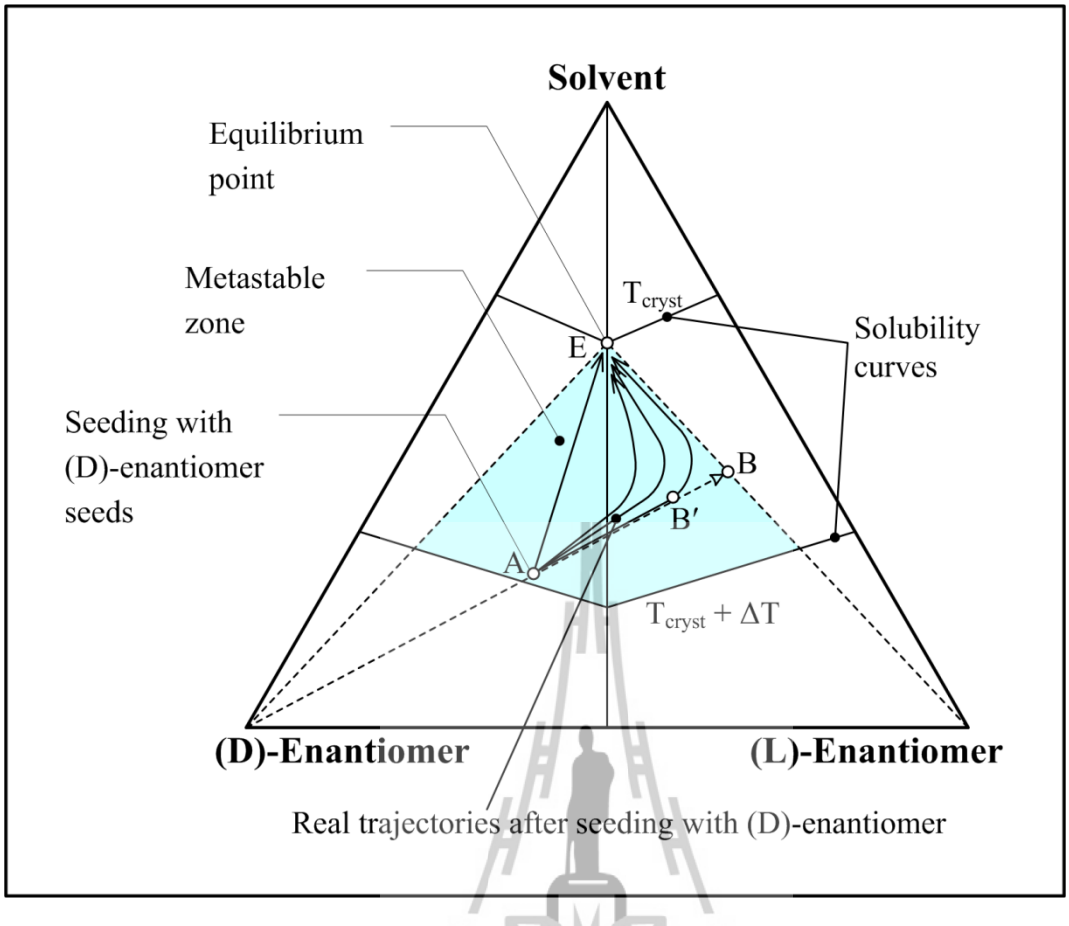

Figure 4.1 Illustration of the principle of preferential crystallization for conglomerate forming system in ternary phase diagram (Qamar, Angelov, Elsner, Ashfaq, Seidel-Morgenstern, and Warnecke, 2009).

In other cases, the composition in liquid phase does not move directly to point E when the crystallizer is seeded with the seeds of pure enantiomer only (in this case the D-enantiomer) at point A. The D-enantiomer at point A begins to crystallize and also the liquid phase composition tends towards point B which is due to the increased mass of D-enantiomer crystal reducing the concentration of the D-enantiomer in solution. This methodology can be used to produce the crystals of just one of the enantiomers by preferential crystallization. However, the spontaneous crystallization of unseeded L-enantiomer is observed after going through a certain period of the experiment. Eventually, the crystallization process is operated along a new trajectory and also reaches to the equilibrium at point E. Therefore, the designed preferential crystallization process must be stopped at point B′ (as an example) before significant nucleation of the unseeded L-enantiomer occurs (Angelov, Raisch, Elsner, and Seidel-Morgenstern, 2008).

4.3.2 Optical Activity Measurement

Polarimetry is one technique in the chiroptical methods that are used in the analysis of optically active compounds, which also include optical rotator dispersion (ORD) and circular dichroism (CD); these are the traditional optical activity measurement techniques (Spencer, Edmonds, Rauh, and Carrabba, 1994; Schreier, Bernreuther, and Huffer, 1995). Optical activity is the ability of a chiral molecule to rotate the plane of polarization of plane-polarized light. Thus, a chiral compound rotates the plane of polarization. The magnitude of the optical rotation (observed rotation; α) in degrees, is measured by a second polarizing filter (called the analyzing polarizer). If the beam has been rotated in a clockwise direction it is called dextrorotatory, (*d*), and the optical rotation is assigned a positive value (+). Conversely, if the beam has been rotated in a counterclockwise direction it is called levorotatory, (*l*), and the optical rotation is assigned a negative value (–) (Carey, 2003; Bruice, 2004).

The nature of a solution of optically active compound was described by introducing the specific rotation of substance. Specific rotation is a physical property of a substance, just like its melting point, boiling point, density, and solubility. The specific rotation is the number of degrees of rotation of the polarized light caused by a solution of 1.0 g of compound/ml of solution in a polarimeter tube 1.0 dm long at specified temperature and wavelength (Bruice, 2004). A recording the specific rotation must be identified with the temperature and wavelength, since the specific rotation depends on the temperature and wavelength also. Each optically active compound has a constant characteristic specific rotation that can be calculated from the observed rotation (optical rotation) obtained in the laboratory by the Biot's law which is given as (Carey, 2003):

$$[\alpha]_{\lambda}^{T} = \frac{100 \times \alpha}{c \times l} \qquad (4.1)$$

where $[\alpha]_{\lambda}^{T}$ is the specific rotation. The conventional unit of specific rotation is degree milliliters per decimeter gram [(°)·ml·dm^{-1}·g^{-1}] but scientific literature uses just degrees (°) (Mohrig, Hammond, and Schatz, 2010). *T* is temperature in degrees Celsius (°C) and λ is the wavelength of the incident light (when the sodium D-line is commonly used for this purpose, λ = 589 nm, λ is indicated as D), respectively, as superscript and subscript. *c* is the concentration of the sample in grams per 100 ml of solution, and *l* is the length of the

polarimeter tube in decimeters (dm). α is a optical rotation (observed rotation) of chiral compound in degrees.

4.4 Experimental Procedure

4.4.1 Materials

DL- and L-met·HCl compounds were prepared similarly to the method in section 2.4.1, Chapter II. Approximately 40 g of total supersaturated solution of DL-met·HCl in water for one sample was prepared at 0.005 and 0.01 relative supersaturation (σ) based on the equilibrium concentration of DL-met·HCl at 10°C. These were prepared by dissolving DL-met·HCl in a heating bath at 40°C until the solution is homogeneous and no nuclei remained. All supersaturated solutions were prepared in 100 ml laboratory glass bottles with screw caps (Schott Duran, Germany), and were maintained at 40°C in a heating bath before starting the experiment. The preferential crystallization temperature is 10°C with temperature control to within ±0.5°C. L-met·HCl crystals were prepared as seed crystals for use to induce the desired product form in the preferential crystallization of DL-met·HCl aqueous solution. Seed crystals were not sieved in this experiment.

4.4.2 Preferential Crystallization of DL-met·HCl Aqueous Solution

In this experiment, a 100 ml beaker (Schott Duran, Germany) was used asa seeded batch crystallizer for preferential crystallization of DL-met·HCl aqueous solution. Supersaturated solutions of DL-met·HCl in water were prepared by dissolution at 40°C until the solution is homogeneous, then the solution was quickly cooled down to 10°C in less than 3 minutes by another cooling bath, to avoid the secondary nucleation in the solution. The DL-met·HCl aqueous solution was maintained at the crystallization temperature within ±0.5°C, which was checked using a mercury thermometer. At the same time, the initial solution concentration at 10±0.5°C was measured to verify the accuracy of the concentration before the start of the experiment using an automatic digital refractometer (Model RFM340, Bellingham and Stanley Ltd.). Approximately 1.00 g of L-met·HCl seed crystals was added to the DL-met·HCl aqueous solution at the start of the experimentfor inducing the crystallization, with experimental resolution times of 2, 5, 8, and 10 minutes. The suspension in the seeded batch crystallizer was agitated by a centrally located, four-blade impeller driven by an overhead stirrer. A constant crystallization temperature was maintained by placing the crystallizer inside a constant temperature water bath.

After the resolution time is reached, at least 4 ml of the suspension was sampled at 10°C and was filtered rapidly through a 61 μm wire mesh sieve for the 2 minute resolution time, and a 104 μm wire mesh sieve for 5, 8, and 10 minute resolution time for separating the solids (the desired product) from the liquid (the undesired product), using a 250 ml filter holder with receiver (Nalgene Labware, USA) connected to an aspirator (Eyela model A-3S, Tokyo): the solution could be filtered within a few minutes at lower than 20°C controlled room temperature. Both solid and liquid contents were weighed on an electronic balance (Sartorius model BP221S, USA) to determine the suspension density of DL-met·HCl. Simultaneously, the concentration of the liquid product was measured for monitoring changes in the concentration using a RFM340 automatic digital refractometer. The solid product was dried in a desiccator over silica gel for 2 or 3 weeks before the measurement of the optical rotation.

4.4.3 Optical Activity of L-met·HCl by Polarimetry

For the preferential crystallization step, the experimental products are the solid content (desired product) and the liquid content after the filtration is complete. The solid product was dried in a desiccator over silica gel for 2 to 3 weeks, and was weighed everyday on an electronic balance, to measure the changes of solid weight until the weight of solid was relatively stable. Between 2.00 g to 5.00 g of solid content was dissolved into distilled water at room temperature to obtain 15.0 ml or 20.0 mlof total aqueous solution; solutions were prepared in a graduated cylinder so that the concentration of the samples was exactly known. All solid solutions were stored in 50 ml laboratory glass bottles and screw caps, which were keptat constant temperature (25°C) in a water bath for one hour. For accurate concentration determination, the solution concentration was measured by a refractive index method using a RFM340 automatic digital refractometer before starting the optical activity. The optical rotations of solid solutions at various the resolution times were determined by polarimetry in a polarimeter (Model P20, Bellingham and Stanley Ltd.) at room temperature (controlled to approximately 25°C by an air conditioner).

The optical rotations (observed rotation) of solutions containing the solids were used to calculate the specific rotation $[\alpha]_{\lambda}^{T}$ of the met·HCl sample, to analyze the percent purity of L-met·HCl in the met·HCl sample after the preferential crystallization is completed. The magnitude of the observed rotation for a particular compound depends on its concentration, the length of the sample tube, the temperature, the solvent, and the wavelength of the light used (Brown, 2000).

4.5 Results and Discussion

4.5.1 The Suspension Density of DL-met·HCl Aqueous Solution during Preferential Crystallization

The preferential crystallization experiments were performed in an isothermal batch process, called seeded isothermal preferential crystallization (SIPC). The experimental results of preferential crystallization of DL-met·HCl aqueous solution at 10°C in two relative supersaturation values ($\sigma = 0.005$ and $\sigma = 0.01$) and four resolution times (t = 2, 5, 8, and 10 minutes) were determined. The preferential crystallization experiments were repeated at each experimental condition at least 4 times to confirm the experimental results were reproducible.

The actual amount of DL-met·HCl used, which is based on the solubility data of DL-met·HCl at 10°C, and also the total amount of DL-met·HCl solution used in each batch experiment were known. The DL-met·HCl solution concentration was measured to check the stability of the solution concentration throughout the experiment in both the initial time and the end time of the crystallization cycle, which was measured by the refractive index method at 25°C using an automatic digital refractometer. When the preferential crystallization was completed, the solid product and the liquid product were separated by filtration and weighed to determine the suspension density (M_T). The suspension density is the primary parameter that indicates the tendency of the quantity of crystal growth in a crystallization process.

The results from the experiments are plotted for the suspension density (g crystal/g solution) versus resolution time (minutes) as shown in Figure 4.2 and Figure 4.3.

The suspension density data were plotted using a scatter plot with multiple error bars (2 standard deviations) and the suspension density curves were fitted using an exponential rise to maximum, 3 parameters, fitted by SigmaPlot® version 11.0.

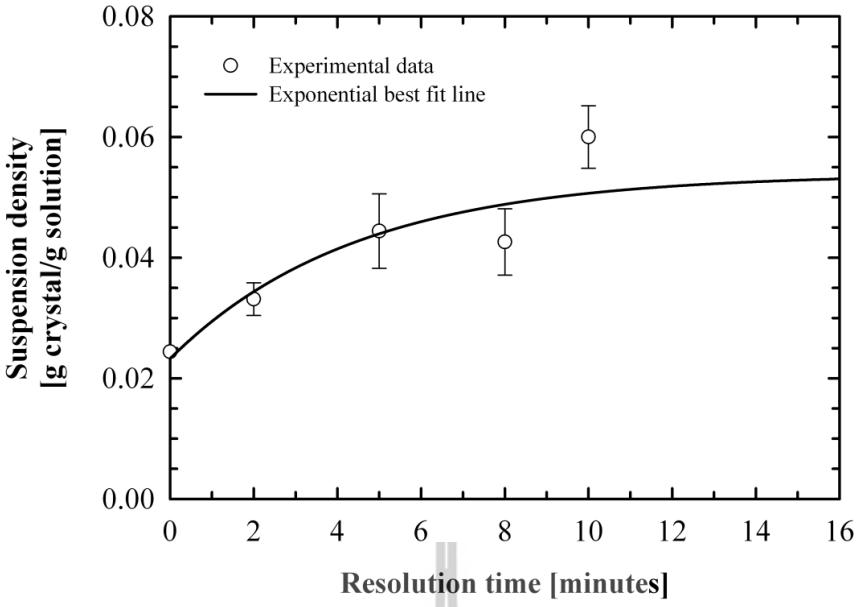

Figure 4.2 Suspension density results for preferential crystallization of DL-met·HCl (σ = 0.005).

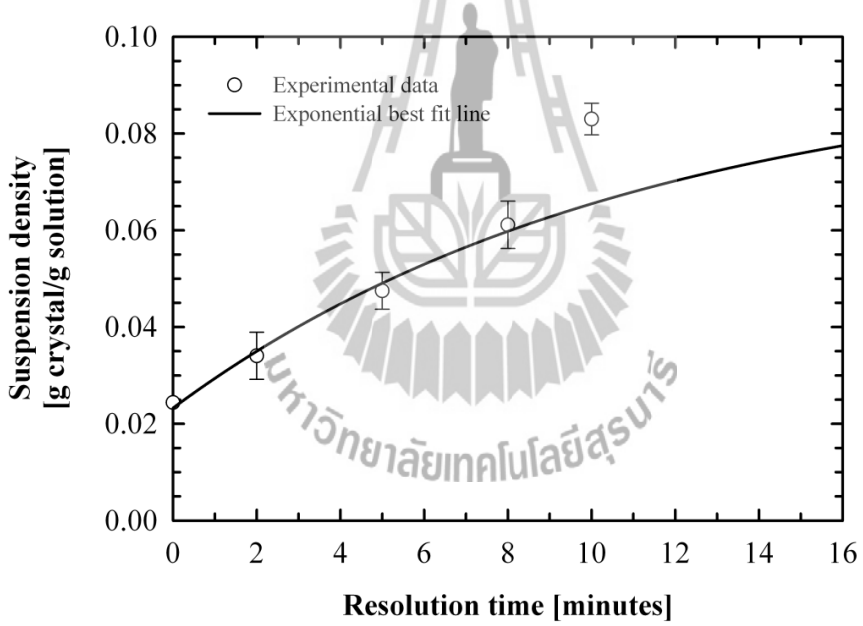

Figure 4.3 Suspension density results for preferential crystallization of DL-met·HCl (σ = 0.01).

These graphs show the tendency of the crystal growth during the preferential crystallization of DL-met·HCl aqueous solution, where the suspension density increases with increasing crystallization cycle time (or resolution time), which indicates the birth of new nuclei and growth of crystals at all times. The suspension density will be taken to the equilibrium condition over time.

4.5.2 Determination of the Percent Purity of L-met·HCl Crystals

The specific rotation, $[\alpha]_{\lambda}^{T}$, can be used to calculate the percent purity of L-met·HCl crystal in mother liquor of DL-met·HCl using the correlation shown in equation (4.2). This equation can be described by the mathematical relationships below and Figure 4.4, which indicates the relationship between the specific rotation at 25°C, sodium D-line wavelength, $[\alpha]_{D}^{25}$, and the percent purity of L-crystal (%L-crystal). Figure 4.4 can be plotted with a linear equation, using SigmaPlot® version 11.0. This graph was used to describe the relationship of the specific rotation of L-met·HCl crystal and the percent purity of L-met·HCl crystal during the preferential crystallization process.

The percent purity of L-met·HCl in crystals can be calculated from equation (4.2).

$$\%\text{Purity of L-crystal} = \left[[\alpha]_{D}^{25} + (18.26°)\right] \times \left[\frac{(100-0)}{(2)\times(18.26°)}\right] \qquad (4.2)$$

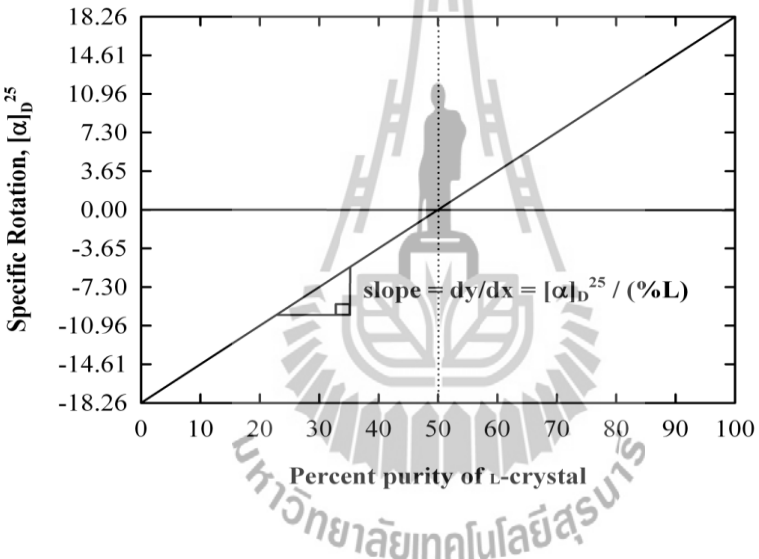

Figure 4.4 The relationship of specific rotation and % L-met·HCl in mixtures of met·HCl.

This calculation method uses the principle that two enantiomers (*d*,*l* or *R*,*S* or +/–) have the same magnitude of specific rotation but that one will have a positive value, and the other will have a negative value. The enantiomer that rotates plane-polarized light to the right will be assigned to the symbol *d* or (+), and the other one is assigned to the symbol *l* or (–). Racemic solutions bend plane-polarized light in both directions, but with equal magnitude and so the specific rotation is zero.

The racemic solution of DL-met·HCl had caused some reduction in purity of the L-met·HCl seed crystals while the preferential crystallization process was operated. The preferential crystallization was started with 100% pure L-met·HCl as seed crystals, with the

specific rotation of pure L-met·HCl solution at 25°C is $[\alpha]_D^{25}$ = +18.26°, as shown in Figure 4.4. The 100% pure L-met·HCl seed crystals decreased in percent purity over time until the purity of L-met·HCl will be 50% purity. At the same time the percent purity of L-met·HCl decreased, the nuclei of the unseeded (counter) enantiomer (D-met·HCl) were occurring and growing that made the percent purity of D-met·HCl increased to 50% purity. In this state, is called the racemic mixture (50% D-met·HCl and 50% L-met·HCl). Similarly, the specific rotation of L-met·HCl crystal will be decreased over time during the preferential crystallization process was operating, until the specific rotation of met·HCl is equal to $[\alpha]_D^{25}$ = ±00.00° that is conglomerate DL-met·HCl crystal as Figure 4.4.

The data can be plotted for the relationship between the percent purity of L-met·HCl in crystals and resolution time (or crystallization cycle time) (min) and these plots are shown in Figure 4.5 and Figure 4.6, and the uncertainty in the graph is represented by 2 standard deviations of the mean. These graphs show the experimental results do not much differ at σ = 0.005 and σ = 0.01, which shows the percent purity of the L-met·HCl crystal decreased rapidly from 100% pure L-met·HCl crystal to the equilibrium state (around 60% to 55% purity) over time. The percent purity of L-met·HCl decreases rapidly at the initial time, with no plateau at the 100% purity state, as shown in the research of Doki et al. The enantiomer ratio of solution is always 1:1 or a racemic mixture when no additive or no seed crystal was added. It indicates that D-enantiomer and L-enantiomer have nucleated simultaneously at all times (Doki, Yokota, Sasaki, and Kubota, 2004), that made the percent purity of L-met·HCl crystal is decreased rapidly at the initial state, and also can be explained by the very short induction time for secondary nucleation threshold in these solutions, which maybe a result of the seed crystals (see section 3.5.1, Chapter III). This research only focuses on the study of the purity drop of L-met·HCl seed crystal in mother liquor of DL-met·HCl via the preferential crystallization, and is without the addition of another D-amino acid to inhibit the birth of new nuclei of the counter enantiomer (D-met·HCl) in the mother liquor.

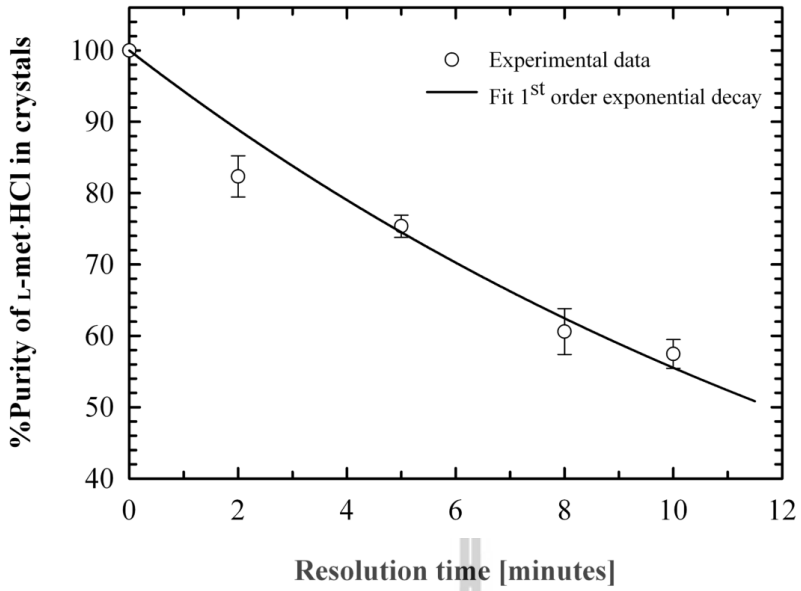

Figure 4.5 Optical purity of the produced L-met·HCl crystal during resolution by preferential crystallization from DL-met·HCl aqueous solution (σ = 0.005); Total solution: 40 g, Solvent: 10.45 cm^3 of distilled water, Seed crystals: 1.000 g of L-met·HCl, crystallization temperature:10±0.5°C.

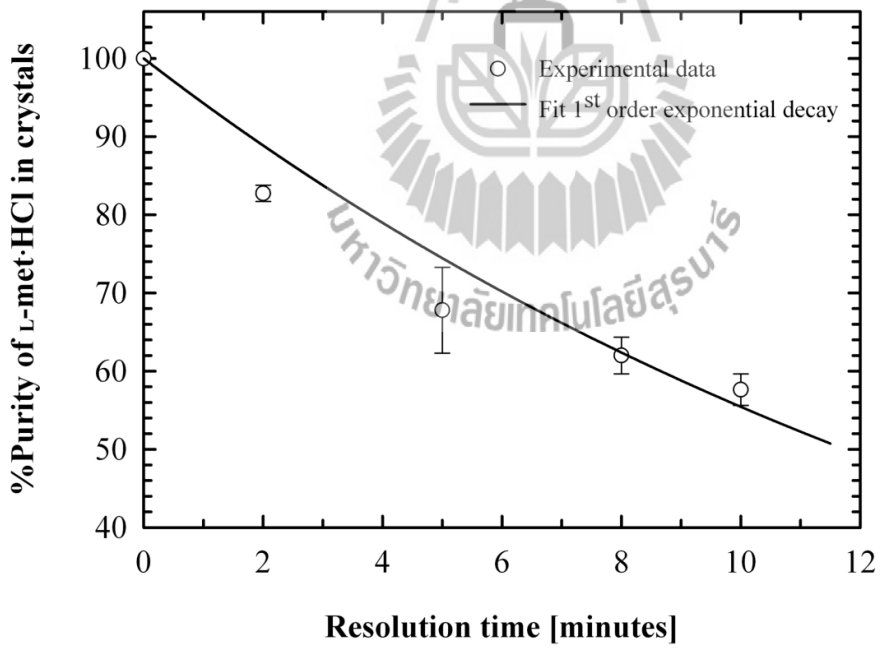

Figure 4.6 Optical purity of the produced L-met·HCl crystal during resolution by preferential crystallization from DL-met·HCl aqueous solution (σ = 0.01); Total solution: 40 g, Solvent: 10.30 cm^3 of distilled water, Seed crystals: 1.000 g of L-met·HCl, crystallization temperature:10±0.5°C.

4.6 Conclusions

The last experiments studied the mechanisms and results of the preferential crystallization of DL-met·HCl, and analyzed the percent purity and purity drop of L-met·HCl in the crystal product by optical resolution using polarimetry. The seeded isothermal preferential crystallization (SIPC) was used in this experiment. The racemic mixture of DL-met·HCl and L-met·HCl crystal are the main chemical that were used in the experiment. DL-met·HCl supersaturated solutions (σ = 0.005 and σ = 0.01) were prepared at 10°C that corresponds to the solubility data of DL-met·HCl at 10°C. About 1.0000 g of L-met·HCl was seeded to the supersaturated solution of DL-met·HCl in preferential crystallization process to induce the L-enantiomer of met·HCl (desired product) in the saturated solution. The resolution time or crystallization cycle time for study the preferential crystallization is 2, 5, 8, and 10 minutes, because of the preferential crystallization period of DL-met·HCl is very short due to the effect of the primary and secondary nucleation threshold measured in the previous chapter.

The suspension density (M_T) during the preferential crystallization of DL-met·HCl aqueous solution increased rapidly with increasing crystallization cycle time in the current experiments partly due to the relatively large growth rates and also due to the large amount of seed crystal, which indicates the birth of new nuclei and growth of crystals all the time during the experiment. Finally, the system will be taken to the equilibrium state (about 0.0380 g crystal/g solution for σ = 0.005, and about 0.0516 g crystal/g solution for σ = 0.01) over time. The solid phase and liquid phase are at the equilibrium condition, which indicates no growth and no dissolution of the crystals anymore. The suspension density was used to indicate the tendency of quantity of crystal growth during the preferential crystallization process, and also to know the total mass of new crystal at any time. Moreover, the suspension density can also be used to know the optimum cycle period for operating the preferential crystallization also. The purity drop and percent purity of L-met·HCl were studied by mathematical calculation of the specific rotation, that reveals the purity of the L-met·HCl crystal decreased rapidly to the equilibrium state (60% to 55% purity) over time, with almost no plateau at 100% purity at initial state. The equilibrium purity is larger than 50% due to the small amount of L-met·HCl seed crystals added at the start of the batch. The quick decrease in purity can be explained by the very short induction time for secondary nucleation in these solutions, which is a result of seed crystals.

This is the first project to develop and improve the chiral resolution (especially the preferential crystallization) technology, which only focuses on the mechanisms and effect of seed crystal to induce the desired form of enantiomer of chiral compounds. It cannot analyze or separate the desired enantiomer to 100% purity. It still needs to use another step to separate the desired enantiomer, such as “tailor-made” additives to inhibit the primary nucleation of the undesired enantiomer, or using a process where one enantiomer (the undesired form) of a compound converts to the other enantiomer (the desired form) by reacting with other compounds, a process called “racemization”.

4.7 References

Angelov, I., Raisch, J., Elsner, M. P., and Seidel-Morgenstern, A. (2008). Optimal operation of enantioseparation by batch-wise preferential crystallization. Chemical Engineering Science 63: 1282-1292.

Bayley, C. R. and Vaidya, N. A. (1992). Resolution of racemates by diastereomeric salt formation. In A. N. Collins, G. Sheldrake, and J. Crosby (Eds.). Chirality in industry: The commercial manufacture and applications of optically active compounds (pp. 69-77). Chichester: John Wiley & Sons.

Blehaut, J. and Nicoud, R. M. (1998). Recent aspects in simulated moving bed. Analusis Magazine 26: M60-M70.

Brown, W. H. (2000). Introduction to organic chemistry. Fort Worth, Texas: Saunders College Publishing.

Bruice, P. Y. (2004). Organic chemistry. Upper Saddle River, New Jersey: Pearson Education.

Carey, F. A. (2003). Organic chemistry. Boston: McGraw-Hill.

Collins, A. N., Sheldrake, G. N., and Crosby, J. (1997). Chirality in industry II: Developments in the manufacture and applications of optically active compounds. Chichester: John Wiley & Sons.

Doki, N., Yokota, M., Sasaki, S., and Kubota, N. (2004). Simultaneous crystallization of D- and L-asparagines in the presence of a tailor-made additive by natural cooling combined with pulse heating. Crystal Growth & Design 4(6): 1359-1363.

Elsner, M. P., Menéndez, D. F., Muslera, E. A., and Seidel-Morgenstern, A. (2005). Experimental study and simplified mathematical description of preferential crystallization. Chirality 17: S183-S195.

Gou, L., Lorenz, H., and Seidel-Morgenstern, A. (2011). Rational design of preferential crystallization. In Poster of the 18th International Symposium on Industrial Crystallization (poster no. 148). Zurich, Switzerland.

Hornback, J. M. (2005). Organic chemistry. New York: W. W. Norton & Company.

Jacques, J., Collet, A., and Wilen, S. H. (1981). Enantiomers, racemates, and resolutions. New York: John Wiley & Sons.

Lorenz, H., Polenske, D., and Seidel-Morgenstern, A. (2006). Application of preferential crystallization to resolve racemic compounds in a hybrid process. Chirality 18: 828-840.

Mohrig, J. R., Hammond, C. N., and Schatz, P. F. (2010). Techniques in organic chemistry. New York: W. H. Freeman & Company.

Nohira, H. and Sakai, K. (2004). Optical resolution by means of crystallization. In F. Toda (Ed.). Enantiomer separation: Fundamentals and practical methods (pp. 165-191). Dordrecht, the Netherlands: Kluwer Academic Publishers.

Polenske, D., Lorenz, H., and Seidel-Morgenstern, A. (2009). Potential of different techniques of preferential crystallization for enantioseparation of racemic compound forming system. Chirality 21: 728-737.

Qamar, S., Angelov, I., Elsner, M. P., Ashfaq, A., Seidel-Morgenstern, A., and Warnecke, G. (2009). Numerical approximations of a population balance model for couple batch preferential crystallizers. Applied Numerical Mathematics 59: 739-753.

Seebach, D., Hoffmann, M., Sting, A. R., Kinkel, J. N., Schulte, M., and Küsters, E. (1998). Chromatographic resolution of synthetically useful chiral glycine derivatives by high-performance liquid chromatography. Journal of Chromatography A 796: 299-307.

Wood, W. M. L. (1997). Crystal science techniques in the manufacture of chiral compounds. In A. N. Collins, G. Sheldrake, and J. Crosby (Eds.). Chirality in industry II: Developments in the manufacture and applications of optically active compounds (pp. 119-156). Chichester: John Wiley & Sons.

Chapter V
Polymorphism and Thermodynamics of DL-Methionine

5.1 Abstract

Pure of the polymorphs α-DL-methionine (α-DL-met) and the γ-DL-methionine (γ-DL-met) were prepared by reaction crystallization of sodium methioninate (Na-Met) aqueous solutions with HCl, and cooling crystallization of aqueous solutions of DL-met, respectively. The polymorphism and thermodynamics of DL-met were studied by a range of techniques including X-ray powder diffractometry (XRPD), determination of the temperatures and enthalpies of fusion by differential scanning calorimetry (DSC), photo microscopy, and solubility measurements. The solubility of each polymorph was determined between 5 and 70 ºC in water. The van't Hoff equation was used to describe the temperature dependence of the solubility. The results showed that XRPD, DSC, photo microscopy, and solubility can be used to describe the differences between the polymorphs. XRPD is the best method for a clear and fast identification and quantification of the polymorphs or polymorphic fraction during crystallization. The solubility of both the α-DL-met and γ-DL-met in water increases with increasing temperature, and the solubility of α-DL-met is higher than γ-DL-met. DSC measurements show that the melting temperature and enthalpy of fusion of γ-DL-met are higher than those of α-DL-met. The enthalpy of dissolution of γ-DL-met is higher than the α-DL-met. The solubility data and the DSC thermograms of the two polymorphs strongly suggest that the system is a monotropic polymorph system with the γ-DL-met being the stable polymorph for all temperature below the melting points of the compounds.

5.2 Introduction

Polymorphism is the ability of a solid compound to exist in more than one crystalline form (Grant, 1999). These crystalline forms, although containing the same molecules, result from a different ordered arrangement of molecules within the crystalline lattice. Polymorphs can have different mechanical, thermal, physical, and chemical properties, such as compressibility, melting point, crystal habit, color, density, dissolution rate, and solubility.

In experimental and industrial crystallizations, it is commonly observed that the metastable form appears first instead of the stable form, and this observation is stated as a

rule known as Ostwald's Rule of Stages (Threlfall, 2003). According to Ostwald's Rule of stages, in crystallization from the melt or from solution, the metastable polymorph (the least stable of the metastable polymorphs if there is more than two polymorphs) forms first, followed by transformation to the more stable polymorph. It is generally known that this rule is not a physical law and that more stable forms can first crystallize directly as well (Roelands *et al*., 2006). The unstable form is sometimes not acceptable from the point of view of obtaining polymorphically pure compounds suitable for sale, particular in the food and other material products. On the other hand, in the field of pharmaceuticals, metastable polymorphs may be more desirable than the stable one (Yamanobe, Takiyama, and Matsuoka, 2002a).

The melting point, enthalpy of fusion, and solubility are important properties which may be used to model the thermodynamics of the system. It known that the solubility of the stable form is always lower than that of the metastable form. If a form is stable relative to all others at all temperatures below the melting point, then the system only ever has one stable form; such a system is known as a monotropic polymorphic system. Where the stable polymorphic form depends on the temperature and pressure of the system, there is reversible transition point below the melting points of the polymorphs where the relative thermodynamics stabilities change; such a system is known as an enantiotropic system.

Currently, there are several techniques that have been used to characterize crystalline solids, and identify the polymorphic forms. Examples of such techniques are microscopy (Cashell, Sutton, Corcoran, and Hodnett, 2003; Ferrari and Davey, 2004; Jiang, Jansens, and ter Horst, 2010), FTIR spectroscopy (Lu, Wang, Yang, and Ching, 2007; Yamanobe, Takiyama, and Matsuoka, 2002b), Raman spectroscopy (Cornel, Kidambi, and Mazzotti, 2010; Jiang *et al*., 2010; Ono, ter Horst, and Jansens, 2004), DSC (Picciochi, Diogo, and Minas da Piedade, 2011; Urakami, Shono, Higashi, Umemoto, and Godo, 2002), XRPD (Dharmayat, Hammond, *et al*., 2008; Grooff, Liebenberg, and De Villiers, 2011; Liu, Wei, and Black, 2009), ^{13}C solid-state nuclear magnetic resonance (SSNMR) spectroscopy (Hughes and Harris, 2008; Dong *et al*., 2002; Shaibat, Casabianca, Siberio-Pérez, Matzger, and Ishii, 2010), and solubility measurement (Anuar, Wan Daud, Roberts, Kamarudin, and Tasirin, 2009; Nordström and Rasmuson, 2006; Urakami *et al*., 2002). In the present study, a number of these techniques were applied to investigate the polymorphic behavior of DL-methionine (DL-met).

In this work DL-met (Figure 5.1) has been chosen as the model substance. It is used in medicines and active pharmaceutical ingredients, and also as a precursor to other amino acids.

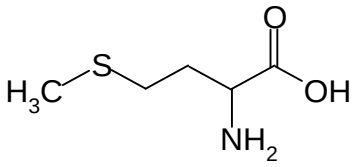

Figure 5.1 Chemical structure of methionine.

DL-met is reported to have three polymorphs; α-DL-met, β-DL-met, and γ-DL-met (Mathieson, 1952; Matsuoka, Yamanobe, Tezuka, Takiyama, and Ishii, 1999). The crystal structures of α-DL-met and β-DL-met are shown by Taniguchi *et al*. (1980), and that of the γ-DL-met is shown by Matsuoka *et al*. (1999). Single crystals of α-DL-met and β-DL-met were grown from an ethanol-water solution by slow evaporation and occur as soft plates (Mathieson, 1952; Taniguchi, Takaki, and Sakurai, 1980). Both the forms were almost equal stability. Ramachandran and Natarajan (2006) showed that β-DL-met crystal was obtained by crystallization in sodium metasilicate gel for the first time by the reduction of solubility method. Matsuoka *et al*. (1999) showed that the α-DL-met crystals were obtained by the reaction crystallization of sodium methioninate (Na-Met) aqueous solutions with liquid acids such as hydrochloric, acetic, nitric, sulfuric or formic acids. Also, Matsuoka *et al*. (1999) reported that γ-DL-met crystals were obtained by the reaction crystallization of Na-Met aqueous solutions with solid benzoic acid, or by cooling crystallization of aqueous solutions of DL-met. The crystallographic data and morphology of each polymorph are shown in Table 5.1 and Figure 5.2, respectively. In this study, the α-DL-met and γ-DL-met were studied because γ-DL-met is found in the cooling crystallization of aqueous solution of DL-met and α-DL-met can transform to γ-DL-met in aqueous solution of DL-met (Yamanobe, Takiyama, and Matsuoka, 2002c).

The aim of this work is to describe the polymorphism and solid-state properties of the α-DL-met and γ-DL-met using analytical thermal methods, X-ray powder diffraction (XRPD), crystal morphology, and the solubility in water. Moreover, the thermodynamic parameters for each polymorph were measured and estimated, and the polymorphic nature of DL-met is described.

Table 5.1 Crystallographic data of each polymorph of DL-met

Form	α^1	β^1	γ^2
a (Å)	16.74	33.13	31.76
b (Å)	4.70	4.70	4.70
c (Å)	9.89	9.912	9.90
β (°)	102.3	106.3	90.98
Z (-)	4	8	8
Space group	$P2_1/c$	I2/c	C2
Crystal system	Monoclinic	Monoclinic	Monoclinic

Sources: [1]Mathieson (1952); [2]Matsuoka *et al*. (1999)

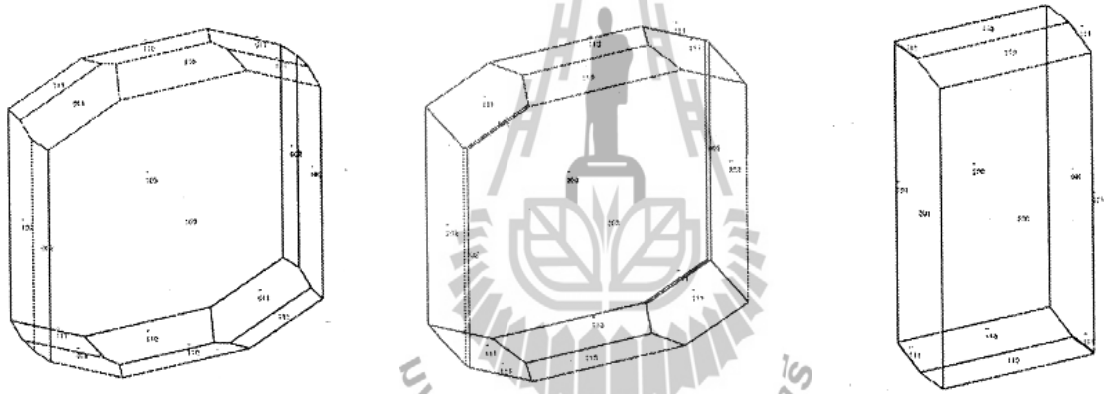

(a) (b) (c)

Figure 5.2 Predicted morphologies of the polymorphs of DL-methionine by the BFDH method. α-DL-met (a), β-DL-met (b) and γ-DL-met (c). (Matsuoka *et al*., 1999)

5.3 Theory

5.3.1 Definition of Polymorphism

Polymorphism occurs when a compound can exist in more than one crystalline form (Grant, 1999). These crystalline forms contain the same molecules but have a different arrangement of molecules within the crystalline lattice. Polymorphs are found among many molecular and ionic compounds.

Polymorphs possess different product properties because of their difference in crystal structures. Example of properties that can be structure-dependent are solubility and dissolution rate, density, stability, melting point, color and morphology (Roelands, 2005). These properties are usually related to the performance of the compound in its application. Only one of the polymorphic structures is thermodynamically stable but the formation of a metastable structure may be kinetically favored, eventually followed by transformation to the stable structure.

Many previous studies concern polymorphism from a pharmaceutical perspective because both polymorphism and formation of solvates are especially widespread among pharmaceutical compounds.

The differences of the properties of each polymorph often are related to the performance of the compound in its application. To obtain the desired polymorphic structure the control over desired performance properties is required. In many chemical, pharmaceutical and food processing industries polymorphism is encountered in crystallization process. There are many parameters influence the formation of polymorphs, such as temperature, pressure, supersaturation, solvent, seeding, and additives. Moreover, understanding of the crystallization mechanism is required with special attention to the process of nucleation, dissolution, growth and transformation.

5.3.2 Solubility and Thermodynamics of Polymorphism

Variations in solubility and dissolution rate may have a serious impact in industrial crystallization processes and in the case of pharmaceutics, bioavailability of drugs. Solubility data are of importance in the study of crystal nucleation and growth kinetics. Solubility, melting temperature, and enthalpy of melting parameters are experimental quantities from which thermodynamics parameters for each polymorph can be calculated.

A number of rules, the heat of transition rule; the heat of fusion rule, and the density rule have been derived by Burger and Ramberger (1979a, 1979b, quoted in Grunenberg *et al*., 1996) are also helpful for checking whether a polymorphic system is monotropic or enantiotropic.

Polymorphic forms differ in solubility because this property is directly proportional to the Gibbs free energy. The fundamental solubility curves of the polymorphic forms of each system are shown in Figures 5.7 and 5.8. Based on ‘Ostwald’s rule’ (Threlfall, 2003), the solubility of the stable form is always lower than the metastable form.

5.4 Materials and Methods

5.4.1 Materials

DL-met was purchased from Acros Organics, purity >99%. NaOH (purity >97%), Na_2CO_3 (purity >99.5%), and HCl (37%) were purchased from Carlo Erba. All chemicals and deionized water were used without further purification.

5.4.2 Apparatus

A 0.5 L batch crystallizer with a sealed glass lid to reduce solvent evaporation was used to prepare γ-DL-met, and to measure the solubility of the α-DL-met and γ-DL-met. The slurry is continuously agitated by a centrally located four-blade impeller driven by an overhead mixer. The crystallizer was placed inside a constant temperature water bath, where the temperature temperature was controlled within ±0.5 °C.

250 mL and 500 mL glass beakers were used as batch crystallizers to prepare α-DL-met and sodium methioninate (Na-Met) aqueous solution, respectively. The temperature control and the agitation systems were the same as used in the 0.5 L batch crystallizer.

5.4.3 Preparation of Na-Met Aqueous Solution

Aqueous solutions of Na-met were prepared by a method previously described (Huthmacher *et al*., 2000). 50 g of DL-met and 13.5 g of NaOH were dissolved in 166.5 mL of water in a 500 mL glass beaker at room temperature, with the addition of 20 g of Na_2CO_3. After mixing, solutions were stirred with a magnetic stirrer for 6 h, and about 150 mL of water was removed from the solution by distillation; the precipitate formed was separated by filtration over a hot (> 100 °C) 8 μm filter by a vacuum pump. The filtrate contained 71% sodium methioninate.

5.4.4 Preparation of Polymorph

α-DL-met was prepared using reaction crystallization of Na-met aqueous solutions as follows: concentrated HCl (37%) was fed slowly into diluted Na-Met aqueous solutions (80 mL of 71% Na-Met aqueous solution diluted by 40 mL of water) in a 250 mL glass beaker at 35 °C. The mixed solutions were continuously agitated by a centrally located four-blade impeller driven by an overhead stirrer at 300 rpm. The pH of the solutions reached the isoelectric point of DL-met (pH = 5.7 - 5.9) after the full amount of HCl was added. The resulting crystals were collected by filtration over a 2 μm filter by a vacuum pump and dried over silica gel. γ-DL-met was prepared by cooling crystallization of aqueous solutions of DL-met as follows. DL-met (21 g) was dissolved in 350 mL of water in

a 0.5 L batch crystallizer maintained above 60 °C. This solution was continuously agitated by a centrally located four-blade impeller driven by an overhead stirrer at 300 rpm, and the solution was cooled and maintained at 25 °C, after which the crystals were removed and filtered. Since these crystals were too large for use as seed crystals a further crystallization was performed. The solution at 25 °C was heated to 30 °C, then cooled to 5 °C and held at this temperature for 24 h. After 24 h, the suspension was filtered over a 2 μm filter by a vacuum pump and dried over silica gel.

5.4.5 Polymorph Characterization

The crystals of the pure polymorph of each form obtained from section 5.4.4 were characterized by X-ray powder diffractometry (XRPD) (Bruker axs, D5005), differential scanning calorimetry (DSC) (PerkinElmer, DSC7), and microscopic observation (Olympus, CH30).

5.4.6 Solubility Measurement

The solubility of each polymorph was determined in water as a function of temperature (5 - 70 ºC), and was measured by a gravimetric method. 200 mL of water was added into a 0.5 L batch crystallizer and stabilized at the desired (measurement) temperature. Excess amounts of each polymorph crystal were then added into the water and the system was agitated. To ensure the equilibrium state, the solutions were stirred (300 rpm) for about 24 h at a constant temperature with an uncertainly ±0.5 ºC. The concentration was periodically recorded by the dry substance method (Garside, Mersmann, and Nyvlt, 2002): the suspensions were withdrawn from the crystallizer using a 10 mL plastic syringe together with a 0.45 μm filter, the clear liquid solutions were evaporated at 100 - 105 ºC, and the weight of the dry DL-met was used to calculate the concentration of DL-met (the weight was repeatedly recorded throughout the drying process with complete dryness determined when the mass of the DL-met remained constant over time). After the water is completely evaporated, the concentration (C) can be determined. The solubility was estimated by averaging the concentration at equilibrium. At equilibrium, the residual solids were analyzed by XRPD to consider the solution-mediated phase transformation between the two forms. Note that at the temperature higher than 25 ºC the syringe and filters must be pre-heated to exceed the solution temperature. This was performed to stop nucleation occurring inside the syringe and filters during sampling.

5.5 Results and Discussions

5.5.1 Polymorphism

The polymorphic form was corroborated through analyses by XRPD, DSC, and photo microscopy.

DSC thermograms of the two polymorphs are shown in Figure 5.3. There is no evidence of significant phase transformation between the polymorphs upon heating. The α-DL-met form melts at 274.0 °C. For γ-DL-met there is small endothermic transition near 52 °C, and this form melts at 277.1 °C. The measured peak fusion temperatures and enthalpies, and estimated entropies of the two polymorphs are shown Table 5.2. From these observations, it appears most likely that there is a conformational difference between α-DL-met and γ-DL-met.

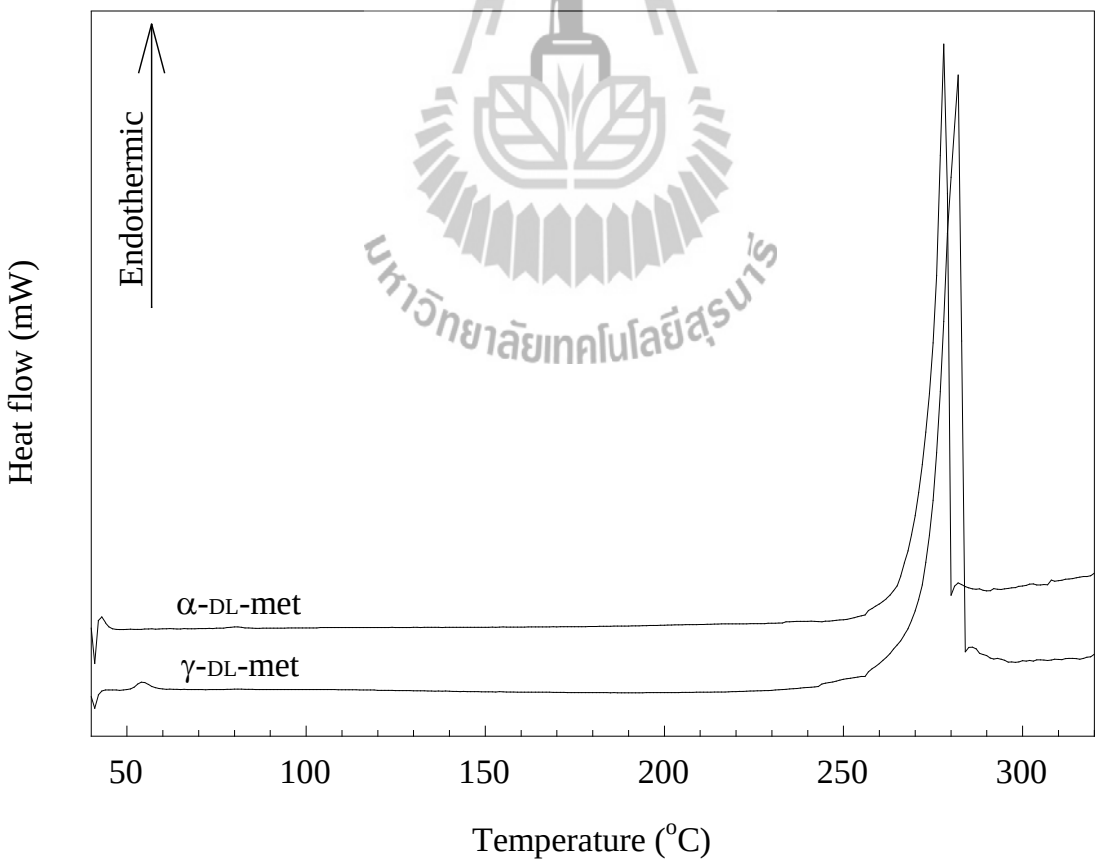

Figure 5.3 DSC curves of α-DL-met and γ-DL-met crystals.

Table 5.2 Thermodynamic parameters of the α-DL-met and γ-DL-met.

Form	α	γ
Peak fusion temperature (ºC)	278.17	281.74
Melting enthalpy (kJ/mol)	88.81	98.76
Melting entropy (kJ/mol/K)	0.1610	0.1780
Dissolution enthalpy (kJ/mol)	17.87	18.23
Dissolution entropy (J/mol/K)	14.83	15.52

XRPD patterns for α-DL-met and γ-DL-met are given in Figure 5.4. The XRPD patterns are identical to patterns given by Matsuoka *et al*. (1999). The XRPD patterns show clearly that the polymorphs possess different crystal structures. The characteristic peaks of the α-DL-met are observed at 25.3°/2θ and 32.8°/2θ, while the characteristic peaks of the γ-DL-met are observed at 28.0°/2θ and 33.8°/2θ. Therefore, the XRPD method is a good method for clear and fast identification and quantification of the polymorphs or polymorphic fraction during crystallization. The composition of γ-DL-met could be estimated using a calibration curve obtained from the relationship between the mass fraction of γ-DL-met and the intensity of characteristic peaks, which is described in chapter V.

The crystal morphology of the two polymorphs differ (Figure 5.5). The crystals of α-DL-met are agglomerated and have laminate structures; the constituent elementary particles are primarily plate-like, whereas the shape of the γ-DL-met crystals is a prism-like hexagon. Therefore, the transformation from the α-DL-met to the γ-DL-met during crystallization could be also followed using a microscope. The morphologies of the two polymorphs obtained are identical to the results given by Matsuoka *et al*. (1999) and Yamanobe-Hada *et al*. (2005).

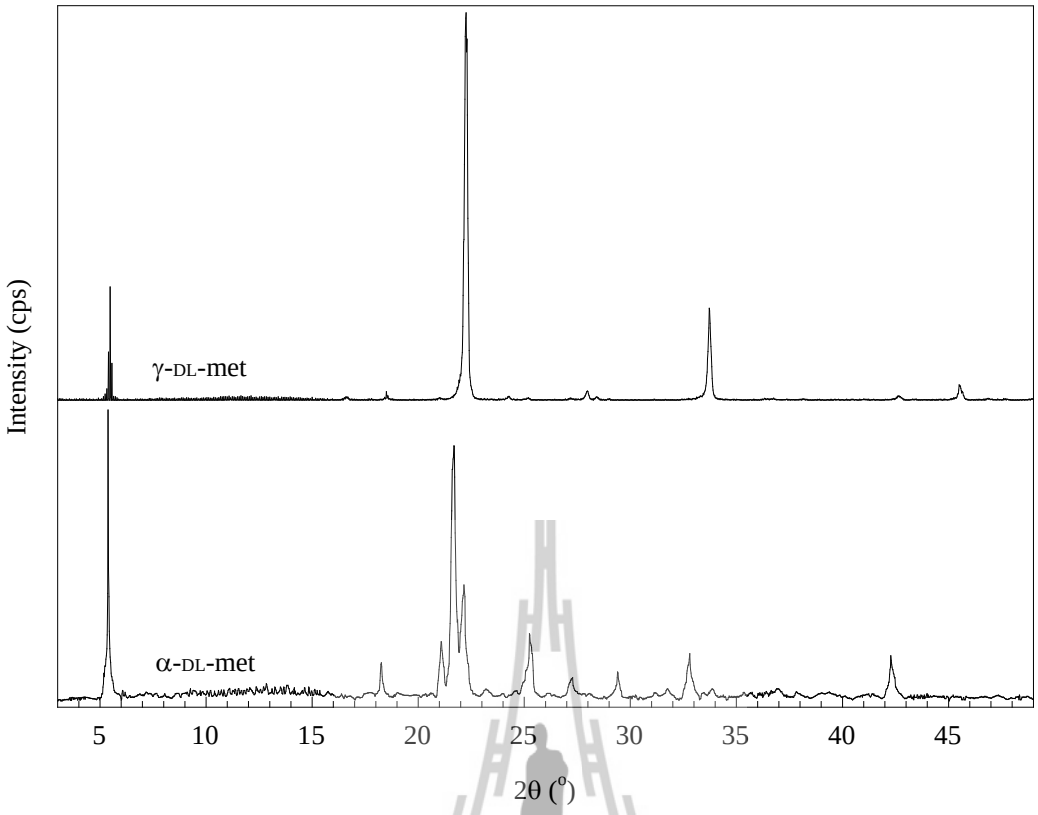

Figure 5.4 PXRD patterns of α-DL-met and γ-DL-met crystals.

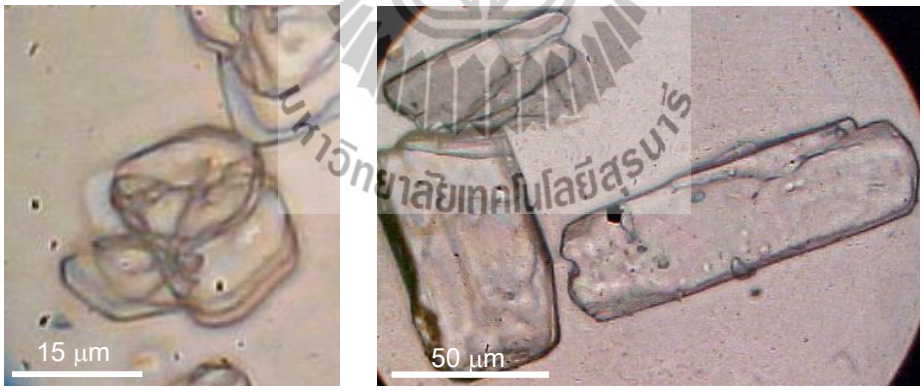

(a) (b)

Figure 5.5 Photomicrographs of α-DL-met (a) and γ-DL-met (b) crystals.

The purity of the crystallized polymorphs was found based on the difference between the two polymorphs, as observed via the different methods of analysis. Particularly XRPD contributed important information, as the two polymorphs showed very different patterns. DSC also provided some knowledge, as analysis of the polymorphic

forms showed differences in the melting properties. Additionally investigation by photo microscopy facilitated in elucidating the purity since the two polymorphs differed in crystal morphology.

5.5.2 Solubility

The dissolution profiles of the α-DL-met and γ-DL-met in water were measured to confirm equilibrium after some time. The solubilities of the two polymorphs are listed in Table 5.3 and shown in Figure 5.6. A sample of the solid phase was examined by XRPD analysis both before and after each solubility measurement.

No conversion of γ-DL-met was observed even after solubility measurement of γ-DL-met. Some conversion from α-DL-met to the γ-DL-met was observed, but the transformation was not close to complete in the time interval of this measurement. From the experimental and simulation results of Yamanobe *et al*. (2002c) it was seen that during transformation from the α-DL-met to the γ-DL-met the concentration of the solution was saturated with the α-DL-met (at the solubility of the α-DL-met) and after all of the α-DL-met transformed to the γ-DL-met the concentration started to decrease to the solubility of the γ-DL-met. Therefore, the saturation concentrations during the transformation of the α-DL-met in this experiment are expected to be the solubility of the α-DL-met. These indicate that γ-DL-met is the stable polymorph and α-DL-met is the metastable polymorph.

The solubility curves showed the solubility of both the α-DL-met and γ-DL-met increased with increasing temperature, and the solubility of the α-DL-met is higher than that of the γ-DL-met over the entire studied temperature range of 5 - 70 ºC. This also indicates that the γ-DL-met is the stable polymorph and the α-DL-met is the metastable polymorph between 5 and 70 ºC: the solubility of the stable form is always lower than that of the metastable form (Threfall, 2003).

Scarce reference data for the solubility data of DL-met is available. The solubility of the γ-DL-met in water is in agreement with the solubility of the industrial DL-met (a mixture of the α-DL-met and γ-DL-met) given by Dalton and Schmidt (1935). This indicates that the solubility of DL-met was determined after all of the α-DL-met transformed to the γ-DL-met.

Table 5.3 Solubility of the α-DL-met and γ-DL-met in water

Temperature (ºC)	Solubility (standard deviation, S) (g DL-met/kg water)	
	α- DL-met	γ- DL-met
5	22.67 (0.27)	20.80 (0.33)
15	28.55 (0.23)	26.69 (0.11)
25	35.62 (0.10)	33.70 (0.20)
35	44.44 (0.13)	42.70 (0.41)
45	56.23 (0.40)	53.03 (0.38)
53	67.91 (0.72)	64.78 (0.32)
69	97.97 (0.38)	-
70	-	94.34 (0.64)

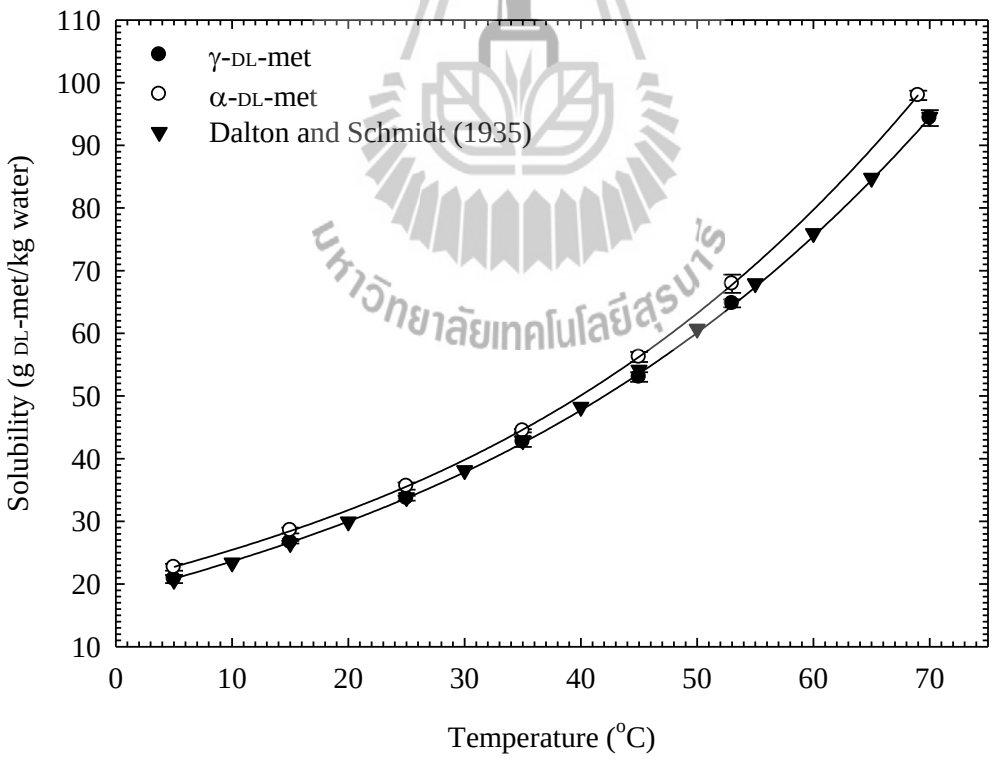

Figure 5.7 Solubility of the α-DL-met and γ-DL-met of in water.

The solubility data in the temperature range of 5 - 70 ºC was fitted using a cubic polynomial equation, with the results shown in equations 5.1 (for α-DL-met) and 5.2 (for γ-DL-met), where C^* is the solubility in g of DL-met/kg of water and T is the experimental temperature in °C.

α-DL-met: $$C^* = 20.02 + 4.897\times10^{-1}T + 2.566\times10^{-3}T^2 + 9.680\times10^{-5}T^3$$
(for 5 ºC ≤ T ≤ 69 ºC) (5.1)

γ-DL-met: $$C^* = 18.23 + 5.053\times10^{-1}T + 2.436\times10^{-3}T^2 + 8.410\times10^{-5}T^3$$
(for 5 ºC ≤ T ≤ 70 ºC) (5.2)

The root mean square deviation (rmsd) is defined as

$$\text{rmsd} = \left[\frac{1}{N} \sum_{i=1}^{N} \frac{(C_c^* - C_i^*)^2}{C_i^*} \right]^{1/2} \quad (5.3)$$

where C_c^* stands for calculated values by equation (5.1) or (5.2), C_i^* stands for experimental values, and N stands for number of experimental points. The rmsd values for the fitting equation of the α-DL-met and γ-DL-met are 0.0021 and 0.0018, respectively. These values indicate that the solubility of the α-DL-met and γ-DL-met in water can be fitted with cubic polynomial equation well.

5.5.3 Thermodynamics

Fitting the mole fraction solubility data (Table 5.4) of the α-DL-met and γ-DL-met in water to the van't Hoff equation ($\ln x$ against $1/T$) will result in a straight line approximation, as shown in Figure 5.7. The $\Delta_{diss}H$ and $\Delta_{diss}S$ can be obtained from the slope of the solubility curve and the intercept with the y axis, respectively. As shown in Figure 5.7, the experimental solubility data fits well for both the α-DL-met and γ-DL-met. The estimated value of the ΔH_{diss} and ΔS_{diss} of the both polymorphs are listed in Table 5.2. The fitting equations of the two polymorphs are shown in equations 5.4 and 5.5.

α-DL-met: $\ln x = -\frac{2.1491 \times 10^3}{T} + 1.7837$ for 5 °C ≤ T ≤ 69 °C (5.4)

γ-DL-met: $\ln x = -\frac{2.1927 \times 10^3}{T} + 1.8673$ for 5 °C ≤ T ≤ 70 °C (5.5)

Table 5.4 Mole fraction solubility (x) of the α-DL-met and γ-DL-met in water.

Temperature	100x (100S) (mole fraction, [-])	
T (K)	α-DL-met	γ-DL-met
278	0.2727 (0.0032)	0.2503 (0.0039)
288	0.3433 (0.0028)	0.3209 (0.0013)
298	0.4279 (0.0053)	0.4049 (0.0023)
308	0.5333 (0.0015)	0.5125 (0.0049)
318	0.6737 (0.0048)	0.6356 (0.0045)
326	0.8126 (0.0086)	0.7754 (0.0038)
342	1.1681 (0.0044)	-
343	-	1.1253 (0.0075)

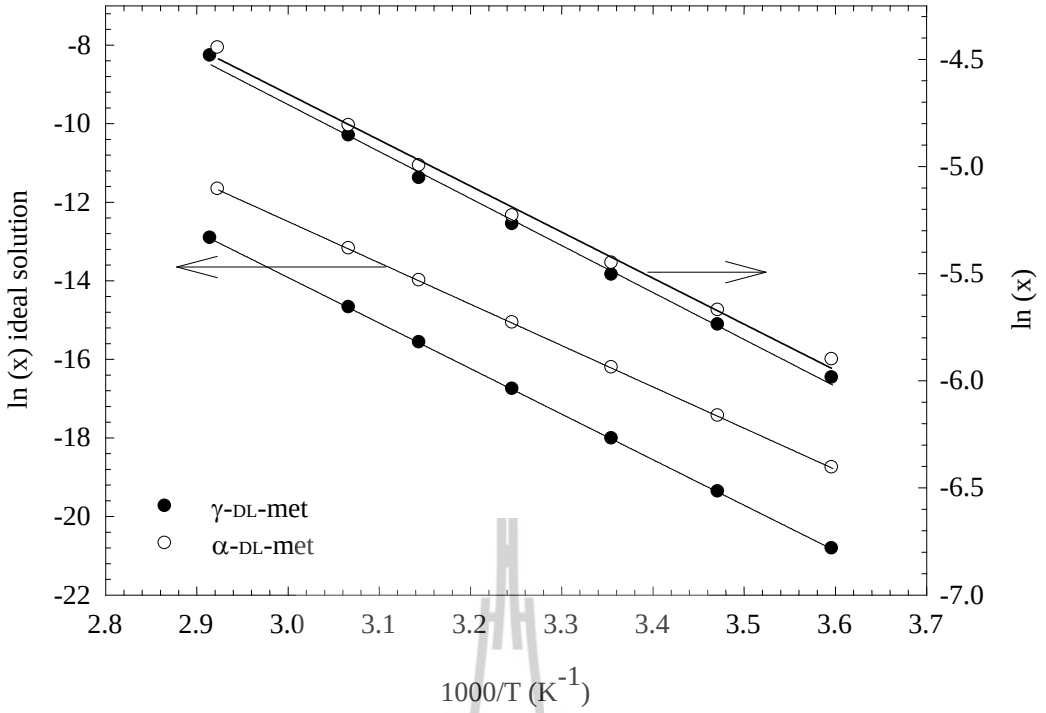

Figure 5.8 Plot of van't Hoff solubility data of real and ideal solubility of α-DL-met and γ-DL-met in water.

The van't Hoff plots of an ideal and real systems are shown in Figures 5.8. These show that the real solubility is higher than the ideal solubility, which indicates strong interactions between DL-met and water molecules (Davey, Mullin, and Whiting, 1982). This means that there are strong interactions between the hydrophilic head of the DL-met molecules (consisting of $-NH_3^+$ and $-COO^-$) and the surrounding water molecules. The ΔH_{diss} shows the dissolution is an endothermic process (ΔH_{diss} is a positive value), and also the ΔS_{diss} shows a positive value; therefore the process will occur spontaneously. The positive value of ΔH_{diss} is due to the endothermic reaction of breaking the hydrogen bonds to create a cavity for the solutes within the aqueous solution (Anuar *et al*., 2009).

The plots of the change of the Gibbs free energy of the two polymorphs using are shown in Figure 5.8. The Gibbs free energy of both polymorphs also confirms that γ-DL-met (which has a lower Gibbs free energy) is the stable polymorph and α-DL-met (which has a higher Gibbs free energy) is the metastable polymorph.

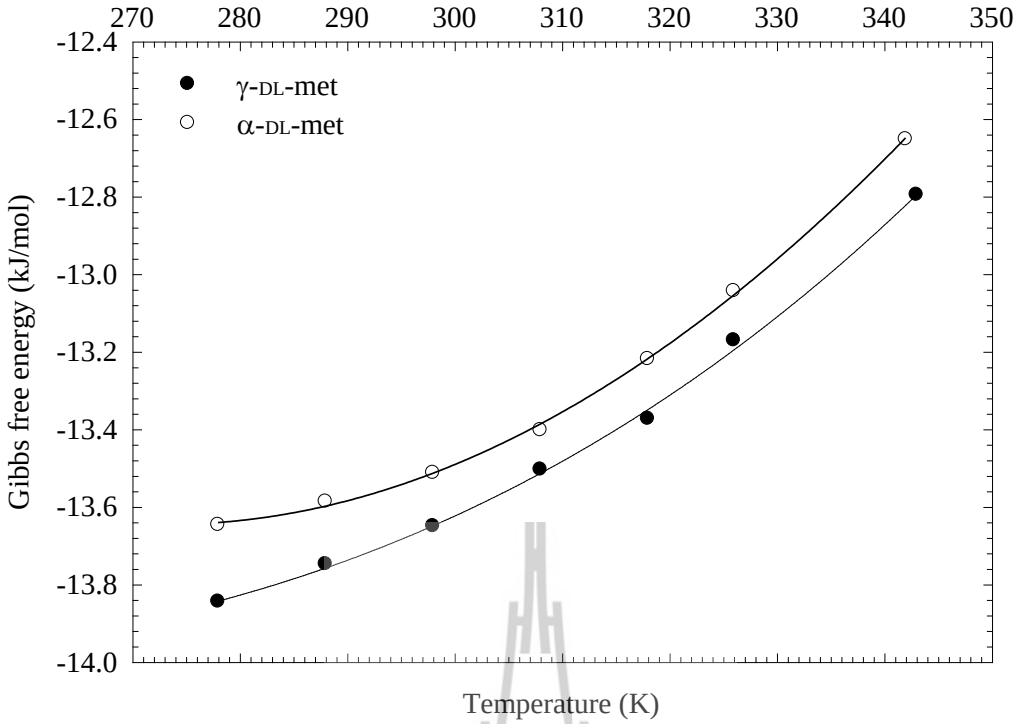

Figure 5.9 Plot of Gibbs free energy of α-DL-met and γ-DL-met.

2.5.4 The Polymorphic Nature of DL-Met

In the DSC thermogram of the two polymorphs, the melting temperature of the γ-DL-met is higher than that of the α-DL-met and the melting enthalpy of the γ-DL-met is also higher than that of the α-DL-met. According to the Burger and Ramberger polymorphic rules (Grunenberg *et al*., 1996), this suggests monotropic polymorphism. Also the solubility curve of van't Hoff plot, and the plot of the Gibbs free energy strongly suggest that the two polymorphs are monotropic, since the γ-DL-met which is stable relative to the α-DL-met at all temperature below the melting point, the polymorphs are not interconvertible, and the solubility of the γ-DL-met is always lower than the α-DL-met.

2.6 Conclusions

The physical and chemical properties of the two main polymorphs of DL-met have been characterized. The polymorphic behavior was confirmed through analyses by XRPD, DSC, photo microscopy, as well as through solubility. It was shown that XRPD is the best method for a clear and fast identification and quantification of the polymorphs or polymorphic fraction during crystallization. DSC measurements show that the melting

temperature and enthalpy of fusion of the γ-DL-met are higher than those of the α-DL-met. The γ-DL-met is shown to be the stable phase and the α-DL-met to be the metastable phase between 5 and 70 °C. The solubility of the metastable polymorph is higher than that of the stable polymorph. The solubility data of the two polymorphs are well fitted with the van't Hoff equation. The enthalpy of dissolution of the two polymorphs can be calculated from the slope of the van't Hoff plot, with the enthalpy of dissolution of the γ-DL-met being higher than that of the α-DL-met. Based on the solubility data and DSC measurements, the polymorphic nature of DL-met is a monotropic system.

2.7 References

Anuar, N., Wan Daud, W. R., Roberts, K. J., Kamarudin, S. K., and Tasirin, S. M. (2009). An examination of the solution chemistry, nucleation kinetics, crystal morphology, and polymorphic behavior of aqueous phase batch crystallized L-isoleucine at 250 mL scale size. Cryst. Growth Des. 9(6): 2853-2862.

Bauer *et al*. (2001). Ritonavir: An extraordinary example of conformational polymorphism. Pharm. Res. 18(6):859-866.

Beckmann, W. (2000). Seeding the desired polymorph: background, possibilities, limitations, and case studies. Org. Process Res. Dev. 4(5): 372-383.

Brečević, L. and Nielsen, A. E. (1993). Solubility of calcium carbonate hexahydrate. Acta Chem. Scand. 47: 668-673.

Burger, A. and Ramberger, R. (1979a). On the polymorphism of pharmaceuticals and other molecular crystals. I Theory of thermodynamic rules. Microchim. Acta. 72: 259-271. Quoted in Grunenberg, A., Henck, J.-O., and Siesler, H. W. (1996). Theoretical derivation and practical application of energy/temperature diagrams as an instrument in preformulation studies of polymorphic drug substances. Inter. J. Pharm. 129(1-2): 147-158.

Burger, A. and Ramberger, R. (1979b). On the polymorphism of pharmaceuticals and other molecular crystals. II Applicability of thermodynamic rules. Microchim. Acta. 72: 273-316. Quoted in Grunenberg, A., Henck, J.-O., and Siesler, H. W. (1996). Theoretical derivation and practical application of energy/temperature diagrams as an instrument in preformulation studies of polymorphic drug substances. Inter. J. Pharm. 129(1-2): 147-158.

Cashell, C., Sutton, D., Corcoran, D., and Hodnett, B. K. (2003). Inclusion of the stable form of a polymorph within crystals of its metastable form. Cryst. Growth Des. 3(6): 869-872.

Chemburkar *et al*. (2000). Dealing with the impact of Ritonavir polymorphs on the late stages of bulk drug process development. Org. Process Res. Dev. 4(5): 413-417.

Cornel, J., Kidambi, P., and Mazzotti, M. (2010). Precipitation and transformation of the three polymorphs of D-mannitol. Ind. Eng. Chem. Res. 49(12): 5854–5862.

Davey, R.J., Mullin, J.W. and Whiting, M.J.L. (1982). Habit modification of succinic acid crystals grown from different solvents. J. Cryst. Growth 58(2): 304–312.

Dalton, J. and Schmidt, C.L.A. (1935). The solubilities of certain amino acids and related compounds in water, the densities of their solutions at twenty-five degrees, and the calculated heats of solution and partial molal volumes. II. J. Biol. Chem. 109(1): 241-248.

Dharmayat, Anda *et al*. (2006). Polymorphic transformation of L-glutamic acid monitored using combined on-line video microscopy and X-ray diffraction. J. Cryst. Growth 294(1): 35-40.

Dharmayat, Hammond *et al*. (2008). An examination of the kinetics of the solution-mediated polymorphic phase transformation between α- and β-forms of L-glutamic acid as determined using online powder X-ray diffraction. Cryst. Growth Des. 8(7): 2205-2216.

Dong *et al*. (2002). Neotame anhydrate polymorphs I: Preparation and characterization. Pharm. Res. 19(3): 330-336.

Ferrari, E. S. and Davey, R. J. (2004). Solution-mediated transformation of α and β L-glutamic acid: Rate enhancement due to secondary nucleation. Cryst. Growth Des. 4(5): 1061-1068.

Garside, J., Mersmann, A., and Nyvlt, J. (2002). Measurement of crystal growth and nucleation rates (2nd). UK: Institute of Chemical Engineering.

Grant, D.J.W. (1999). Theory and origin of polymorphism, in: H.G. Brittain (Ed.), Polymorphism in pharmaceutical solids, drugs and the pharmaceutical sciences, Marcel Dekker, New York, 1999, pp. 1–34 Vol. 95.

Grooff, D., Liebenberg, W., and De Villiers, M. M. (2011). Preparation and transformation of true nifedipine polymorphs: Investigated with differential scanning calorimetry and X-ray diffraction pattern fitting methods. J. Pharm. Sci. 100(5): 1944-1957.

Grunenberg, A., Henck, J.-O., and Siesler, H. W. (1996). Theoretical derivation and practical application of energy/temperature diagrams as an instrument in preformulation studies of polymorphic drug substances. Inter. J. Pharm. 129(1-2): 147-158.

Himawan, C. (2005). Characterization and population balance modeling of eutectic freeze crystallization. Ph.D. Thesis, Delft University of Technology, The Netherlands.

Hughes, C. E. and Harris, K. D. M. (2008). A Technique for in situ monitoring of crystallization from solution by solid-state ^{13}C CPMAS NMR spectroscopy. J. Phys. Chem. A, 112(30): 6808-6810.

Huthmacher, K; Binder, W; Hasselbach, H. J; Korfer, M; Rohland, L; Alt, H. C; Kniesel, H. Process for the preparation of aqueous sodium methioninate solutions and use of those solutions in the production of a granulate. U.S. 6,126,972, October 3, 2000.

Jiang, S., Jansens, P. J., and ter Horst, J. H. (2010). Mechanism and kinetics of the polymorphic transformation of o-aminobenzoic acid. Cryst. Growth Des. 10(5): 2123-2128.

Kaneniwa, N. and Otsuka, M. (1985). Effect of grinding on the transformations of polymorphs of chloramphenicol palmitate. Chem. Pharm. Bull. 33(4): 1660-1668.

Kee, N. C. S., Tan, R. B. H. and Braatz, R. D. (2009). Selective crystallization of the metastable α-form of L-glutamic acid using concentration feedback control. Cryst. Growth Des. 9(7): 3044-3051.

Kitamura, M. (1993). Crystallization behavior and transformation kinetics of L-histidine polymorphs. J. Chem. Eng. Jpn. 26(3): 303-307.

Kitamura, M. (2001). Crystallization and transformation mechanism of calcium carbonate polymorphs and the effect of magnesium ion. J. Colloid Interface Sci. 236(2): 318-327.

Kitamura, M., Konno, H., Yasui, A. and Masuoka, H. (2002). Controlling factors and mechanism of reactive crystallization of calcium carbonate polymorphs from calcium hydroxide suspensions. J. Cryst. Growth. 236(1-3): 323–332.

Kolar, Z., Binsma, J. J. M., Subotić, B. (1986). The formation of orthorhombic BaF_2 by precipitation from aqueous solutions and its transformation into cubic BaF_2. J. Cryst. Growth. 76(2): 408-412. Quoted in C. P. M. Roelands. (2005). Polymorphism in precipitation process. Ph.D. thesis, Delft University of Technology, The Netherlands.

Liu, W., Wei, H., and Black, S. (2009). An investigation of the transformation of carbamazepine from anhydrate to hydrate using in situ FBRM and PVM. Org. Process Res. Dev. 13(3):494-500.

Lu, J., Wang, X-J., Yang, X., and Ching, C-B. (2007). Polymorphism and crystallization of famotidine. Cryst. Growth Des. 7(9): 1590-1598.

Maruyama, S. and Ooshima, H. (2000). Crystallization behavior of taltirelin polymorphs in a mixture of water and methanol. J. Cryst. Growth 212(1-2): 239-245.

Mathieson, A. M. (1952). The crystal structures of the dimorphs of DL-methionine. Acta Cryst. 5: 332-341.

Matsunaga, J., Nambu, N., and Nagai, T. (1976). Polymorphism of phenylbutazone. Chem. Pharm. Bull. 24(6): 1169-1172.

Matsuoka, M., Yamanobe, M., Tezuka, N., Takiyama, H. and Ishii, H. (1999). Polymorphism, morphologies and bulk densities of DL-methionine agglomerate crystals. J. Cryst. Growth 198-199: 1299-1306.

Miyazaki, S., Arita, T, Hori, R., and Ito, K. (1974). Effect of polymorphism on the dissolution behavior and gastrointestinal absorption of chlortetracycline hydrochloride. Chem. Pharm. Bull. 22(3): 638-642.

Mohan, R., Koo, K-K., Strege, C., and Myerson, A. S. (2001). Effect of additives on the transformation behavior of L-phenylalanine in aqueous solution. Ind. Eng. Chem. Res. 40(26): 6111-6117.

Mullin, J. W. (2001). Crystallization (4th ed.). Oxford: Butterworth-Heinemann.

Nordström, F. L. and Rasmuson, Å. C. (2006). Polymorphism and thermodynamics of m-hydroxybenzoic acid. Eur. J. Pharm. Sci. 28(5):377-384.

Ono, T., ter Horst, J. H., and Jansens, P. J. (2004). Quantitative measurement of the polymorphic transformation of L-glutamic acid using in-situ Raman spectroscopy. Cryst. Growth Des. 4(3): 465-469.

Picciochi, R., Diogo, H. P., Minas da Piedade, M. E. (2011). Thermodynamic characterization of three polymorphic forms of piracetam. J. Pharm. Sci. 100(2): 594-603.

Ramachandran, E. and Natarajan, S. (2006). Gel growth and characterization of β-DL-methionine. Cryst. Res. Technol. 41(4): 411-415.

Roelands, C. P. M. (2005). Polymorphism in Precipitation Process. Ph.D. thesis, Delft University of Technology, The Netherlands.

Roelands, C. P. M., Jiang, S., Kitamura, M., ter Horst, J. H., Kramer, H. J. M., and Jansens, P. J. (2006). Antisolvent crystallization of the polymorphs of L-histidine as a function of supersaturation ratio and of solvent composition. Cryst. Growth Des. 6(4): 955-963.

Schmidt, A. C. (2005). Solid-state characterization of chloroprocaine hydrochloride: part VI. Crystal polymorphism of local anaesthetic drugs. J. Therm. Anal. Cal. 81(2): 291-297.

Shaibat, M. A., Casabianca, L. B., Siberio-Pérez, D. Y., Matzger, A. J., and Ishii, Y. (2010). Distinguishing polymorphs of the semiconducting pigment copper phthalocyanine by solid-state NMR and Raman Spectroscopy. J. Phys. Chem. B 114(13): 4400–4406.

Takayama, K., Nambu, N., and Nagai, T. (1980). Dissolution kinetics for coprecipitates of indomethacin with polyvinylpyrrolidone. Chem. Pharm. Bull. 28(11): 3304-3309.

Taniguchi, T., Takaki, Y. and Sakurai, K. (1980). The crystal structures of the α and β forms of DL-methionine. Bull. Chem. Soc. Jpn. 53(3): 803-804.

Threlfall, T. (2003). Structural and thermodynamic explanations of Ostwald's rule. Org. Process Res. Dev. 7(6): 1017-1027.

Umeda *et al*. (1984). Kinetics of the thermal transition of carbamazepine polymorphic forms in the solid state. Yakugaku Zasshi 104(7): 786-792.

Urakami, K., Shono, Y., Higashi, A., Umemoto, K., and Godo, M. (2002). A novel method for estimation of transition temperature for polymorphic pairs in pharmaceuticals using heat of solution and solubility data. Chem. Pharm. Bull. 50(2): 263-267.

Vippagunta, S. R., Brittain, H. G., and Grant, D. J .W. (2001). Crystalline solids. Adv. Drug Del. Rev. 48(1): 3-26.

Yamanobe, M., Takiyama, H., and Matsuoka, M. (2002a). Kinetic study on polymorphic solid-state transformation of organic compound: Bisphenol A and DL-methionine. J. Chem. Eng. Jpn. 35: 247-254.

Yamanobe, M., Takiyama, H., and Matsuoka, M. (2002b). FT-IR study on the effect of solvents on polymorphic crystallization of organic compounds. J. Chem. Eng. Jpn. 35(6): 569-573.

Yamanobe, M., Takiyama, H., and Matsuoka, M. (2002c). Polymorphic transformation of DL-methionine crystals in aqueous solutions. J. Cryst. Growth. 237-239: 2221-2226.

Yamanobe-Hada, M., Ito, A., and Shindo, H. (2005). Study of spontaneous cleavage and change in surface structure of DL-methionine crystals. J. Cryst. Growth. 275(1-2): e1739-e1743.

Yu, L., Reutzel, S. M., and Stephenson, G. A. (1998). Physical characterization of polymorphic drugs: An integrated characterization strategy. Pharm. Sci. Technol. Today 1(3): 118-127.

Chapter VI

Crystal growth rates and secondary nucleation threshold for γ-DL-methionine in aqueous solution [Published in J. Crystal Growth©]

6.1 Abstract

The secondary nucleation threshold (SNT) of γ-DL-methionine (DL-met) in aqueous solution was measured for the temperature range 10 to 61 ºC. The width of the SNT is weakly temperature dependent with slightly smaller induction times at higher temperatures. Seeded batch crystallizations of γ-DL-met were performed isothermally at 10, 25, and 40 ºC in an agitated batch crystallizer, and within the SNT region to avoid nucleation. The effect of the initial supersaturation and seed mass on crystal growth were also studied at 25 ºC. The initial growth rate (during the first 20 minutes of the batch) is significantly higher than subsequent crystal growth, a phenomenon previously seen with other species. The measured growth rates are independent of seed mass, as expected, for the usable portion of the growth rate data. The growth rates were found to linearly depend on the relative supersaturation of the total DL-met in the system. The growth rate constants increase with increasing temperature and follow an Arrhenius relationship. The growth kinetics of the γ-DL-met will be used to study in order to begin characterization of the polymorphic transformations and the overall crystallization rate of DL-met.

6.1 Introduction

Polymorphism occurs when a compound can exist in more than one crystalline form (Grant, 1999). These crystalline forms contain the same molecules but have a different arrangement of molecules within the crystalline lattice. Polymorphs can have different mechanical, thermal, physical, and chemical properties, which greatly influence their suitability for a wide variety of uses, particularly for pharmaceutical products, and affects their suitability for further processing.

Crystallization processes where polymorphs may form consist of competitive nucleation, crystal growth, and the transformation from the metastable to the stable form. In most cases the most important factor for the control of polymorphic crystallization is the nucleation process. However, the mechanism of each elementary step in the crystallization process needs to be clear in relation to the operational conditions in order to selectively crystallize polymorphs. The most important process in crystallization of polymorphs is

solution-mediated transformation (SMT) which consists of the dissolution of the metastable form and the growth of the stable form (Kitamura, 2009).

The crystal growth process is described by two successive mechanisms, mass transfer (by diffusion or convection) of solute molecules from the bulk solution to the crystal surface and integration of solute molecules into the surface (a reaction step) (Randolph and Larson, 1988). Crystals can grow without significant birth of new crystals (nuclei) in a metastable zone which is often exhibited by supersaturated solutions. When the supersaturation is sufficiently high, secondary nucleation in the presence of prior crystals occurs; the limit of this regime is referred to as the metastable limit for secondary nucleation (Srisa-nga *et al.*, 2006) or the secondary nucleation threshold, depending on the method of measurement. The secondary nucleation threshold (SNT) is the upper limit of the metastable zone with regard to secondary nucleation. Nucleation is typically avoided or minimized in crystallization processes because it is difficult to control and gives a bad product size distribution. In batch processes the operation is usually undertaken in the metastable zone, and crystallization is initiated through the addition of seed crystals, thus avoiding large amounts of nucleation.

DL-methionine (DL-met) is an essential amino acid in the human diet, and is also used as dietary component in poultry and animal feeds. It is also used in active pharmaceutical ingredients, and as a precursor to other amino acids. DL-met has previously been shown to exhibit polymorphism and exists in the solid phase as α-DL-met, β-DL-met, and γ-DL-met (Mathieson, 1952; Matsuoka *et al.*, 1999). α-DL-met and β-DL-met forms are almost equally stable (Mathieson, 1952), and the crystal structures of each polymorph are known (Taniguchi *et al.*, 1980). Single crystals of both forms were grown from an ethanol-water solution by slow evaporation and occur as soft plates. β-DL-met was discovered accidentally while attempting to grow α-DL-met crystals of greater plate thickness. Moreover, α-DL-met crystals can be obtained by the reaction crystallization of aqueous solutions of sodium methioninate (Na-met) using liquid acids such as hydrochloric, acetic, nitric, sulfuric, or formic acids (Matsuoka *et al.*, 1999). Matsuoka *et al.* reported the third polymorph, γ-DL-met, as well as its preparation method and crystal structure. γ-DL-met crystals were obtained by reaction crystallization of aqueous solutions of Na-Met with a solid benzoic acid, or by cooling crystallization of aqueous solutions of DL-met.

The transformation of DL-met crystals in solution has been reported to consist of the solid-state transformation (SST) of γ-DL-met to α-DL-met in the charged crystals and

solvent-mediated transformation (SMT) of α-DL-met to γ-DL-met which is caused by the dissolution of α-DL-met and crystal growth of γ-DL-met (Yamanobe *et al.*, 2002). This indicates that the crystallization kinetics (particularly dissolution of α-DL-met and growth of γ-DL-met) for the polymorphs produced also have to be studied in order to characterize the phase transformation in the system.

There is no published data on the SNT and crystal growth kinetics of γ-DL-met in aqueous solution. Therefore, in the present study the growth rate of the γ-DL-met in aqueous solution was measured to attempt to begin to characterize the polymorphic transformation in solution. The SNT of this system was determined to ensure that the system is operated under convenient non-nucleating conditions.

6.2 Materials and methods

6.2.1 Materials

DL-met (>99%, Acros Organics) and deionized water were used to prepare the supersaturated solution in all experiments. γ-DL-met was prepared by cooling crystallization of aqueous solutions of DL-met as follows. DL-met (21 g) was dissolved in 350 mL of water in a 0.5-L batch crystallizer maintained above 60 ºC. This solution was continuously agitated by an overhead stirrer at 300 rpm, and the solution was cooled and maintained at 25 ºC, after which the crystals were removed and filtered. Since these crystals were too large for use as seed crystals a further crystallization was performed. The solution at 25 ºC was heated to 30 ºC, then cooled to 5 ºC and held at this temperature for 24 h. After 24 h, the suspension was filtered, washed, and dried. γ-DL-met was identified using X-ray powder diffractometry (Bruker axs, D5005). The pure γ-DL-met crystals were sieved, and the cut between 180 and 250 μm was used as seeds for crystal growth rate measurement.

6.2.2 Secondary nucleation threshold measurement

Secondary nucleation threshold experiments were performed at 10, 25, 40, and 61 ºC in a 0.5-L batch crystallizer for a range of supersaturated solutions containing γ-DL-met seed crystals using a method similar to that of Srisa-nga *et al.* A series of supersaturated solutions were prepared and heated to 20 ºC above the experimental temperature for 30 to 40 min to ensure that no ghost nuclei remained in the solution. Approximately 3 mg of sieved γ-DL-met crystals, 75-105 μm in size, was added to each solution to induce

secondary nucleation. Nucleation was observed by the naked eye at particular time intervals, with nucleation being indicated by precipitation or clouding due to the very fine nuclei particles. The clouding occurring in the experiments was clearly visible and the distinction between solutions that had precipitated at a particular measurement time and those that had not was clear. The highest concentration solution that had not nucleated at a particular time and the lowest concentration that had nucleated were both recorded. All experiments were duplicated to check reproducibility.

6.2.3 Crystal growth rate measurement

The growth kinetics of γ-DL-met were studied via seeded batch desupersaturation experiments using time dependent measurements of both particle size distributions (PSDs) and solute concentrations (Scholl, 2006; Garside *et al.*, 2002). Experiments were performed at 10, 25, and 40 ºC in a 0.5-L batch crystallizer agitated at 350 rpm by an overhead stirrer, and performed within the SNT region to avoid nucleation. The solute concentration in the clear liquor was measured periodically using dry substance determination (Garside *et al.*, 2002), and the PSD of crystalline samples was measured using a Malvern Mastersizer/E (Malvern Instrument, Mastersizer S). Volume percent distributions were converted mathematically to number density distributions in order to determine the number mean growth rate of the crystals, which is most suitable for use in population balance modeling. Nucleation was not detected in any seeded batch crystallization for growth determination. Growth rate was determined as the time rate of change of the number mean crystal size.

De-supersaturation experiments were performed on supersaturated solutions within the SNT region that had previously been heated to 20 ºC above the experimental temperature for 30 to 40 min to ensure that no ghost nuclei remained in the solution. The solutions were then cooled to the experimental temperature, after which a quantity of dry seeds were fed to the crystallizer. A small volume of the suspension was sampled at particular times during the batch to determine the PSDs and solute concentration. All experiments were duplicated to determine reproducibility.

6.3 Results and discussion

6.3.1 Secondary nucleation threshold

The effect of induction time on the measured SNT at different temperature is shown in Figure 6.1. In this figure the upper point on each vertical line represents the

lowest absolute supersaturation that had nucleated and the lower point represents the highest absolute supersaturation that had not nucleated. This means that the true value of the SNT must lie between these two points. The mean value of these two points is an approximation for the true SNT at this experimental time. This figure shows the time dependence of the SNT, with the SNT decreasing as the induction time increases. In terms of absolute supersaturation, initial time SNT are about 11.8 g of DL-met/kg of water for 10 and 25 ºC, and 12.1 g of DL-met/kg of water for 40 and 61 ºC. At large induction times, greater than 50 h, the SNT is about 3.2 g of DL-met/kg of water for 10 and 25 ºC, and 2.2 g of DL-met/kg of water for 40 and 61 ºC. After 2 days there were still some solutions of low supersaturation which had not nucleated.

Since the SNTs at temperatures of 10 and 25, and 40 and 61 ºC do not overlap when plotted in terms of absolute value of supersaturation, the induction time dependence of the SNT were plotted separately. This indicates that temperature has an effect on the SNT over the range of temperatures that DL-met is likely to be crystallized.

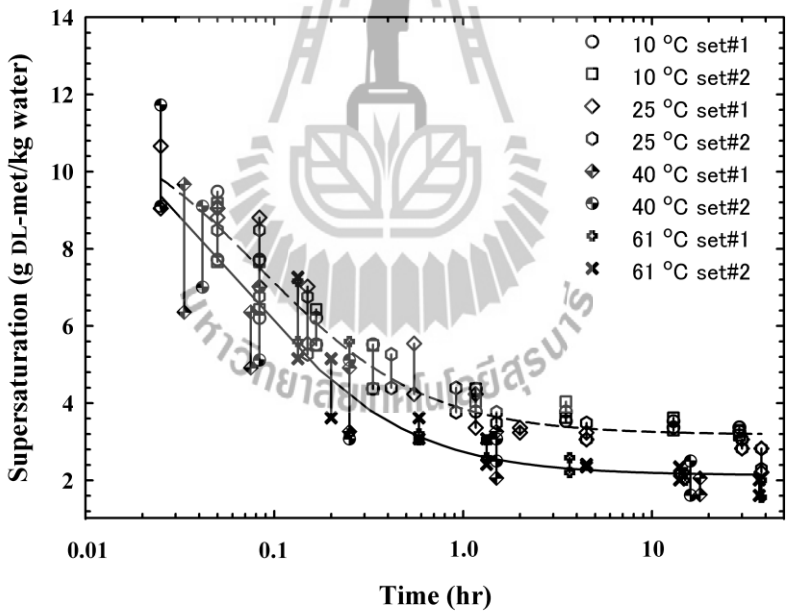

Figure 6.1 The time dependence of the secondary nucleation zone width based on DL-met concentrations at temperatures of 10, 25, 40 and 61 ºC. The dashed line represents the model for data at 10 and 25 ºC. The solid line represents the model for 40 and 61 ºC.

The data in Figure 6.1 were fitted with a hyperbolic decay with three parameters. Eqs. (6.1) and (6.2) show the fitted equations, where *C* represents the total DL-met concentration

(g of DL-met/kg of water) for the SNT, C^* is the solubility, and t_{ind} is the observation time in hours.

$$C - C^* = 3.1828 + \frac{0.7266}{0.0845 + t_{ind}} \qquad \text{(For 5 ºC < T < 40 ºC} \qquad (6.1)$$

$$C - C^* = 2.1287 + \frac{0.6519}{0.0651 + t_{ind}} \qquad \text{(For 40 ºC < T < 70 ºC)} \qquad (6.2)$$

The solubility data of α-DL-met and γ-DL-met in the temperature range of 5 to 70 ºC has been measured previously (Wantha and Flood, 2009) and is plotted as a function of temperature in Figure 6.2. The solubility of γ-DL-met (g of DL-met/kg of water) was fitted using a cubic polynomial with the result shown in Eq. 6.3, where T represents the experimental temperature in ºC.

$$C^* = 18.23 + 5.053\times10^{-1}T + 2.436\times10^{-3}T^2 + 8.410\times10^{-5}T^3 \qquad (6.3)$$

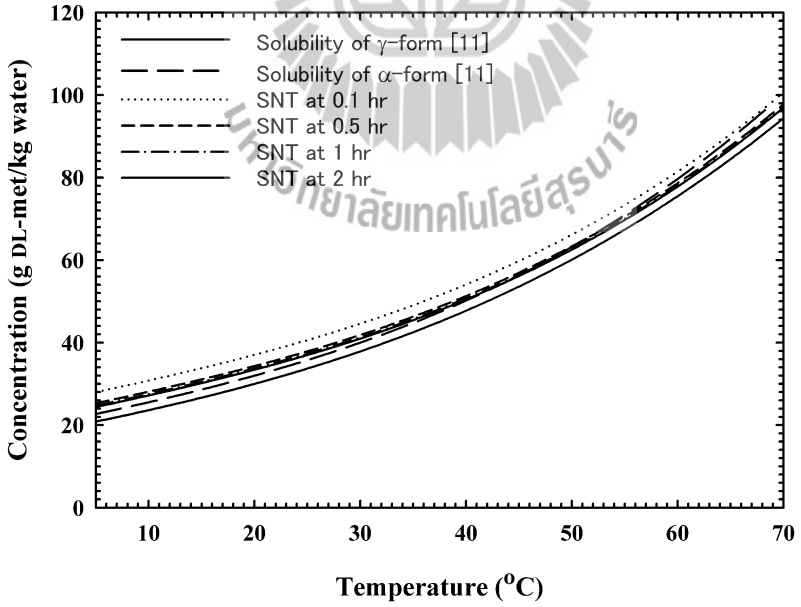

Figure 6.2 Secondary nucleation thresholds for γ-DL-met at operating times of 0.1, 0.5, 1.0, and 2.0 hr.

Substitution of Eq. (6.3) into Eq. (6.1) gives the SNT concentration as a function of time between 5 ºC and 40 ºC, and substitution of Eq. (6.3) into Eq. (6.2) gives the SNT concentration as a function of time between 40 ºC and 70 ºC.

The induction time dependence of SNT of γ-DL-met in aqueous solution is shown in Figure 6.2. SNT shows limitations on either the operating concentration or the batch time to ensure that nuclei are not formed, so it is very important for control of seeded batch crystallizations. For example, when the crystallization is performed at 25 ºC and the operating time is within 1 h, the initial concentration that can operate without a significant birth of new crystals is up to 37 g of DL-met/kg of water.

The SNT of α-DL-met was not measured in this work since experiments were performed in regions where only the γ-form will nucleate. The SNT technique used by Lu *et al.* is appropriate for the metastable form. However, growth experiments for the α-form can only be performed within the area between the SNT of γ-DL-met and the solubility of α-DL-met. This is reasonable for the temperature range 5 to 35 ºC.

3.2 Crystal growth kinetics

An example of PSDs from a batch run at 25 ºC is shown in Figure 6.3. The PSD is plotted on a log-scale to show that the volume-based PSD is a log-normal distribution, and hence appears as a normal distribution on a log-scale. Photomicrographs of seed crystals and product crystals from a batch run at 25 ºC were also analyzed. These indicated that there is no nucleation occurring during the growth process because there is only one peak in the PSD and no particles smaller than the seed crystals. PSDs of product crystals are uniform, which lead to a good product quality.

The morphology of γ-DL-met is thin rod-like, prism-like, or plate-like having a hexagonal cross section (Matsuoka *et al.*, 1999; Yamanobe *et al.* 2005). For this study the shape of the seed crystals (γ-DL-met crystals) obtained from an aqueous solution is plate-like having a hexagonal cross section, but the shape is not perfect. After the growth process the morphology of the crystals has not changed, but the shape is more perfect than the seed crystals. This means that there is no phase transformation during the growth of the γ-DL-met crystals in aqueous solution. Similar results are seen at all experimental temperatures (10, 25, and 40 ºC), which indicates that γ-DL-met is the stable polymorphic form at these temperatures. The improved shape and features of the product crystals show that correct operation of the batch can lead to improved product quality.

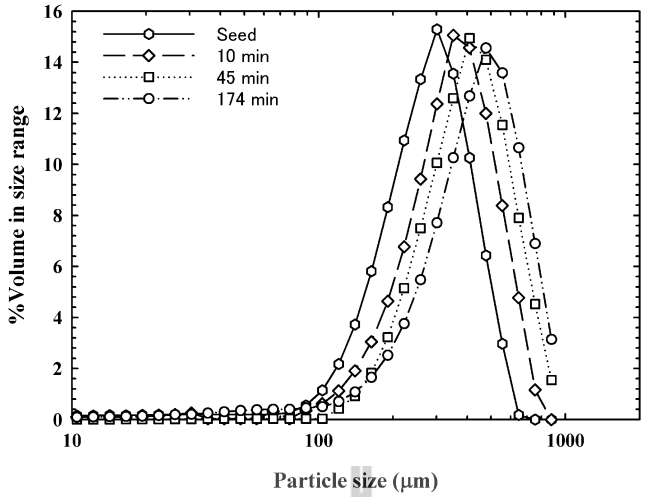

Figure 6.3 Particle size distributions of seed and product crystals from a batch run at 25 ºC and $\sigma_0 = 0.11$.

A log-normal volume-based PSD indicates that the number distribution is also log-normal with the same geometric standard deviation (Allen, 1997). The number mean size may then be calculated from the following equation:

$$\ln x_{NL} = \ln x_{mV} - 2.5 \ln^2 \sigma_g \tag{6.4}$$

where x_{NL} is the number mean crystal size, x_{mV} is the median of the volume distribution, and σ_g is the geometric standard deviation of the volume distribution. The PSDs of this work were confirmed by discretizing the volume density distribution into small elements (of 1 μm width), and calculating the number of particles in each element and number mean crystal size. The geometric standard deviation of the volume distribution was constant over the time period of the experiment, indicating common history seed (Srisa-nga *et al.*,2006). The mean growth rate was determined as the time rate of change of the number mean crystal size. The growth rate was calculated directly from the slope of a plot between the number mean crystal size and time of each measurement. Figure 6.4 is an example of this plot.

Figure 6.4 also shows the batch crystallization profiles for the condition of 0.5 g of γ-DL-met seed crystals having an average size of approximately 178 μm, with the crystallization temperature being 25 ºC and for initial relative supersaturations (σ) equal to

0.09 and 0.11. Figure 6.4 shows that an increase in the initial supersaturation results in an increase final crystal sizes. This is since the higher solute concentration in excess of the solubility leads to a higher amount of solute addition onto the same seed mass. In addition, experiments varying the seed mass show that an increase of the total seed surface leads to a faster decrease in supersaturation, and smaller final crystal sizes. This is since the higher seed surface area results in an increased solid integration rate through crystal growth. The higher seed mass leads to a smaller final crystal sizes since the same amount of solute is added to a larger number of seed crystals. The de-supersaturation rate increases with increasing temperature since the integration of solute into the crystal surface increases with increasing temperature.

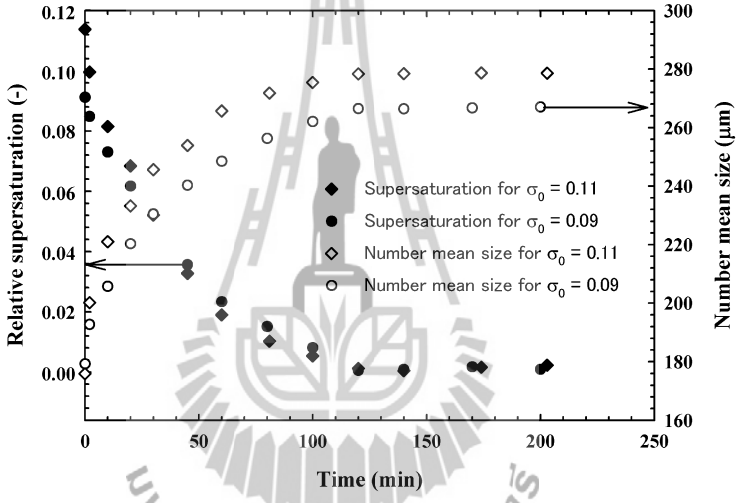

Figure 6.4 Desupersaturation curves and time dependence of crystal sizes from a batch run at 25 ºC with different initial supersaturations.

The growth rates were calculated using the number mean crystal size. The crystal growth experiments allowed growth kinetics to be determined as a function of relative supersaturation, as shown in Figures 6.5 and 6.6. It can be seen that, at constant temperature, the growth rates increase with increasing supersaturation. The results of the experiments with different initial supersaturation (Figure 6.5) agree very well for all but the first three data points of each experiment, where there were different growth rates predicted for the same supersaturation value. Also the results of the experiments with different seed mass (Figure 6.6) agree very well for all but at early periods of the experiment, where there is some differences between data for different seed masses.

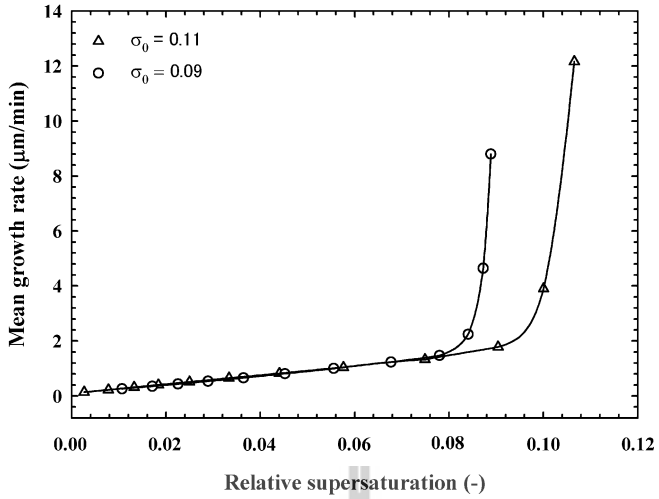

Figure 6.5 Mean crystal growth rates for γ-DL-met as a function of relative supersaturation at 25 ºC with different initial supersaturations.

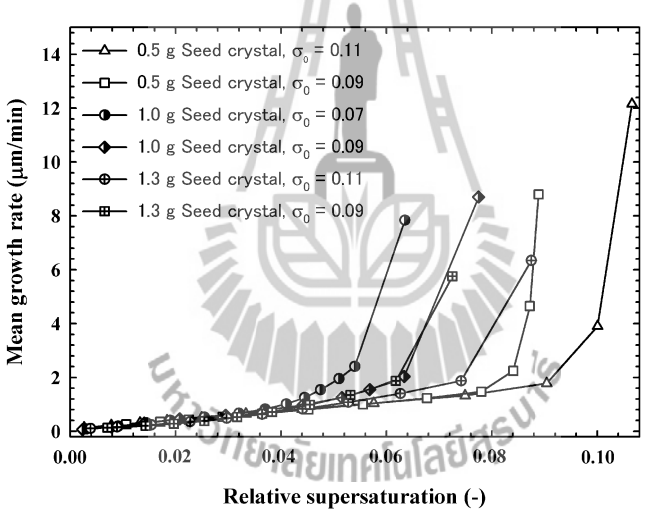

Figure 6.6 Mean crystal growth rates for γ-DL-met as a function of relative supersaturation at 25 ºC with different seed masses.

The explanation for the difference between the growth rates at early periods of the experiment is unknown, although this has been noted earlier many other species, with the phenomenon initially being seen for fructose (Flood *et al.*1996). Many explanations have been proposed for this behavior including: initial fast crystal growth as seed crystals repair their surface; later crystal growth being slowed by slow surface adsorption of impurity molecules (Flood *et al.*1996); and the effect of growth rate history on the crystal surface (Pantaraks and Flood, 2005; Pantaraks et al., 2007; Promraksa *et al.*, 2009; Flood, 2010).

The unusually high growth rates during the early period of all experiments were ignored in subsequent analysis of crystallization kinetics. The growth kinetics can be described for each set of conditions by the power-law model (Myerson *et al.* 2002):

$$\overline{G} = K_G \sigma^n \tag{6.5}$$

where $\overline{G}$ is the mean growth rate in μm/min, K_G is the growth rate constant in μm/min, σ is relative supersaturation, and n is the growth rate order. The experimental data were fitted using Eq. 6.5, with the result shown in Figure 6.7. The resulting equations show that the growth rate order is unity for all conditions. The values of growth rate constant (K_G) obtained from linear regression of the experimental data (Figure 6.7) are 10.39, 18.87, and 27.83 μm/min respectively for 10, 25, and 40 °C. This indicates that the growth rate constant is strongly temperature dependent. The growth rate constant can be modeled by Arrhenius relationship of the form (Mullin, 2001):

$$K_G = k_G \exp\left[\frac{-E_G}{RT}\right] \tag{6.6}$$

where E_G is the activation energy of growth in kJ/mol, T is temperature in K, and R is the ideal gas constant (8.314 J/mol/K). The results (Figure 6.8) indicate an activation energy of growth for γ-DL-met of 24.26 kJ/mol.

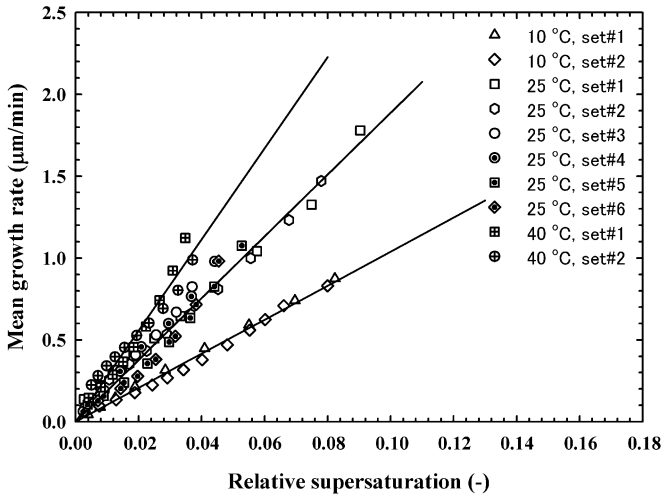

Figure 6.7 Mean crystal growth rates of γ-DL-met as a function of relative supersaturation and temperature.

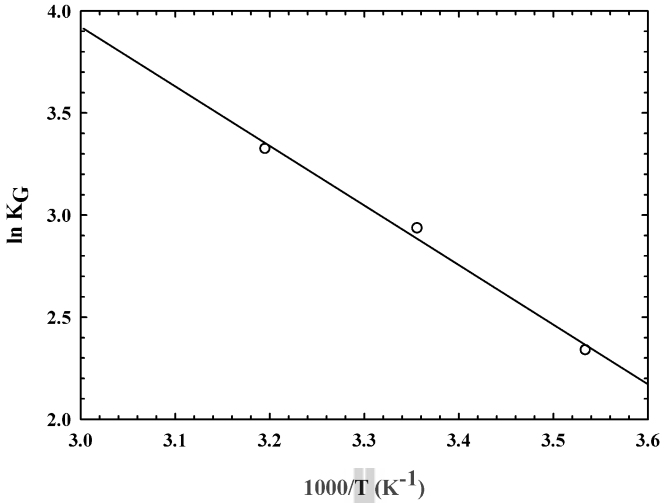

Figure 6.8 An Arrhenius plot of the growth rate constant for DL-met for determination of the activation energy of crystal growth.

The value of the growth rate order is very important in understanding the controlling mechanism. In general a growth rate order of n = 1 indicates that mass transfer becomes more important as a rate controlling mechanism and a growth rate order between 1 and 2 indicate that the surface integration step is more pronounced (Mullin, 2001). In the case of γ-DL-met growth at all temperature studied, with growth rate order of 1, indicates that the mass transfer process plays an important role in explaining the growth process.

Further work needs to be performed in order to characterize both the crystal growth and dissolution kinetics of the α-form of DL-met, and also the nucleation rates of the two polymorphs in order to fully characterize the phase transitions in the system.

6.4 Conclusions

The SNT of γ-DL-met in aqueous solution decreases with increasing induction time. The SNT in these measurement units is temperature independent for all induction times. The crystallization of γ-DL-met from aqueous solution should be operated within the SNT region if nucleation is to be avoided. The initial growth rate (at higher supersaturation) is significantly higher than subsequent crystal growth (at lower supersaturation). During the early periods of the experiments there were much larger growth rates than would be expected from extrapolation of the data determined during the later time periods. This is due to the effect of the growth history on the crystal surface, with crystals grown more

quickly at higher supersaturation having a rougher surface on a microscopic level than the seed crystals they were grown from. The crystal growth rate orders are 1, and the growth rate constants are temperature dependent and follow an Arrhenius relationship with an activation energy of 24.26 kJ/mol. Further crystal nucleation, growth and dissolution experiments will be performed on the α-form. This should allow a complete model of the SMT between the polymorphs to be achieved.

References

Grant, D.J.W. Theory and Origin of Polymorphism, in: H.G. Brittain (Ed.), Polymorphism in Pharmaceutical Solids, Drugs and the Pharmaceutical Sciences Vol. 95, Marcel Dekker, New York, 1999, pp1–34.

Kitamura, M. Strategy for control of crystallization of polymorphs, CrystEngComm. 11 (2009) 949–964.

Randolph, A.D., Larson, M.A. Theory of Particulate Processes: Analysis and Techniques of Continuous Crystallization, second ed., Academic Press, California, 1988.

Srisa-nga, S., Flood, A.E., White, E.T. The secondary nucleation threshold and crystal growth of α-glucose monohydrate in aqueous solution, Cryst. Growth Des. 6 (2006) 795–801.

Mathieson, A.M. The crystal structures of the dimorphs of DL-methionine, Acta Cryst. 5 (1952) 332–341.

Matsuoka, M. Yamanobe, M., Tezuka, N. Takiyama, H. Ishii, H. Polymorphism, morphologies and bulk densities of DL-methionine agglomerate crystals, J. Cryst. Growth 198-199 (1999) 1299–1306.

Taniguchi, T. Takaki, Y. Sakurai, K. The crystal structures of the α- and β-forms of DL-methionine, Bull. Chem. Soc. Japan 53 (1980) 803–804.

Yamanobe, M. Takiyama, H. Matsuoka, M. Polymorphic transformation of DL-methionine crystals in aqueous solution, J. Cryst. Growth 237-239 (2002) 2221–2226.

Schöll, S. Nucleation, growth, and solid phase transformations during precipitation processes, Ph.D. Thesis, Swiss Federal Institute of Technology Zurich, Zurich, Switzerland, 2006.

Garside, J. Mersmann, A. Nyvlt, J. Measurement of crystal growth and nucleation rates, second ed., Institute of Chemical Engineering, UK, 2002.

Wantha, L., Flood, A.E. Thermodynamics and kinetics of crystallization of the polymorphs of DL-methionine, in: M. Louhi-Kultanen, H. Hatakka (Eds.), Proceedings of the 16th International Workshop on Industrial Crystallization: BIWIC 2009, Lappeenranta University of Technology, Finland, 2009, pp. 173–180.

Lu, J., Wang, X-J., Yang, X., Ching, C-B. Polymorphism and crystallization of famotidine, Cryst. Growth Des. 7 (2007) 1590–1598.

Yamanobe-Hada, M., Ito, A., Shindo, H. Study of spontaneous cleavage and change in surface structure of DL-methionine crystals, J. Cryst. Growth 275 (2005) e1739–e1743.

Allen, T. Particle size measurement: Volume 1 Powder Sampling and Particle Size Measurement, fifth ed., Chapman&Hall, London, 1997.

Flood, A.E. , Johns, M.R., White, E.T. Crystal growth rates and dispersion for D-fructose from aqueous ethanol, AIChE J. 46 (2000) 239–246.

Pantaraks, P., Flood, A. E. Effect of growth rate history on current crystal growth: A second look at surface effects on crystal growth rates, Cryst. Growth Des. 5 (2005) 365–371.

Pantaraks, P., Matsuoka, M., Flood, A.E. Effect of growth rate history on current crystal growth. 2: Crystal growth of sucrose, $KAl(SO_4)_2{\cdot}12H_2O$, KH_2PO_4, and K_2SO_4, Cryst. Growth Des. 7 (2007) 2635–2642.

Promraksa, A., Flood, A. E., Schneider, P. A. Measurement and analysis of the dextran partition coefficient in sucrose crystallization, J. Cryst. Growth 311 (2009) 3667-3673.

Flood, A. E. Feedback between crystal growth rates and surface roughness, CrystEngComm 12 (2010) 313–323.

Myerson, A. S., Ginde, R. Crystals, crystal growth, and nucleation, in: A.S. Myerson (Ed.), Handbook of Industrial Crystallization, second ed., Butterworth-Heinemann, USA, 2002, pp33–65.

Mullin, J.W. Crystallization, fourth ed., Butterworth-Heinemann, Oxford, 2001.

Chapter VII

Growth and dissolution kinetics of α and γ polymorphs of DL-methionine [Published in J. Crystal Growth©]

7.1 Abstract

Growth kinetics of the two common polymorphs of DL-methionine (DL-met), α-DL-met and γ-DL-met, and dissolution kinetics of γ-DL-met, were studied in aqueous solution as part of an attempt to complete an *a-priori* model of the solution-mediated transformation (SMT) of polymorphs in this system, which will then be compared to measured rates of polymorph transformation. The growth rates of α-DL-met and γ-DL-met were found to be linearly dependent on the relative supersaturation of DL-met in the system. The dissolution rate of γ-DL-met was found to linearly depend on the relative undersaturation of DL-met in the system. Both the growth and dissolution rate constants are temperature dependent and follow an Arrhenius relationship. At all temperatures studied, both the growth rate of α-DL-met and the dissolution rate of γ-DL-met are faster than the growth rate of γ-DL-met, indicating that if the dissolution is a diffusion controlled process, then the SMT of the polymorphs of DL-met is likely to be controlled by the growth rate of γ-DL-met.

7.2 Introduction

Crystallization processes which include transformation of polymorphs consist of the competitive nucleation and crystal growth of the polymorphs, and the transformation from the metastable form to the stable form, usually via a solution-mediated transformation (SMT), which consists of the nucleation and crystal growth of the stable form and the dissolution of the metastable form. To understand and control polymorph formation, the mechanism of each elementary step in the crystallization process needs to be understood and be able to be modeled for inclusion in crystal population balances for each polymorph involved in the transformation.

Crystal growth from solution is a two step process (Randolph and Larson, 1988). The first step is the mass transfer (by diffusion and/or convection) of solute molecules from the bulk solution to the surface of the growing crystal. The second step is the adsorption of solute molecules to the surface of the crystal, and integration of the adsorbed molecules into the crystal lattice if they find a suitable integration site via a surface diffusion mechanism before they desorb. The growth rate depends on the level of driving force for crystal growth, which

is the supersaturation. Crystals can grow without significant birth of new crystals (nuclei) in a region which lies between the saturation and nucleation limits, called the metastable zone, which is time dependent.

Dissolution has traditionally been considered as a one step process which is diffusion controlled. The dissolution rate depends on the level of the driving force for dissolution, which is the undersaturation.

DL-methionine (DL-met) is an essential amino acid which has previously been shown to exhibit polymorphism and exists in the solid phase as α-DL-met, β-DL-met, and γ-DL-met (Mathieson, 1952; Matsuoka *et al.*, 1999). The SMT of DL-met has been studied by Yamanobe et al. which showed that the transformation of α-DL-met to γ-DL-met occurs via the dissolution of α-DL-met and crystal growth of γ-DL-met. To improve understanding of the behavior of the polymorphic crystallization of DL-met, growth kinetics, dissolution kinetics, and nucleation kinetics need to be studied. The crystal growth rates of γ-DL-met have been reported in a previous study (Wantha and Flood, 2011), as have nucleation kinetics for γ-DL-met (Wantha and Flood, 2011b). In the present study, the growth and dissolution kinetics of α-DL-met and γ-DL-met were measured and analyzed using batch experiments containing substantial populations of crystals. Similar data can also be obtained using results from measurements in a small growth cell under a microscope (Dowling *et al.*, 2010; Han *et al.*, 2010) however this technique may be more time consuming if a large number of crystals are analyzed to obtain the extent of growth rate dispersion. The influence of the supersaturation and temperature on crystal growth, and undersaturation and temperature on dissolution, were investigated. The solubility data used for the calculation of supersaturation and undersaturation of the two polymorphs was from a recent study (Wantha and Flood, 2011). The results in the current article will be used with the results of the nucleation study in order to *a-priori* model the SMT of the methionine polymorphs with population balances, and compare the model to measured rates of transformation; this will be discussed in a later article. Previous research has shown that population balance models can be used to *fit* mechanistic models of nucleation, dissolution and growth in SMT systems, however it is also important to show how accurate the population balance models are when measured data are used to describe the fundamental mechanisms.

7.2 Materials and methods

7.2.1 Materials

DL-met (>99%, Acros Organics), NaOH (>97%, Carlo Erba), Na_2CO_3 (>99.5%, Carlo Erba), and HCl (37%, Carlo Erba) were used without further purification. Deionized water was used to prepare all solutions. Sodium methioninate (Na-met) was also required for acidic precipitations of DL-met to prepare α-DL-met. Aqueous solutions of Na-met were prepared by a method previously described (Huthmacher *et al.*, 2000). 50 g of DL-met and 13.5 g of NaOH were dissolved in 166.5 mL of water, with the addition of 20 g of Na_2CO_3. After mixing, solutions were stirred with a magnetic stirrer for 6 h, and about 150 mL of water was removed from the solution by distillation; the precipitate formed was separated by filtration over a hot (> 100 °C) 8 μm filter by a vacuum pump. The filtrate contained 71% sodium methioninate.

7.2.2 Preparation of the polymorphic forms of DL-met

α-DL-met was prepared using reaction crystallization of Na-met aqueous solutions as follows: concentrated HCl (37%) was fed slowly into diluted Na-Met aqueous solutions (80 mL of 71% Na-Met aqueous solution diluted by 40 mL of water) in a 250 mL glass beaker at 35 °C. The mixed solutions were continuously agitated by a centrally located four-blade impeller driven by an overhead stirrer at 300 rpm. The pH of the solutions reached the isoelectric point of DL-met (pH = 5.7-5.9) after the full amount of HCl was added. The resulting crystals were collected by filtration and dried over silica gel. γ-DL-met was prepared by cooling crystallization of aqueous solutions of DL-met, which has been described in a previous paper [5]. The seed of pure α-DL-met were obtained by collecting sieved crystals in the size range of 64 - 125 μm. The seed of pure γ-DL-met were obtained by collecting sieved crystals in the size ranges of 180 - 250 and 250 - 300 μm. Pure crystal polymorphs of each form were also characterized by X-ray powder diffractometry (XRPD) (Bruker axs, D5005).

7.2.3 Crystal growth and dissolution rates measurement

The growth kinetics of α-DL-met were studied via seeded batch desupersaturation experiments, as described in a previous paper (Wantha and Flood, 2011). The experiments were performed at 5, 15, and 25 ºC in a 0.5-L stirred glass crystallizer agitated by a centrally located four-blade impeller driven by an overhead stirrer at 350 rpm. Experiments were performed within the area between the secondary nucleation threshold (SNT) of γ-DL-met (the stable polymorph) and the solubility of α-DL-met, to avoid nucleation (Wantha and Flood, 2011). Concentration was measured periodically using dry substance determination (Garside *et al*., 2002), and the particle size distribution (PSD) of crystalline samples was

measured using a Malvern Mastersizer/S (Malvern Instrument, Mastersizer S). Volume percent distributions were converted mathematically to number density distributions in order to determine the number mean growth rate of the crystals, which is most suitable for use in population balance modeling (Wantha and Flood, 2011; Allen, 1997). Nucleation was not detected in any seeded batch crystallizations for growth rate determination. Growth rate was determined as the time rate of change of the number mean crystal size using a number of experiments using different seeds and different starting supersaturation values. Crystal growth rate at a particular supersaturation was measured to ±0.05 μm/min (95% confidence).

The dissolution experiments for γ-DL-met were studied using a similar method to the growth experiments, except the experiments were performed at 10, 25, and 40 ºC, and under the solubility of γ-DL-met. The dissolution rate at a particular undersaturation was measured to ±0.07 μm/min (95% confidence).

7.3 Results and Discussion

7.3.1 Growth and dissolution kinetics of the polymorphic forms

Examples of PSDs from dissolution and growth experiments at 25 °C are shown in Figures 7.1 and 7.2, respectively. The PSD is plotted on a log-scale to show that the volume-based PSD is a log–normal distribution, and hence appears as a normal distribution on a log-scale. Photomicrographs of seed crystals and product crystals from growth, and final crystals from dissolution experiments at 25 °C were also analyzed. The analysis showed that there is no nucleation occurring during the growth process because there is only one peak in the PSD and no particles smaller than the seed crystals. Good quality product crystals were obtained because these are uniform PSDs. The product crystals obtained from growth and the final crystals obtained from the dissolution processes showed only one peak, which indicates that the growth and dissolution rates can be easily calculated from the change of the mean crystal size. The product and final crystals were also examined by XRPD analysis. The XRPD patterns of the product and final crystals were the same as the seed crystals; this indicates that there was no phase transformation during the growth and dissolution processes during the relatively short batch times used. After the growth process of α-DL-met the concentration reaches the solubility of α-DL-met and then remains constant for some period of time. At this concentration α-DL-met starts to transform to γ-DL-met. Therefore the growth rate is measured from the time of seed addition until the concentration reaches the solubility of α-DL-met.

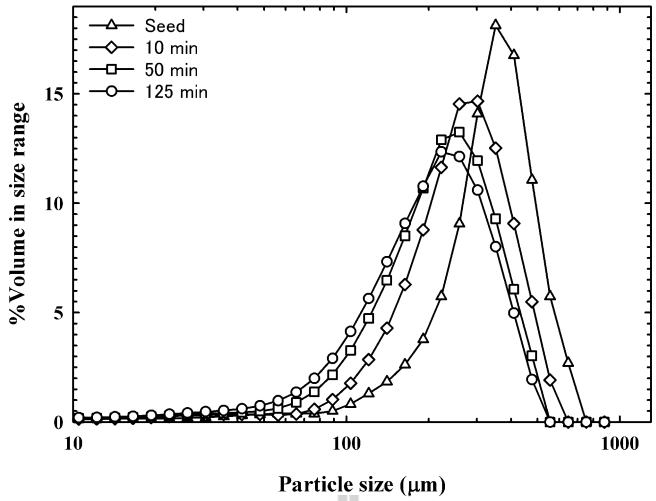

Figure 7.1 Particle size distributions of seed and final crystals from a dissolution experiment at 25 °C.

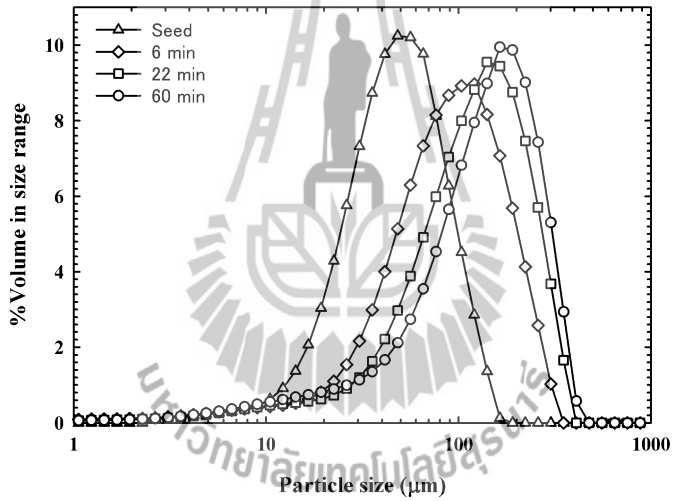

Figure 7.2 Particle size distributions of seed and product crystals from a growth experiment at 25 °C.

A log-normal volume-based PSD indicates that the number distribution is also log-normal with the same geometric standard deviation (Allen, 1997). The number mean crystal size was calculated using a method described in a previous paper (Wantha and Flood, 2011). The mean growth and dissolution rates were determined as the change of the number mean crystal size with time. The number-basis was used to calculate the growth rate because the growth rate data can only be obtained from batch growth using the population balance, which is a number-based balance. If other mean sizes (i.e. the volume or mass mean sizes) are used then the result is not suitable for use in the population balance, and therefore far less useful. The

growth and dissolution rates can calculated from the slope of the plot between the number mean crystal size and the time of each measurement, with these being correlated with the measured supersaturation at the same time point.

The crystals of α-DL-met prepared by precipitation of the aqueous solutions of Na-met produce crystals are small and partly aggregated, which makes them unsuited for determination of average dissolution rates. At the same undersaturation values used for γ-DL-met the α-DL-met crystals dissolved too quickly for the determination of the dissolution rate to any suitable accuracy, and the time rate of change in the mean size of the crystals changed to rapidly to measure. Where the undersaturation was small enough that dissolution was sufficiently slow the concentration is so close to the solubility of α-DL-met that the undersaturation cannot be predicted to sufficient accuracy. Hence, in the current study dissolution rates were measured using γ-DL-met seed crystals only.

In a preliminary model of the SMT the dissolution rates of α-DL-met and γ-DL-met as a function of undersaturation may be assumed to be the same based on the assumption that dissolution is a single step (diffusion controlled) process. A bulk diffusion controlled process does not depend on the crystal structure at the surface (since diffusion occurs in the liquid phase where the molecule does not occur in a polymorphic form). The assumption of common dissolution kinetics does not mean that the dissolution rates of the two forms will be the same at the same concentration of DL-met, however: the two forms will have different undersaturation levels for a particular value of the DL-met concentration, since they have a different solubility. There is currently some debate about whether dissolution is really a two-step process, and hence this assumption will be verified in later work. It is quite possible that this assumption is not sufficiently accurate; confirmation of the validity of this assumption can be demonstrated when SMT data for the transformation of α-DL-met to γ-DL-met is compared to the population balance model.

The crystal growth of either of the two polymorphs is a two step process (mass transfer to the surface of the crystal, and a reaction step which integrates the solute into the crystal surface) [1], and therefore the growth kinetics of the two forms will not be the same. The second step (solute integration into the lattice) depends on the characteristics of the surface of the crystal, and therefore on the crystal structure of the polymorph.

The crystal dissolution experiments allowed dissolution kinetics to be determined as a function of relative undersaturation and the dissolution rates of γ-DL-met increased linearly with increasing undersaturation, as expected. The crystal growth experiments allowed growth

kinetics to be determined as a function of relative supersaturation and the growth rates of α-DL-met also increased with increasing supersaturation. The initial growth rates of α-DL-met (the first one or two growth rate data points) are significantly higher than expected based on extrapolation of data from subsequent crystal growth measurements, as was found previously in the case of γ-DL-met (Wantha and Flood, 2011). This is due to the effect of the growth history on the crystal surface, with crystals grown more quickly at higher supersaturation having a rougher surface than the seed crystals they were grown (Pantaraks and Flood, 2005; Pantaraks et al., 2007; Promraksa *et al.*, 2009; Flood, 2010). A similar phenomenon was also found in the dissolution experiments of γ-DL-met; that is the initial dissolution rate of γ-DL-met at early periods of the experiment (at higher undersaturation) is significantly higher than would be expected from subsequent crystal dissolution (at lower undersaturation). This may be due to a change in the surface structure of the crystals as dissolution progressed; the seeds at the initial undersaturation may have a rougher surface (on a microscopic scale) than they had after a period of dissolution, leading to a small difference in thermodynamic stability due to the increased surface energy of the rougher crystals.

The growth rate of the seed crystal in the size range of 64 - 355 μm is size independent growth (Scholl *et al.*, 2007). The dissolution rate of two different sets of seed crystals, in the size ranges of 180 - 250 and 250 - 300 μm were measured at 25 °C to determine if any size dependence was found in the dissolution rate. The results showed that the dissolution rates of both seed sizes are the same. Therefore, when considering the transformation kinetics, the growth rate of α-DL-met (seed size: 64 - 125 μm), the dissolution rates of γ-DL-met (seed size: 250 - 300 μm), and the growth rate of γ-DL-met (seed size: 180 - 250 μm) [5] can be reasonably compared with each other.

The initial crystal dissolution and growth rates of all experiments were disregarded in subsequent analysis of crystallization kinetics. The growth and dissolution kinetics were described for each set of conditions by the power-law model [17, 18]

$$\overline{D} = K_D \sigma_D^m \tag{7.1}$$

$$\overline{G} = K_G \sigma_G^n \tag{7.2}$$

where $\overline{D}$ and $\overline{G}$ are the mean dissolution and growth rates in μm/min, respectively; K_D and K_G are the dissolution and growth rate constants in μm/min, respectively; σ_D and σ_G are the

relative undersaturation and supersaturation, respectively; *m* and *n* are the dissolution and growth rates orders, respectively. The experimental results of the dissolution of γ-DL-met and growth of α-DL-met were fitted with Eqs. (7.1) and (7.2), and the results are shown in Figures 7.3 and 7.4. The resulting equations show that the dissolution and growth rate order are unity for all conditions. The values of the dissolution and growth rate constants obtained from the linear regression of the experimental data are shown in Table 7.1.

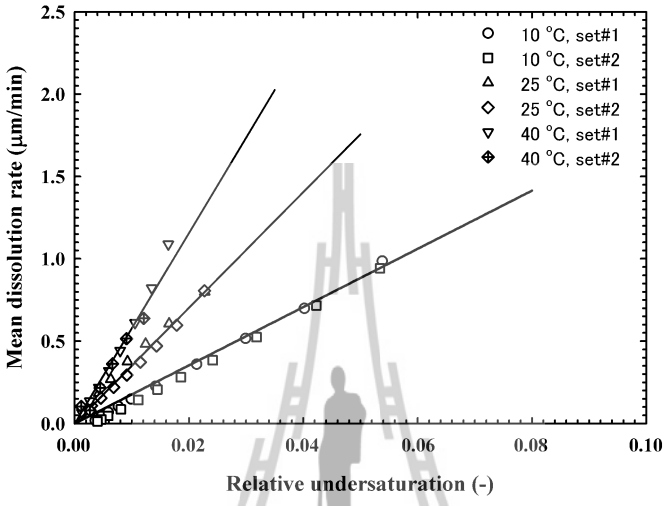

Figure 7.3 Mean dissolution rates of DL-met as a function of relative undersaturation and temperature.

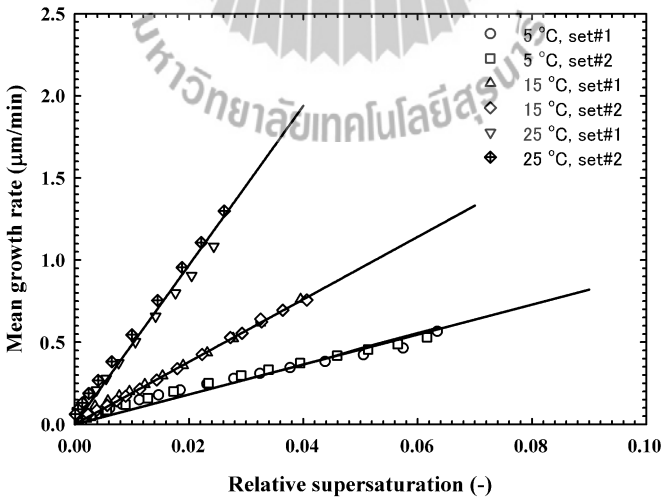

Figure 7.4 Mean crystal growth rates of α-DL-met as a function of relative supersaturation and temperature.

The results indicated that the dissolution and growth rate constants are strongly temperature dependent. The dissolution and growth rate constants can be modeled by Arrhenius relationship of the form (Gougazeh *et al*., 2009)

$$K_D = k_D \exp\left[\frac{-E_D}{RT}\right] \tag{7.3}$$

$$K_G = k_G \exp\left[\frac{-E_G}{RT}\right] \tag{7.4}$$

where E_D and E_G are the activation energies of dissolution and growth in J/mol, respectively; T is the temperature in K, and R is the ideal gas constant (8.314 J/mol/K). The dissolution rate constant of γ-DL-met and growth rate constant of α-DL-met were fitted with Eqs. (7.3) and (7.4), and the results are shown in Figure 7.5 together with the growth of γ-DL-met (Wantha and Flood, 2011). The values of activation energy of dissolution and growth obtained from the linear regression of the dissolution and growth rate constants are shown in Table 7.1.

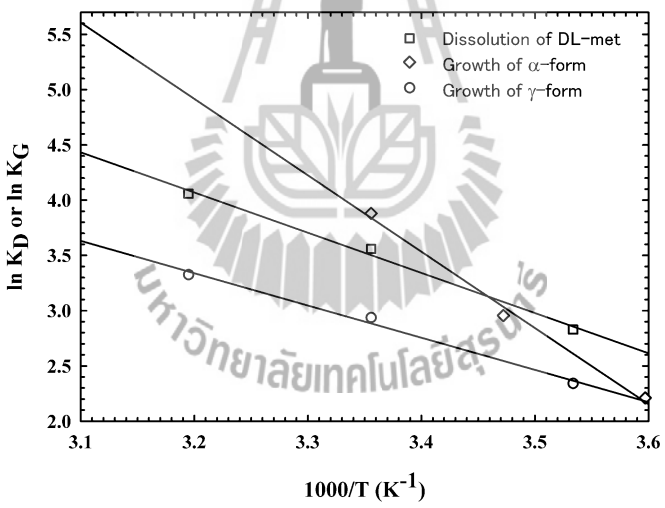

Figure 7.5 An Arrhenius plot of the growth rate and dissolution rate constants for DL-met for determination of the activation energy of crystal growth and dissolution.

Table 7.1 Dissolution and growth kinetic parameters of the polymorphs of DL-met.

Temp. (°C)	α-DL-met		γ-DL-met[a]		DL-met[b]	
	K_G (μm/min)	E_G (kJ/mol)	K_G (μm/min)	E_G (kJ/mol)	K_D (μm/min)	E_D (kJ/mol)
5	9.11		-		-	
10	-		10.39		16.93	
15	19.23	56.00	-	24.26	-	29.16
25	48.46		18.87		35.13	
40	-		27.83		57.87	

[a] Data from Wantha and Flood. [b]Dissolution kinetics of α-DL-met or γ-DL-met are assumed to be the same.

7.3.2 Discussion

The SMT is usually the most important process in crystallization of polymorphs from solution. If α-DL-met crystals are put in a saturated aqueous solution, a SMT from the α-DL-met to the γ-DL-met will take place. The dissolution of the α-DL-met and growth of the γ-DL-met are the main kinetics of SMT. Table 7.1 shows that the dissolution rate constants of α-DL-met (assuming they are similar to the dissolution rates of γ-DL-met) are likely to be larger than the growth rate constants of γ-DL-met at all temperatures studied. Therefore, the rate of the SMT is likely to be controlled by the growth of γ-DL-met. This conclusion is similar to the SMT of other crystalline substances, for example, L-histidine (Kitamura, 1993), and L-glutamic acid (Ono *et al*., 2004). Moreover, the growth rate constant of α-DL-met is larger than the growth rate constant of γ-DL-met, except at low temperature. This is reasonable because the crystallization kinetics of the metastable forms should be faster than the stable forms when the metastable forms appear first and then transform to more stable forms (Jiang *et al*., *et al*., 2008), although the increased crystallization rates of the metastable form could also be due to larger nucleation rates for the metastable form rather than larger growth rates. Nucleation rates in general have a larger effect on the overall rate of crystallization of a species since differences in nucleation rate can have very large effects on the population density of crystals in the system, however in many cases the differences in growth rates are sufficiently large that differences in the growth kinetics are more significant. For instance it has been shown that, for an equal supersaturation, the growth rate of α-glycine

(the metastable polymorph) is 500 times faster than the growth rate of γ-glycine (the stable polymorph) (Chew *et al*., 2007).

7.4. Conclusions

In this work, the kinetics of the processes which contribute to the rate of transformation between the polymorphs have been studied. The growth kinetics of the two polymorphs and the dissolution kinetics of γ-DL-met were measured between 5 and 40 °C in an agitated batch crystallizer. At all temperatures studied, the growth rate orders of both the α-DL-met and γ-DL-met are 1. The dissolution rate order of γ-DL-met is also 1. The growth and dissolution rate constants increase with increasing temperature and follow an Arrhenius relationship. At all temperatures studied, the growth rate constant for α-DL-met and the dissolution rate constant for γ-DL-met are larger than the growth rate constant for γ-DL-met, indicating that the SMT of the polymorph of DL-met may be controlled by the growth of γ-DL-met.

References

Randolph, A.D., Larson, M.A. Theory of Particulate Processes: Analysis and Techniques of Continuous Crystallization, second ed., Academic Press, California, 1988.

Mathieson, A.M. The crystal structures of the dimorphs of DL-methionine, Acta Cryst. 5 (1952) 332–341.

Matsuoka, M. Yamanobe, M., Tezuka, N., Takiyama, H., Ishii, H. Polymorphism, morphologies and bulk densities of DL-methionine agglomerate crystals, J. Cryst. Growth 198-199 (1999) 1299–1306.

Yamanobe, M. , Takiyama, T., Matsuoka, M. Polymorphic transformation of DL-methionine crystals in aqueous solution, J. Cryst. Growth 237-239 (2002) 2221–2226.

Wantha, L., Flood, A.E. Crystal growth rates and secondary nucleation threshold for γ-DL-methionine in aqueous solution, J. Cryst. Growth 318 (2011) 117-121.

Wantha, L., Flood, A.E. Nucleation kinetics of the γ-polymorph of DL-methionine, in: J.H. ter Horst (Ed.), Proceedings of BIWIC 2011, IOS Press, Delft, 2011, pp 302-307.

Dowling, R. , Davey, R. J., Curtis, R. A., Han, G., Poornachary, S. K., Chow, P. S., Tan, R. B. H. Acceleration of crystal growth rates: an unexpected effect of tailor-made additives, ChemComm 46 (2010) 5924-6926.

Han, G., Poornachary, S. K., Chow, P. S., Tan, R. B. H. Understanding Growth Morphology Changes of γ-Glycine and dl-Alanine Polar Crystals in Pure Aqueous Solutions, Cryst. Growth Des. 10 (2010) 4883-4889.

Huthmacher, K., Binder, W., Hasselbach, H. J., Korfer, M., Rohland, L., Alt, H.C., Kniesel, H. Process for the preparation of aqueous sodium methioninate solutions and use of those solutions in the production of a granulate, U.S. 6,126,972, October 3, 2000.

Garside, J., Mersmann, A., Nyvlt, J. Measurement of Crystal Growth and Nucleation Rates, second ed., Institute of Chemical Engineering, UK, 2002.

Allen, T. Particle Size Measurement: Volume 1 Powder Sampling and Particle Size Measurement, fifth ed., Chapman&Hall, London, 1997.

Pantaraks, P., Flood, A.E. Effect of growth rate history on current crystal growth: A second look at surface effects on crystal growth rates, Cryst. Growth Des. 5 (2005) 365–371.

Pantaraks, P., Matsuoka, M., Flood, A.E. Effect of growth rate history on current crystal growth. 2: Crystal growth of sucrose, $KAl(SO_4)2{:}12H_2O$, KH_2PO_4, and K_2SO_4, Cryst. Growth Des. 7 (2007) 2635–2642.

Promraksa, A., Flood, A. E., Schneider, P. A. Measurement and analysis of the dextran partition coefficient in sucrose crystallization, J. Cryst. Growth 311 (2009) 3667-3673.

Flood, A. E. Feedback between crystal growth rates and surface roughness, CrystEngComm 12 (2010) 313–323.

Schöll, J., Lindenberg, C., Vicum, L., Brozio, J., Mazzotti, M. Precipitation of α L-glutamic acid: determination of growth kinetics, Faraday Discuss. 136 (2007) 247–264.

Myerson, A.S., Ginde, R. Crystals, crystal growth, and nucleation, in: A.S. Myerson (Ed.), Handbook of Industrial Crystallization, second ed., Butterworth-Heinemann, USA, 2002, pp. 33–65.

Gougazeh, M., Omar, W., Ulrich, J. Growth and dissolution kinetics of potassium sulfate in pure solutions and in the presence of Cr^{3+} ions, Cryst. Res. Technol. 44 (2009) 1205-1210.

Mullin, J. W. Crystallization, fourth ed., Butterworth-Heinemann, Oxford, 2001.

Kitamura, M. Crystallization behavior and transformation kinetics of L-histidine polymorphs, J. Chem. Eng. Jpn. 26 (1993) 303-307.

Ono, T., Kramer, H.J.M., ter Horst, J.H., Jansens, P.J. Process modeling of the polymorphic transformation of L-glutamic acid, Cryst. Growth Des. 4 (2004) 1161-1167.

Jiang, S., ter Horst, J.H., Jansens, P.J. Concomitant polymorphism of o-aminobenzoic acid in antisolvent crystallization, Cryst. Growth Des. 8 (2008) 37-43.

Chew, J. W., Black, S. N. Chow, P. S., Tan, R. B. H., Carpenter, K. J. Stable polymorphs: difficult to make and difficult to predict, CrystEngComm 9 (2007) 128-130.

Chapter VIII
Polymorphic Transformation of DL-methionine in Aqueous Solution

8.1 Abstract

In this work, the solution mediated transformation (SMT) of α-DL-met into γ-DL-met in water at 25 °C via a seeded batch crystallization process was studied by measurement of the change of the solute concentration and the fraction of γ-DL-met in the crystal phase with time during the crystallization process. The solute concentration and was measured off-line using the dry substance method, since this is recognized as the most accurate method for concentration determination. The fraction of γ-DL-met was measured off-line by XRPD by setting a calibration curve using the internal standard method. The internal standard method was done by setting up the calibration curve using mixtures of α-DL-met, γ-DL-met, and NaCl, where NaCl was the internal standard. The mechanism of the SMT was interpreted to be a two step process, consisting of the dissolution process of α-DL-met and the crystallization process (nucleation and growth) of γ-DL-met. The dissolution of α-DL-met is the rate controlling step during the transformation. The transformation time for the case where the seed was added to a supersaturated solution within the SNT region is longer than the case which the seed was added to a supersaturated solution above the SNT region.

8.2 Introduction

When the driving force is created in a solution of a polymorphic compound, the system tends to minimize its free energy. Theoretically, this leads to the crystallization of the stable polymorph. However, if the crystallization kinetics of the metastable polymorph are faster the compound may crystallize into this metastable polymorph first. Eventually the metastable polymorph should transform into the stable one (Roelands, 2005). This phenomenon of formation of the kinetically controlled polymorph over the thermodynamically favored form is known as Ostwald's Rule of Stages (Threlfall, 2003). This rule is based on observation and is not a physical law (Roelands *et. al*., 2006); it is often incorrect, particularly in cases where the solution is either below the solubility of the metastable form, or below the nucleation threshold of the metastable form. Moreover, if both polymorphs crystallize at similar rates a mixture of the two polymorphs is initially obtained; this is called concomitant polymorphism (Bernstein, Davey, and Henck, 1999).

The metastable polymorph will transform to the stable polymorph via solid-state transformation (SST) (O'Brien, Timmins, Williams, and York, 2004; Jiang, Jansens, and ter

Horst, 2010a) or solution-mediated transformation (SMT) (Schöll, Bonalumi, Vicum, and Mazzotti, 2006; Jiang, Jansens, and ter Horst, 2010b). In the case of true SST the crystal lattice transforms into the different arrangement, for instance when the temperature is raised. Studies of SST are important, for example the sudden appearance or disappearance of a polymorphic form in pharmaceutical products can lead to serious consequences if the transformation occurs in the dosage forms (Vippagunta, Brittain, and Grant, 2001). The transformation in the solid state is often much slower than in the solution. For the SMT the transformation of the metastable polymorph into the stable polymorph occurs when a liquid phase surrounds the crystals. SMT consists of the nucleation and crystal growth of the stable polymorph and the dissolution of the metastable polymorph. There are two mechanisms that could control the transformation rate: either the dissolution rate of the metastable polymorph is limiting or the crystallization rate of the stable polymorph is limiting (Mangin, Puel, and Veesler, 2009). SMT is found in the crystallization of polymorphic compounds in solution. Crystallization with seeding (which is commonly found in industrial crystallization) is the easy way to study the SMT mechanisms. However, the SMT can be studied via unseeded crystallization where the metastable polymorph forms first, followed by transformation to the more stable polymorph (Ostwald's Rule). Therefore, crystallization processes involving polymorphs consist of the competitive nucleation and crystal growth of the polymorphs, and the transformation from the metastable to the stable polymorph. In this work the focus is on the SMT of the polymorphs of DL-methionine (DL-met).

To study the mechanisms of SMT and identify which mechanism is the limiting step the polymorphic composition of the slurry has to be followed in time in combination with the concentration of the solute in the solution. For example, the SMT of the metastable α polymorph of L-glutamic acid was studied by Garti and Zour (1997), by Ono, Kramer, ter Horst, and Jansens, (2004), by Schöll *et al*., (2006), and by Dharmayat *et al*. (2008). In all studies the aqueous suspension was stirred in an agitated crystallizer. It was concluded that the growth rate of the stable β polymorph was the rate controlling step during the transformation processes. In addition, the experimental results of Garti and Zour showed that the transformation could be inhibited by the addition of surfactants. Kitamura (1993) found that the dissolution rate constant of the metastable B polymorph was nearly six times larger than the growth rate constant of the stable A polymorph, which indicated the transformation process in aqueous solution was growth controlled. The SMT of the metastable α polymorph of taltireline to the stable β polymorph in water at 10 °C was studied by Maruyama, Ooshima, and Kato, (1999). It found that the growth rate of the stable β polymorph was the rate

controlling step during the transformation process, and the coexistence of methanol promoted the transformation rate. Qu, Louhi-Kultanen, Rantanen, and Kallas (2006) found that the crystallization of (nucleation and growth) of dihydrate form (CBZH) of carbamazepine was the rate controlling step for the transformation of anhydrous form (CBZA) into CBZH in water-ethanol mixed solvent.

Usually, the transformation rate is controlled by the growth rate of the stable polymorph as described in the above examples. However, the transformation rate can be controlled by the dissolution rate of the metastable polymorph. For example, the transformation rate of the metastable β polymorph of glycine to the stable α polymorph in water-ethanol mixed solvent was limited by the slow dissolution rate of the metastable β polymorph (Ferrari, Davey, Cross, Gillon, and Towler, 2003). In this work it was concluded that increased attrition of the metastable polymorph created additional surface area which facilitated the rate-limiting dissolution process.

The experiment to study the SMT can be performed by monitoring the transformation of the metastable polymorph to the stable polymorph during the crystallization. Monitoring the transformation involves measuring the change of the supersaturation (or solute concentration) and polymorphic fraction with time during the crystallization process. Several methods have been used to measure the solute concentration during the SMT experiments, for example the dry substance method (Qu *et al*., 2006; Roelands *et. al*., 2006; Jiang, ter Horst, and Jansens, 2008), using UV spectroscopy (Kitamura, 1993; Garti and Zour, 1997; Lu, Wang, Yang, and Ching, 2007), and using HPLC (Maruyama *et al*., 1999). There are many analytical methods which have been used for measuring the polymorphic fraction off-line, for example Raman spectroscopy (Ono, Kramer *et al*., 2004; Qu *et al*., 2006; Roelands *et. al*., 2006), X-ray powder diffractometry (XRPD) (Kitamura 1993; Garti and Zour, 1997; Maruyama *et al*., 1999; Kitamura and Sugimoto, 2003), and Fourier transform infrared spectroscopy (FT-IR) (Ferrari *et al*., 2003; Lu *et al*., 2007). However, for this purpose there are at least two techniques have been applied in-situ during crystallization: XRPD (Davis *et al*., 2003; Hammond, Lai, Roberts, Thomas, and White, 2004; Dharmayat *et al*., 2008) and Raman spectroscopy (Ono, ter Horst, and Jansens, 2004; Qu *et al*., 2006; Schöll *et al*., 2006; Jiang *et al*., 2010b). During the crystallization experiment simultaneous in-situ measurements and off-line measurements of the polymorphs fraction were done by Ono, ter Horst *et al*. (2004) and by Qu *et al*. (2006), and the two techniques showed good agreement.

All of the above techniques are accurate enough for determining the solute concentration and polymorphic fraction during the crystallization process. The accuracy depends on the performance of each equipment, and the reliability and robustness of the sampling techniques, data analysis, etc. Usually, off-line handling rather than in-situ measurements may be the cause of the observed deviations. However, the studies of Ono, ter Horst *et al*. (2004) and Qu *et al*. (2006) showed that the off-line result is accurate enough for this purpose as described above. Therefore, in this work the dry substance method was used to determine the solute concentration and XRPD was used for measuring the polymorphic fraction off-line. The aim of this work is to study the SMT of the metastable α-DL-methionine (α-DL-met) to the stable γ-DL-methionine (γ-DL-met) in aqueous solution at 25 °C. The polymorphic transformation was studied by measuring the changes of the polymorphic fraction and the solute concentration with time during the crystallization process. The off-line measurements of the solute concentration and polymorphic fraction were measured by the dry substance method and XRPD, respectively.

8.3 Theory

The transformation of polymorphs can be carried out only from the less stable polymorphs to the most stable one. During crystallization from solution of a polymorphic compound the phase transformation phenomena are often promoted by the liquid phase surrounding the crystals. This is usually called solution-mediated transformation (SMT).

If the polymorphic system is far away from the transformation temperature, as shown in Figure 8.1(a), the metastable polymorph (polymorph II) has a higher solubility than the stable polymorph (polymorph I). Initially, the solution at concentration C_i and temperature T is supersaturated with respect to both polymorphs. For Ostwald's Rule of Stages, when the crystallization kinetics, determined by both the nucleation rate and the growth rate, of polymorph II are faster than that of polymorph I, polymorph II crystals will initially nucleate and grow (Jiang *et al*., 2010b; Roelands, 2005). The solute concentration C_i drops to the solubility of polymorph II, C_{II}^{*}. This is since the crystal growth is of polymorph II. At this point, the solution is saturated with respect to polymorph II while still supersaturated with respect to polymorph I. This corresponds with the beginning of region 1 in Figure 5.1(b), where the supersaturation ratios S_I of polymorph I and S_{II} of polymorph II are a function of time, and both the supersaturation ratios decrease because of the decrease of the solute concentration C_i.

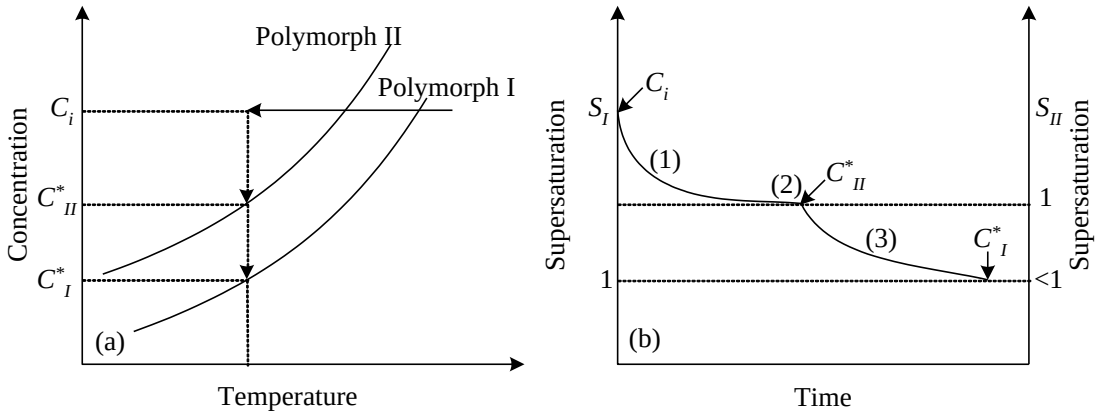

Figure 8.1 Thermodynamic and kinetic features of the SMT: (a) typical solubility curves of a monotropically related stable polymorph (polymorph I) and metastable polymorph (polymorph II), (b) general features of the time dependence of supersaturation ratios a SMT. (Adapted from Jiang *et al*., 2010b)

Because the solution is still supersaturated with respect to polymorph I, polymorph I crystals start nucleating and growing, and polymorph II start dissolving when the supersaturation ratio of polymorph II becomes $S_{II} < 1$. This is the start of SMT, which consists of the nucleation and crystal growth of the stable polymorph and the dissolution of the metastable polymorph (Jiang *et al*., 2010b; Schöll *et al*., 2006). The solute concentration is balanced by the decrease in the solute concentration due to the growth of polymorph I crystals and the increase the solute concentration due to the dissolution of polymorph II crystals. In many cases, the phase transformation is a growth-controlled transformation. During the transformation the solute concentration C_i is maintained at or close to the solubility C^*_{II} of polymorph II because the dissolution of polymorph II crystals is rapid enough to maintain the solution concentration C_i. This coincides with region 2 in Figure 5.1(b) which the supersaturation ratio S_I remains at a plateau value of $S_I \approx C^*_{II} / C^*_I$.

The solute concentration (or supersaturation ratio) remains constant until polymorph II crystals have completely dissolved. The solute concentration starts to decrease upon the further growth of polymorph I crystals, and the whole transformation process is complete when the solute concentration C_i reaches the solubility C^*_I of polymorph I. At this point the supersaturation ratio of polymorph I $S_I = 1$, and supersaturation ratio of polymorph II becomes $S_{II} < 1$. This is indicated as region 3 in Figure 8.1(b).

It is important to note that if the phase transformation is a growth-controlled transformation, the concentration profile corresponds to curve (1) in Figure 8.2 where the plateau of solute concentration is located in the vicinity of the solubility of the metastable polymorph (Mangin *et al*., 2009). This indicates the growth rate constant is much smaller than the dissolution rate constant. If the solute concentration dropping immediately to the solubility of the stable polymorph (as shown curve (2) in Figure 8.2), the phase transformation is a dissolution-controlled transformation. This indicates the dissolution rate constant of the metastable polymorph is much smaller than that the growth rate constant of the stable polymorph.

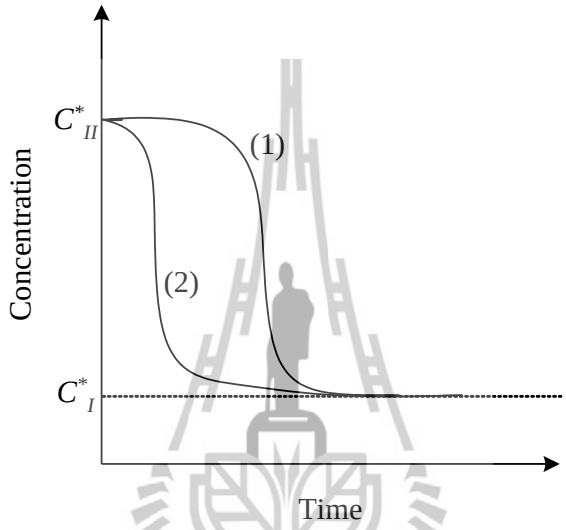

Figure 8.2 Concentration as a function of time during SMT: curve (1) growth-controlled transformation, curve (2) dissolution-controlled transformation. (Adapted from Mangin *et al*., 2009)

8.4 Experimental Methods

8.4.1 Materials

DL-met (>99%, Acros Organics), NaOH (>97%, Carlo Erba), Na_2CO_3 (>99.5%, Carlo Erba), HCl (37%, Carlo Erba) and deionized water were used without further purification. DL-met and deionized water were used to prepare the supersaturated solutions in all SMT experiments. Sodium methioninate (Na-met) was also required for acidic precipitations of DL-met to prepare α-DL-met. Aqueous solutions of Na-met were prepared by the method previously described in Chapter V.

8.4.2 Apparatus

A 0.5-L batch crystallizer with a sealed glass lid to reduce solvent evaporation was used to study the SMT. The slurry is continuously agitated at the set speed by a centrally located four-blade impeller driven by an overhead stirrer. The crystallizer was placed inside a constant temperature water bath, where the temperature was controlled within ±0.5°C.

250 mL and 500 mL glass beakers were used as batch crystallizers to prepare α-DL-met and sodium methioninate (Na-Met) aqueous solutions, respectively. The temperature control and the agitation systems were the same as for the 0.5 L batch crystallizer.

8.4.3 Preparation of Polymorph

α-DL-met was prepared using reaction crystallization of Na-met aqueous solutions with HCl as described in Chapter V. The obtained pure α-DL-met with the size range of 64 - 250 μm was used as seed.

8.4.4 Analysis of the Polymorphic Fraction

X-ray powder diffractometry (XRPD) (Bruker axs, D5005) was used for the measurement of the polymorphic content during crystallization (or polymorphic transformation experiments). XRPD have been used to quantify the polymorphic crystalline material off-line in the literature (Takahashi, Takenishi, and Nagashima, 1962; Kitamura 1993; Garti and Zour, 1997; Maruyama *et al*., 1999; Kitamura and Sugimoto, 2003). This method is based on a calibration curve using prepared polymorphic mixtures as dry powder. Takahashi *et al*. (1962) showed that an exponential calibration line was obtained from the direct method (a binary mixture of the two polymorphs), while a linear calibration line was obtained from the internal standard method (mixtures of the two polymorphs with a known amount of the internal standard). This indicates that the internal standard method is more efficient and more accurate than the direct method. A suitable internal standard should have satisfactory purity, sharp diffraction lines, and a suitable line free from interference and superposition (Takahashi *et al*., 1962). In this work the internal standard is NaCl. The XRPD patterns of NaCl, α-DL-met, and γ-DL-met are shown in Figure 8.3.

From Figure 8.3, the characteristic peaks are at $2\theta = 31.7°$ for NaCl, $2\theta = 25.3°$ and 32.84° for α-DL-met, and $2\theta = 28.06°$ and 33.82° for γ-DL-met. The following equations were used for construction the calibration lines.

Based on peak intensities:

$$Y_I = \frac{\left[\frac{I_{\gamma,33.82^\circ} + I_{\gamma,28.06^\circ}}{I_{N,31.7^\circ}} + \left(1 - \frac{I_{\alpha,32.84^\circ}}{I_{N,31.7^\circ}}\right) + \left(1 - \frac{I_{\alpha,25.3^\circ}}{I_{N,31.7^\circ}}\right)\right]}{4} \quad (8.1)$$

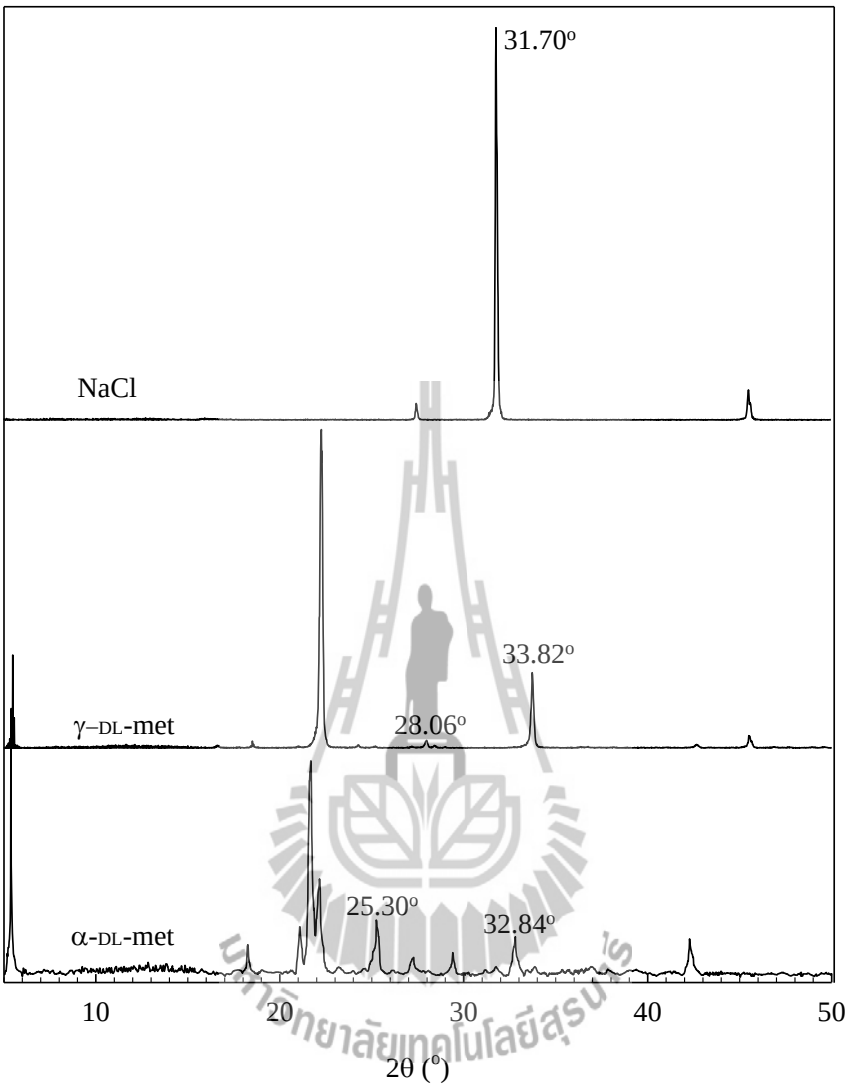

Figure 8.3 XRPD patterns for α-DL-met, γ-DL-met, and NaCl.

Based on area of the peaks:

$$Y_A = \frac{\left[\frac{A_{\gamma,33.82^\circ} + A_{\gamma,28.06^\circ}}{A_{N,31.7^\circ}} + \left(1 - \frac{A_{\alpha,32.84^\circ}}{A_{N,31.7^\circ}}\right) + \left(1 - \frac{A_{\alpha,25.3^\circ}}{A_{N,31.7^\circ}}\right)\right]}{4} \quad (8.2)$$

where I is the characteristic peak intensity, A is the area under curve of the characteristic peak, and Y is the calculation factor. The calibration curves were thus obtained from plotting Y against the concentration of γ-DL-met in standard samples. The standard samples were prepared as mixtures of the two polymorphs and NaCl, in various mass fractions with a constant mass of NaCl. The mixing was done in a mortar by hand, with grinding for more than 10 min. The mixing should be done softly to avoid the transformation of the metastable α-DL-met to the stable γ-DL-met due to the heat effect from grinding.

8.4.5 Polymorphic Transformation Experiments

The polymorphic transformation experiments were studied by seeded batch crystallization. There are two distinct experiments (as shown in Table 8.1): (1) seed crystals were added to a supersaturated solution where the supersaturation level is above the secondary nucleation threshold (SNT) for γ-DL-met, and (2) seed crystals were added to a supersaturated solution where the supersaturation level is in the SNT for γ-DL-met. All experiments were performed at 25 ºC in a 0.5-L batch crystallizer agitated by a centrally located four-blade impeller driven by an overhead stirrer at 350 rpm. The solute concentration in the clear liquor was measured periodically using dry substance determination (Garside, Mersmann, and Nyvlt, 2002). In addition, the solid fraction in wt.% was measured periodically using the calibration curve which is given in Section 8.4.3.

At the beginning of all experiments, the supersaturated solutions were prepared by dissolving DL-met in deionized water at 55 °C (at least 20 ºC above saturation temperature) for 30 to 40 min to ensure that no ghost nuclei remained in the solution. After complete dissolution of the solid material the solutions were then cooled to the experimental temperature, which was then held constant throughout the process, and a quantity of dry seeds was fed to the crystallizer. A small volume of the suspension was sampled at particular times during the batch to determine the solid fraction and the solute concentration.

The experimental conditions are shown in Table 8.1, where C_0 is the initial concentration, and $S_{\alpha 0}$ and $S_{\gamma 0}$ are the initial supersaturations with respect to α-DL-met and γ-DL-met, respectively.

Table 8.1 Experimental conditions of the polymorphic transformation experiments where the seed is α-DL-met. SNT indicates the SNT for γ-DL-met.

Exp. no.	Amount of seed (g)	C_0 (g DL-met/ kg water)	$S_{\alpha 0}$	$S_{\gamma 0}$	Level of C_0
1	1	40.50	1.14	1.20	above SNT
2	1	40.50	1.14	1.20	above SNT
3	1	40.50	1.14	1.20	above SNT
4	1	40.50	1.14	1.20	above SNT
5	2	37.00	1.04	1.10	in SNT
6	2	37.00	1.04	1.10	in SNT
7	2	37.00	1.04	1.10	in SNT

8.5 Results and Discussions

8.5.1 Analysis of the Polymorphic Fraction

The obtained XRPD patterns for the reference mixture samples (for replicate number 1) are shown in Figure 8.4. This shows that the characteristic peaks of each polymorph and NaCl do not overlap (in the case of pure α-DL-met or γ-DL-met). The characteristic peaks of α-DL-met and γ-DL-met overlapped for the mixture samples. It is observed that as the fraction of γ-DL-met changes the height and area of the characteristic peaks change correspondingly. Therefore, quantitative analysis can be done by the calibration line which was constructed from the overlapped peak intensities or area under the characteristic peaks of each polymorph as described in Section 8.4.4. This illustrates how the characteristic peaks of each polymorph change with the polymorphic fraction. These indicate that PXRD can be used to analyze the quantitative of the solid composition of polymorphic forms during the transformation process well.

The plots of the calculated factor Y against the fraction of γ-DL-met in the standard samples are shown in Figures 8.4 (for Y_I) and 8.5 (for Y_A). The linear relationships are

$$Y_I = 0.2992x + 0.4521 \tag{8.3}$$

$$Y_A = 0.3322x + 0.4405 \tag{8.4}$$

where x is the mass fraction of γ-DL-met (wt.%) and the mass fraction of α-DL-met is $1 - x$. The calibration line (Figures 8.4 and 8.5) exhibits good linearity over the entire concentration range studied. The rmsd values for the fitting equation of Y_I and Y_A are 0.0098 and 0.0109, respectively. These two figures suggest that the calibration line applied in this work for the quantification of the polymorphic mixture of DL-met via XRPD is practical. These two equations were used to determine the polymorphic fractions of γ-DL-met obtained during the polymorphic transformation experiments. The fraction x is the average value that is obtained from equations (8.3) and (8.4).

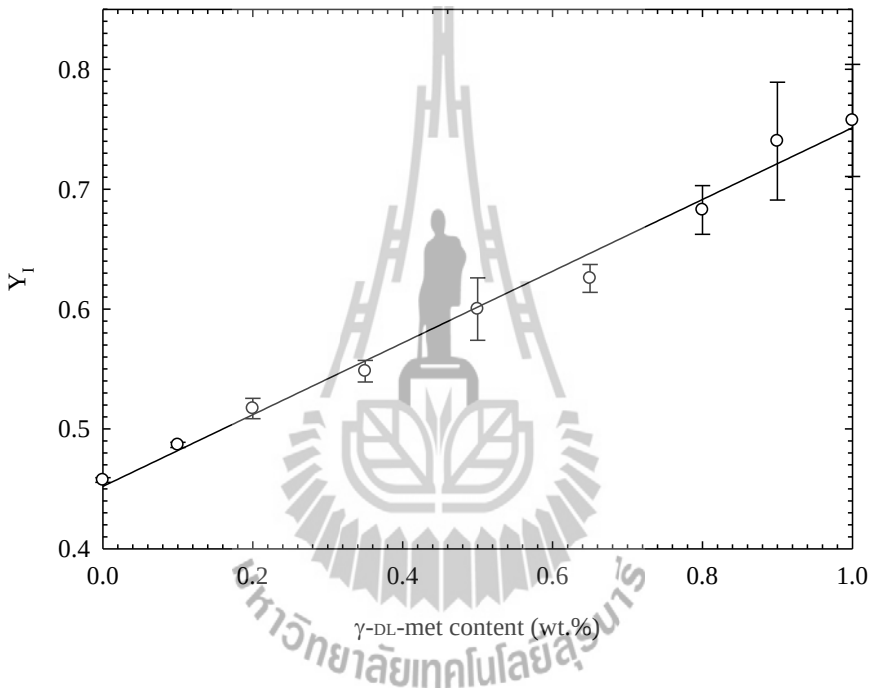

Figure 8.4 The calibration curve for analysis of the fraction of γ-DL-met based on the peak intensities. XRPD measurements (circle) and the fit (solid line).

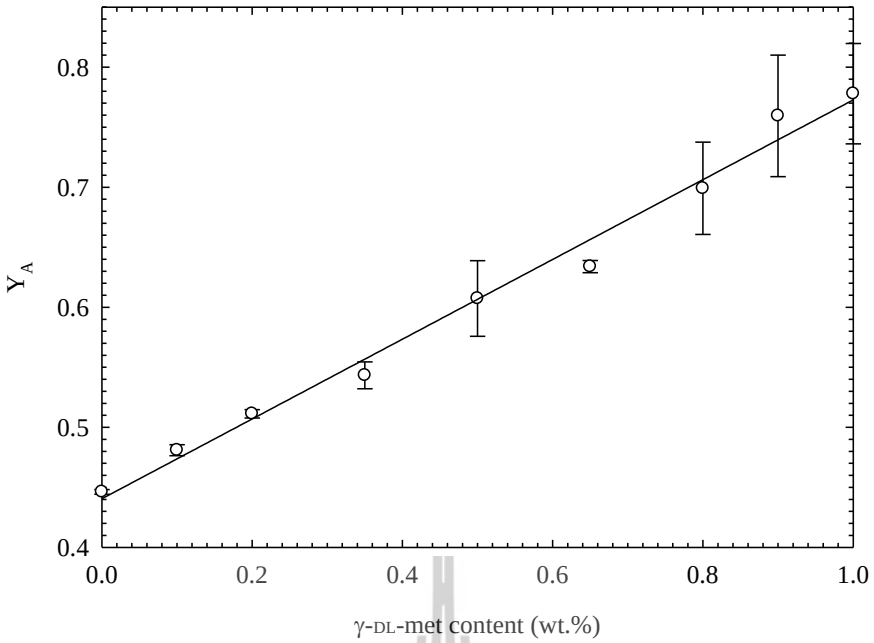

Figure 8.5 The calibration curve for analysis of the fraction of γ-DL-met based on the area of the peaks. XRPD measurements (circle) and the fit (solid line).

8.5.2 Polymorphic Transformation

Figure 5.6 shows the typical change in the XRPD patterns of the product crystals relative to the crystallization time from the seeded batch crystallization at 25 °C and C_0 = 40.5 g DL-met/kg water (for which the initial supersaturation level is above the SNT for γ-DL-met). It was found that the characteristic peak heights of each polymorph (e.g. peaks at 32.84° for α-DL-met and 33.82° for γ-DL-met) gradually changed with crystallization time because of the spontaneous generation of γ-DL-met and the transformation of polymorphs during crystallization process. The characteristic peaks for γ-DL-met increase with crystallization time, while the characteristic peaks for α-DL-met decrease with crystallization time. This indicates that there is a transformation of α-DL-met into γ-DL-met during the crystallization process. Therefore, according to the SMT mechanism of the polymorphs (Mangin *et al*., 2009; Jiang *et al*., 2010b), the stable γ-DL-met is nucleated, and then simultaneously the metastable α-DL-met is dissolved and the stable γ-DL-met is grown. Figure 8.6 also shows that the characteristic peaks of γ-DL-met appear clearly at 1 h. This leads to the conclusion that γ-DL-met is nucleated at or close to 1h. This indicates that there is an induction time for nucleation of γ-DL-met. Only γ-DL-met was nucleated because only γ-DL-met was found to nucleate during the crystallization of DL-met from aqueous solution (Matsuoka, Yamanobe, Tezuka, Takiyama, and Ishii, 1999). The resulting peaks indicate the

amount of α-DL-met and γ-DL-met in the solid (which can be calculated from equations (5.3) and (5.4)) present as a function of crystallization time, as shown in Figure 5.9.

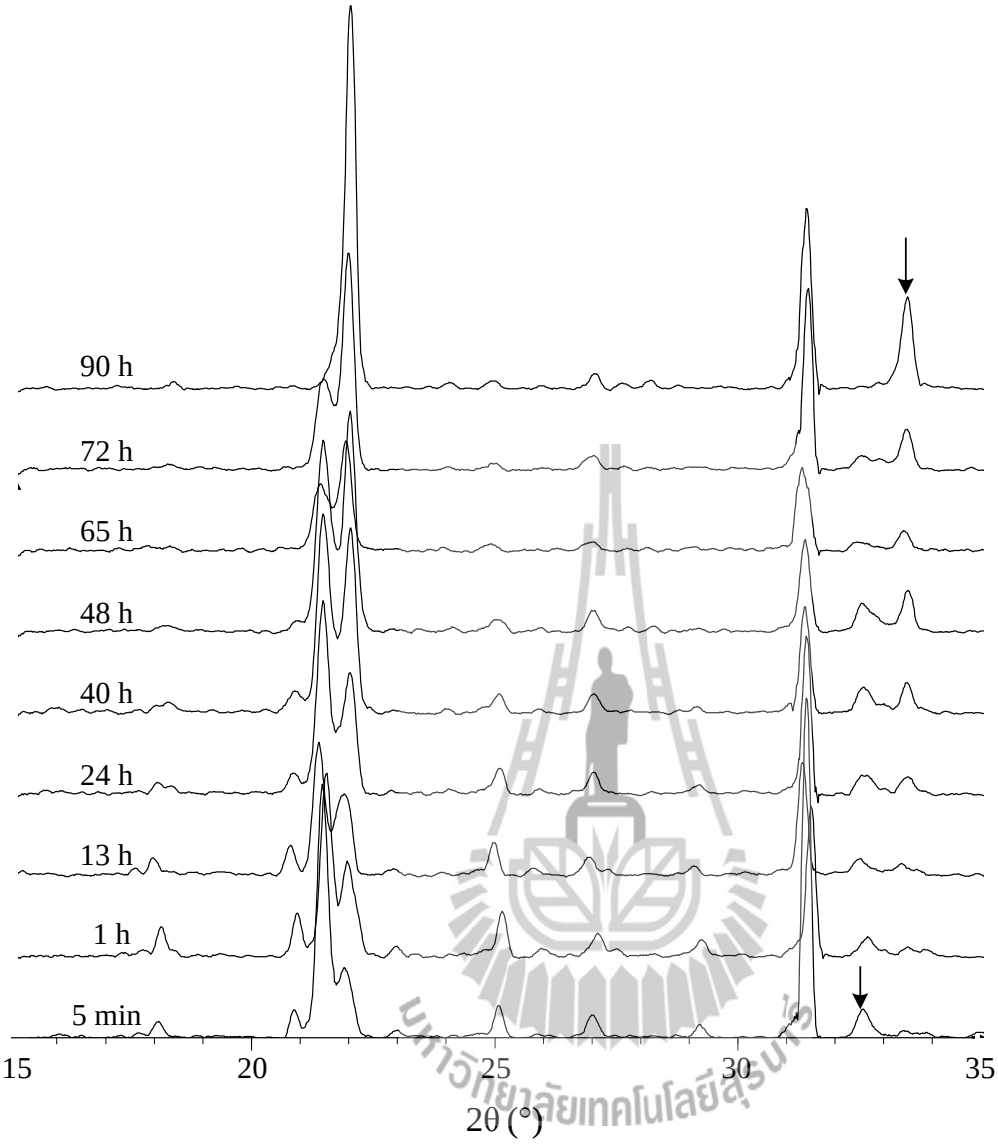

Figure 8.6 XRPD patterns of the solid mixture taken at various times during the polymorphic transformation of α-DL-met into γ-DL-met at 25 °C and C_0 = 40.5 g DL-met/kg water.

The SMT is a complex process because there are several mechanisms, including the dissolution of the metastable polymorph and the nucleation and growth of the stable polymorph, which are both involved in the transformation. The comparison of the solute concentration profile and the solid phase composition measured using XRPD allows for the identification of the mechanisms during the transformation. The measured solute concentration and the solid phase composition (γ-DL-met fraction) obtained from the seeded

batch crystallization at 25 °C and C_0 = 40.5 g DL-met/kg water (where the initial supersaturation level is above the SNT for γ-DL-met) are shown in Figure 8.7. A magnification of the rapid decrease in the solute concentration in the range of 0 - 60 min is shown in Figure 8.8.

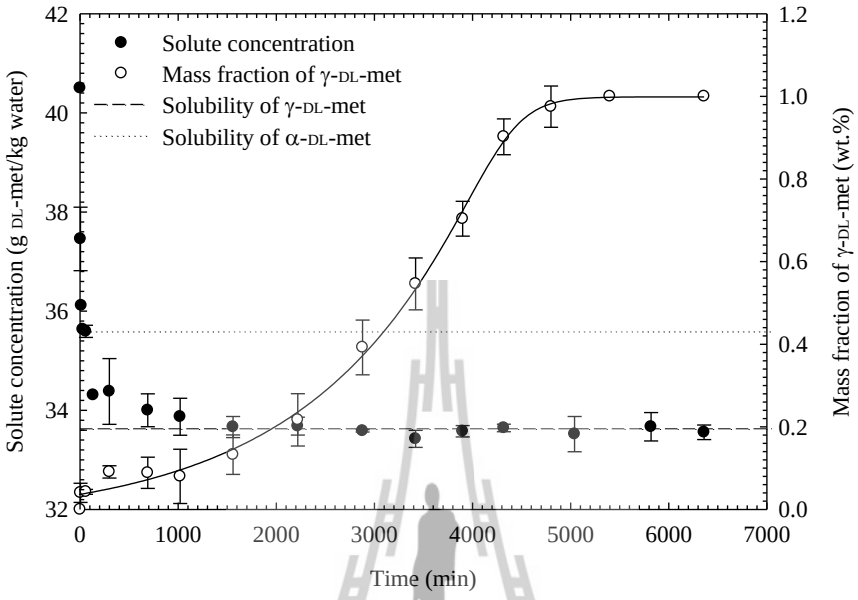

Figure 8.7 Solute concentration and fraction of γ-DL-met in the solution during the polymorphic transformation of α-DL-met into γ-DL-met at 25 °C and C_0 = 40.5 g DL-met/kg water.

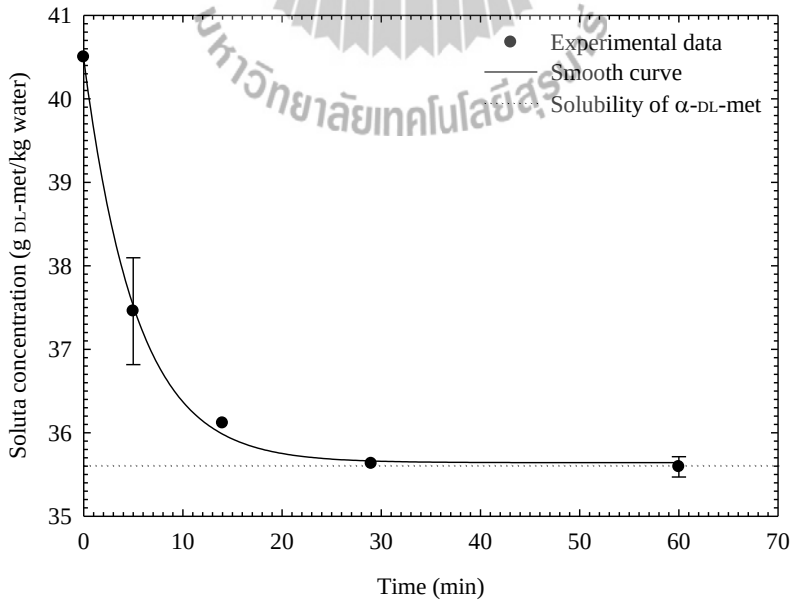

Figure 8.8 The magnification of the solute concentration in Figure 5.9 in the range of 0 – 60 min.

Figure 8.7 clearly illustrates the transformation process where α-DL-met seeds have been added to the supersaturated solution. Initially, the solute concentration is supersaturated with respect to both polymorphs, and α-DL-met crystals were seeded. The growth of α-DL-met initially occurs since crystals of this polymorph are already present in the solution. This leads to a drop in the solute concentration, to the solubility of α-DL-met, within 30 min (Figure 8.8). At this point, the solution is saturated with respect to α-DL-met, while still being supersaturated with respect to γ-DL-met. The solute concentration is maintained at, or close to, the solubility of α-DL-met during a short period (30 min). Since the solution is still supersaturated with respect to γ-DL-met, γ-DL-met crystals start nucleating and growing, and α-DL-met start dissolving as the solute concentration drops lower than the solubility of α-DL-met ($S_\alpha < 1$). This is the start of the SMT of α-DL-met into γ-DL-met, which consists of the nucleation and crystal growth of the stable γ-DL-met and the dissolution of the metastable α-DL-met. This also indicates that the induction time for nucleation of γ-DL-met is approximately 30 min. As shown in Figure 8.7, the amount of γ-DL-met begins to increase at this point. The increase in solute concentration due to dissolution of α-DL-met is balanced by the decrease in the solute concentration due to the growth of γ-DL-met crystals at this point. The dissolution of α-DL-met crystals is rapid enough to maintain the solute concentration for only a short period of time (30 min). After that the solute concentration drops rapidly to the solubility of γ-DL-met within the crystallization time of 1,000 – 1,600 min, while the transformation still occurs continually (the γ-DL-met fraction still increases). After 1,600 min the transformation still occurs until the fraction of γ-DL-met reaches 1 (complete transformation) at approximately 5,400 min. The solute concentration is maintained at or close to the solubility of γ-DL-met. This means that from 60 min until 5400 min the dissolution of the α-DL-met crystals is not rapid enough to maintain the solute concentration at or close to the solubility of α-DL-met. This can demonstrate that the dissolution rate of α-DL-met is slower than the crystallization rate of γ-DL-met. The transformation process in this period depends on the simultaneous growth of γ-DL-met and the dissolution of α-DL-met. The supersaturated solution is created by the slower dissolution of α-DL-met, but the solute concentration drop is more rapid due to the faster growth of γ-DL-met. These two processes are occur simultaneously until the α-DL-met crystals are completely dissolved, which means that the transformation is complete. The transformation time in this case is approximately 5,400 min.

The results in the case where α-DL-met crystals were seeded to a supersatured solution where the supersaturation level is within the SNT for γ-DL-met are shown Figures 8.9-8.11. Figure 8.9 shows the typical change in the XRPD patterns for this case. There is noise (or a lot of the small peaks) in the XRPD patterns. A possible explanation is a reduction in the performance of the XRPD in Suranaree University of Technology. After the changes to the machine the XRPD works, and patterns of sample are the same as previous measurements, but there is some noise in the spectra and all peak intensities are reduced. However, the ratios of the peak or peak areas are still the same. This indicates that the quantification of the polymorphic fraction still works.

Figure 8.9 shows that the change in the XRPD patterns is similar to the previous case, but the transformation time is longer. It seems that the nucleation of γ-DL-met does not start during the initial period which indicates that the transformation does not occur during this period either. This can be confirmed from the fact that the characteristic peaks of γ-DL-met appear clearly at around 2 - 3 days (48 - 72 h). This indicates that there is an induction time which is required for the nucleation of γ-DL-met. This is reasonable because the seed was added to the supersatured solution where the supersaturation level is within the SNT of γ-DL-met.

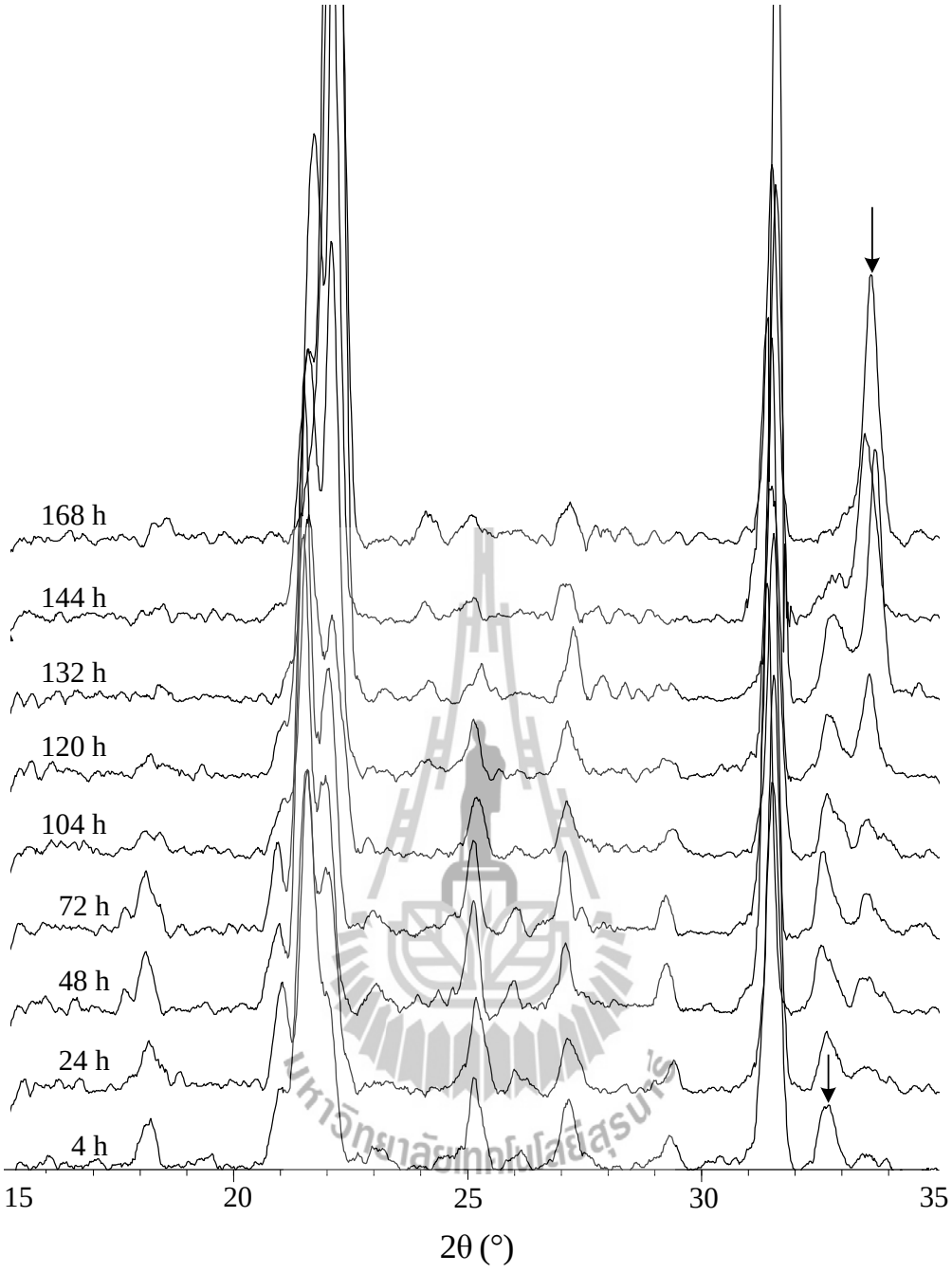

Figure 8.9 XRPD patterns of the solid mixture taken at various times during the polymorphic transformation of α-DL-met into γ-DL-met at 25 °C and C_0 = 37.0 g DL-met/kg water.

The measured solute concentration and the solid phase composition (γ-DL-met fraction) obtained from the seeded batch crystallization at 25 °C and C_0 = 37.0 g DL-met/kg water (where the initial supersaturation level is within the SNT for γ-DL-met) are shown in Figure 5.12. The magnification of the rapid decrease of the solute concentration in Figure 8.10, in the range of 0 - 70 min, is shown in Figure 8.11.

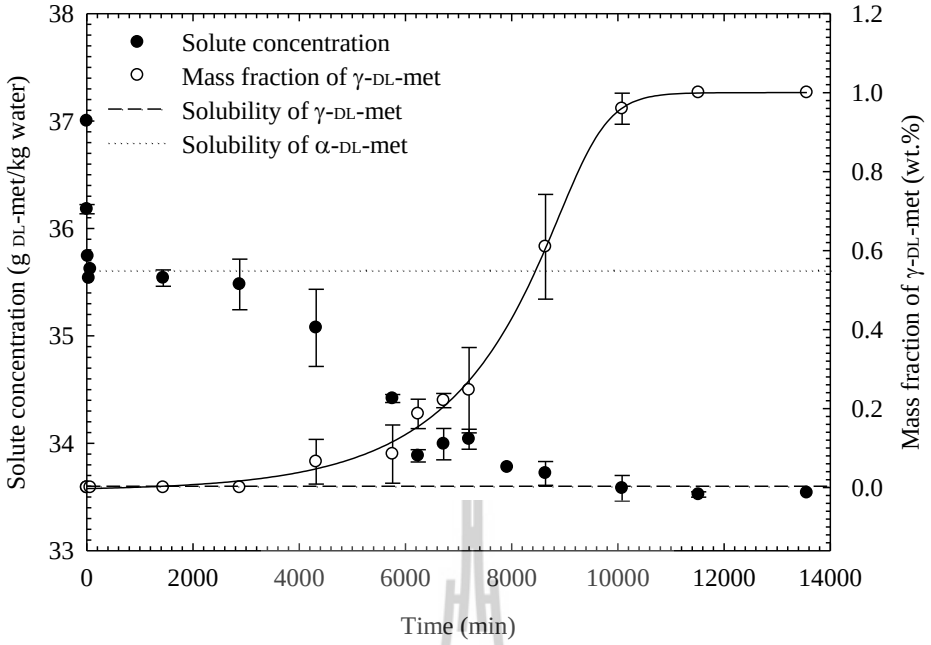

Figure 8.10 Solute concentration and fraction of γ-DL-met in the solution during the polymorphic transformation of α-DL-met into γ-DL-met at 25 °C and C_0 = 37.0 g DL-met/kg water.

Figure 8.10 clearly illustrates the transformation process where α-DL-met seeds are added to the supersaturated solution. Since the seed was added to a supersaturated solution within the SNT region, there is an induction time for the nucleation of γ-DL-met. As shown in Figure 8.10, the induction time (the time where the fraction of γ-DL-met starts to increase from zero) is more than 2 days (2,880 min); due to the measurement uncertainty the induction time is around 2 - 3 days.

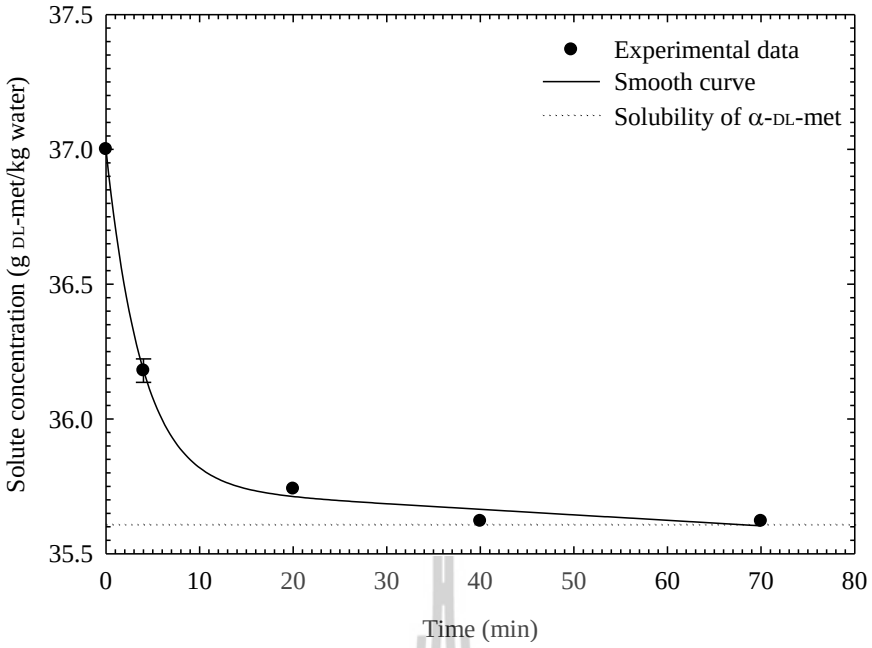

Figure 8.11 The magnification of the solute concentration in Figure 8.10 in the range of 0 – 70 min.

As shown in Figure 8.10, initially the solute is supersaturated with respect to both polymorphs, and α-DL-met crystals were seeded. However the initial supersaturated solution is within the SNT region so that the only growth of α-DL-met was occurred initially. This leads to the solute concentration dropping to the solubility of α-DL-met within 40 min (Figure 5.13). At this point, the solution is in equilibrium with respect to α-DL-met, and the solution will remain at this equilibrium until the crystallization time reaches the induction time for the nucleation of γ-DL-met (around 2 - 3 days). When the system reaches this induction time, γ-DL-met crystals start nucleating (the γ-DL-met fraction starts to increase from zero) and growing, which causes the α-DL-met to start dissolving when the supersaturation ratio of α-DL-met becomes $S_\alpha < 1$. This is the start of the SMT of α-DL-met into γ-DL-met, where the behavior of the SMT is similar to the previous case. The solute concentration is balanced by the decrease in the solute concentration due to the growth of γ-DL-met crystals and the increase the solute concentration due to the dissolution of α-DL-met crystals. In this case, after the start of the transformation, the solute concentration drops slowly to the solubility of γ-DL-met (not remaining constant at the solubility of α-DL-met), while the γ-DL-met fraction increases slowly until it reaches 1 (complete transformation). This can be explained in a similar way to the previous case. Namely, the dissolution rate of α-DL-met is slower than the growth rate of γ-DL-met. Therefore, the transformation process

depends on the simultaneous growth of γ-DL-met and the dissolution of α-DL-met. These two processes simultaneously occur until α-DL-met crystals are completely dissolved, which means that the transformation is complete. In this case, the transformation is complete at approximately 8 days (11,520 min). The transformation time is around 5 - 6 days, which is the time between the induction time and the complete transformation time. The transformation time is longer than the previous case due to a slower crystallization of γ-DL-met.

8.5.3 Discussion

The transformation experiments showed the SMT of α-DL-met into γ-DL-met at 25 °C is a dissolution controlled process, where the mass transfer of solute to the growing phase rapidly depletes the solute concentration to the value consistent with the minimum level of supersaturation required to maintain the growth of the stable polymorph (Dharmayat *et al*., 2008). This is since the solute concentration dropping immediately to the solubility of the stable polymorph as shown curves 8.7 and 8.10. In the literature there are a lot of studies showing that the growth of the stable polymorph was the limiting step, for example L-glutamic acid (Garti and Zour, 1997; Ono, Kramer *et al*., 2004; Schöll *et al*., 2006; Dharmayat *et al*., 2008), L-histidine (Kitamura, 1993), taltireline (Maruyama *et al*., 1999), and carbamazepine (Qu *et al*., 2006). The SMT of glycine is at least one example where the dissolution of the metastable polymorph was the limiting step (Ferrari *et al*., 2003).

The conclusion here indicates that the assumption behind the dissolution measurement in Chapter VII is not true. Namely, in Chapter VII the dissolution rates were measured based on γ-DL-met seed crystals and then assuming the same dissolution rate for both α-DL-met and γ-DL-met due to the dissolution being considered as a single step (a diffusion controlled process). This result showed that the dissolution rate of α-DL-met was faster than the growth rate of γ-DL-met. But the results of the SMT experiments in this chapter showed that the dissolution rate of α-DL-met is slower than the growth rate of γ-DL-met. Therefore, in reality the dissolution rate of α-DL-met is slower than γ-DL-met based on the result of this chapter. This leads to the conclusion that the dissolution process of the polymorphs of DL-met is a two step process. These are the surface reaction and the detachment of the species followed by transfer of these species toward the bulk solution across the diffusion layer which surrounds the crystals (Kramer and van Rosmalen, 2009). The value of the dissolution rate constant of α-DL-met at 25 °C can be estimated from the simulation of the SMT process.

5.6 Conclusions

The kinetics of the SMT of α-DL-met into γ-DL-met in water at 25 °C via seeded batch crystallization process was studied by the change of the solute concentration and γ-DL-met fraction with time during the crystallization process. The solute concentration profile was measured by off-line sampling using the dry substance method. Off-line quantitative measurement of the fraction of γ-DL-met in suspension was accomplished with XRPD by setting up a calibration curve using the mixtures of α-DL-met, γ-DL-met, and NaCl. NaCl was the internal standard sample and the composition was fixed to a constant value. A linear calibration line was obtained. The SMT is a two step process, consisting of the dissolution process of α-DL-met and the crystallization process (nucleation and growth) of γ-DL-met. The dissolution of α-DL-met is the rate controlling step during the transformation due the solute concentration dropping immediately to the solubility of the stable γ-DL-met. The transformation time for the case where the seed was added to the supersaturated solution in the SNT region is longer than the case in which the seed was added to the supersaturated solution above the SNT region. There is the induction time for the nucleation of γ-DL-met for the first case, but for the second case γ-DL-met is nucleates quickly (there is little or no induction time).

8.7 References

Bernstein, J., Davey, R. J., and Henck, J. O. (1999). Concomitant polymorphs. Angew. Chem. Int. Ed. 38(23): 3440-3461.

Davis *et al.* (2003). *In situ* monitoring of wet granulation using online X-Ray Powder Diffraction. Pharm. Res. 20(11): 1851-1857.

Dharmayat *et al*. (2008). An examination of the kinetics of the solution-mediated polymorphic phase transformation between α- and β-forms of L-glutamic acid as determined using online Powder X-ray Diffraction. Cryst. Growth Des. 8(7): 2205-2216.

Ferrari, E. S., Davey, R. J., Cross, W. I., Gillon, A. L., and Towler, C. S. (2003). Crystallization in polymorphic systems: The solution-mediated transformation of β to α glycine. Cryst. Growth Des. 3(1): 53-60.

Garti, N. and Zour, H. (1997). The effect of surfactants on the crystallization and polymorphic transformation of glutamic acid. J. Cryst. Growth 172(3-4): 486-498.

Garside, J., Mersmann, A., and Nyvlt, J. (2002). Measurement of crystal growth and nucleation rates (2nd ed.). UK: Institute of Chemical Engineering.

Hammond, R. B., Lai, X., Roberts, K. J., Thomas, A., and White, G. (2004). Application of in-process X-ray powder diffraction for the identification of polymorphic forms during batch crystallization reactions. Cryst. Growth Des. 4(5): 943-948.

Jiang, S., Jansens, P. J., and ter Horst, J. H. (2010a). Mechanism and kinetics of the polymorphic transformation of o-aminobenzoic acid. Cryst. Growth Des. 10(5): 2123-2128.

Jiang, S., Jansens, P. J., and ter Horst, J. H. (2010b). Control over polymorph formation of o-aminobenzoic acid. Cryst. Growth Des. 10(6): 2541-2547.

Jiang, S., ter Horst, J. H., and Jansens, P. J. (2008). Concomitant polymorphism of o-aminobenzoic acid in antisolvent crystallization. Cryst. Growth Des. 8(1): 37-43.

Kitamura, M. (1993). Crystallization behavior and transformation kinetics of L-histidine polymorphs. J. Chem. Eng. Jpn. 26(3): 303-307.

Kitamura, M. and Sugimoto, M. (2003). Anti-solvent crystallization and transformation of thiazole-derivative polymorphs-I: effect of addition rate and initial caoncentrations. J. Cryst. Growth 257(1-2): 177-184.

Kramer, H. J. M. and van Rosmalen, G. M. (2009). Crystallization. In: I. A., Wilson and C. F., Poole (ed.). Handbook of methods and instrumentation in separation science volume 2 (pp 1-20). London: Academic Press.

Lu, J., Wang, X-J., Yang, X., and Ching, C-B. (2007). Polymorphism and crystallization of famotidine. Cryst. Growth Des. 7(9): 1590-1598.

Mangin, D., Puel, F., and Veesler, S. (2009). Polymorphism in processes of crystallization in solution: A practical review. Org. Process Res. Dev. 13(6): 1241-1253.

Maruyama, S., Ooshima, H., and Kato, J. (1999). Crystal structures and solvent-mediated transformation of taltireline polymorphs. Chem. Eng. J. 75(3): 193-200.

Matsuoka, M., Yamanobe, M., Tezuka, N., Takiyama, H. and Ishii, H. (1999). Polymorphism, morphologies and bulk densities of DL-methionine agglomerate crystals. J. Cryst. Growth 198-199: 1299-1306.

O'Brien, L. E., Timmins, P., Williams, A. C., and York, P. (2004). Use of in situ FT-Raman spectroscopy to study the kinetics of the transformation of carbamazepine polymorphs. J. Pharm. Biomed. Anal. 36 (2) 335-340.

Ono, T., Kramer, H. J. M., ter Horst, J. H., and Jansens, P. J. (2004). Process modeling of the polymorphic transformation of L-glutamic acid. Cryst. Growth Des. 4 (6): 1161-1167.

Ono, T., ter Horst, J. H., and Jansens, P. J. (2004). Quantitative Measurement of the polymorphic transformation of L-glutamic acid using in-situ Raman Spectroscopy. Cryst. Growth Des. 4 (3): 465-469.

Qu, H., Louhi-Kultanen, M., Rantanen, J., and Kallas, J. (2006). Solvent-mediated phase transformation kinetics of an anhydrate/hydrate system. Cryst. Growth Des. 6(9): 2053-2060.

Roelands, C. P. M. (2005). Polymorphism in Precipitation Process. Ph.D. thesis, Delft University of Technology, The Netherlands.

Roelands *et al*. (2006). Antisolvent crystallization of the polymorphs of L-histidine as a function of supersaturation ratio and of solvent composition. Cryst. Growth Des. 6(4): 955-963.

Schöll, J., Bonalumi, D., Vicum, L., and Mazzotti, M. (2006). In situ monitoring and modeling of the solvent-mediated polymorphic transformation of L-glutamic acid. Cryst. Growth Des. 6(4): 881-891.

Takahashi, H., Takenishi, T., and Nagashima, N. (1962). Quantitative analysis of mixtures of L-glutamic acid polymorphs by X-ray diffraction. Bull. Chem. Soc. Jpn. 35 (6): 923-926.

Threlfall, T. (2003). Structural and thermodynamic explanations of Ostwald's Rule. Org. Process Res. Dev. 7(6): 1017-1027.

Vippagunta, S. R., Brittain, H. G., and Grant, D. J .W. (2001). Crystalline solids. Adv. Drug Del. Rev. 48(1): 3-26.

Chapter IX
Summary

The study has been successful in furthering understanding of two key parts of purification of amino acids through industrial crystallization. The first part of the project successfully studied the preferential crystallization of an amino acid component, methionine hydrochloride, and investigated this in terms of the physical properties of the system, mainly solubility, crystallization properties including metastable zone width and crystal growth rates, and also the preferential crystallization. The second part successfully studied the solution mediated phase transformation between two different polymorphs using the system DL-methionine. The two polymorphs studied were the alpha and gamma forms of this racemic amino acid. The properties, crystal growth, crystal dissolution, metastable zone width, and nucleation were all studied.

The project also helped support 2 graduate students. The project fully supported the study and research of Mr. Watcharagarn Simahaprom, who has graduated from his M.E. degree, and published a paper on his thesis in J. Crystal Growth as well as having a paper accepted in the journal of Prince of Songkhla University. The project also helped support the research of Dr. Lek Wantha, who received salary support for his Ph.D. from the M.O.E. He already has three international journal papers from this work published, 2 in J. Crystal Growth (independent of the paper of the other student) and 1 in Chemical Engineering and Technology. These students also have several conference proceedings papers, and several conference abstracts. Thus the project has also been successful in training students to perform internationally recognized research.

Appendix

Accepted / Published International Journal Articles Fully or Partially Supported by this Research

L. Wantha and A. E. Flood "Nucleation Kinetics of the γ-Polymorph of DL-Methionine" Chemical Engineering and Technology, 35(6) 1024-1030 (2012).

L. Wantha and A. E. Flood "Growth and dissolution kinetics of α and γ polymorphs of dl-methionine" J. Cryst. Growth, in press (2011). doi:10.1016/j.jcrysgro.2011.10.064.

W. Srimahaprom, A. E. Flood "Crystal growth rates and optical resolution of dl-methionine hydrochloride by preferential crystallization from aqueous solution" J. Cryst. Growth, in press (2011). doi:10.1016/j.jcrysgro.2011.10.056.